Aalborg Universitet

AALBORG UNIVERSITY
DENMARK

Modeling and Optimization of CatLiq® Liquid Biofuel Process

Toor, Saqib

Publication date:
2010

Document Version
Accepted author manuscript, peer reviewed version

Link to publication from Aalborg University

Citation for published version (APA):
Toor, S. (2010). *Modeling and Optimization of CatLiq® Liquid Biofuel Process*. Department of Energy Technology, Aalborg University.

General rights
Copyright and moral rights for the publications made accessible in the public portal are retained by the authors and/or other copyright owners and it is a condition of accessing publications that users recognise and abide by the legal requirements associated with these rights.

- Users may download and print one copy of any publication from the public portal for the purpose of private study or research.
- You may not further distribute the material or use it for any profit-making activity or commercial gain
- You may freely distribute the URL identifying the publication in the public portal -

Take down policy
If you believe that this document breaches copyright please contact us at vbn@aub.aau.dk providing details, and we will remove access to the work immediately and investigate your claim.

Downloaded from vbn.aau.dk on: May 05, 2023

Modelling and Optimization of Catliq® Liquid Biofuel Process

by

Saqib Sohail Toor

Aalborg University
Department of Energy Technology
July 2010

Aalborg University
Department of Energy Technology
Pontoppidanstræde 101
DK-9220 Aalborg East

ISBN: 978-87-89179-91-9

Printed in Denmark by Aalborg University

PREFACE

First, I would like to express my sincere gratitude to my supervisor, Prof. Lasse Rosendahl (Department of Energy Technology, AAU), his expert guidance, suggestions and many good advices.
I would like to thank my co-supervisor Mads Pagh Nielsen for his support and helpful comments and suggestions during this PhD study.
A great part of my work was done at Esbjerg Institute of Technology, Colloidal and Interface Chemistry research group (CIChem), Aalborg University. I would like to thank Erik G. Søgaard and his research group especially Rudi P. Nielsen, for his excellent cooperation and many advices. This cooperation was extremely useful, I have learnt a lot from them.
The second parts of my experiments were carried out at Department of Petroleum Engineering, Stavanger University, Norway. I would like to thank Tor Austad and Sivert Bakken Drangeid in assisting me to complete the experimental work.
At the University of Birmingham, UK my thanks goes to Regina Santos, Muhammad Noman Baig, and Phillip Robbins, I spent three months there, learning much of thermodynamic modeling and optimization work.
There are a number of people. Without them, I could not have completed this work and I owe them my gratitude. I thank to Andreas Rudolf, SCF Technologies A/S for his continuous support and inviting me to visit the pilot plant of the CatLiq® process. I am also grateful to Andreas for providing me useful data and product samples of the pilot plant for experimental work.
Finally, I would like to thank my family and friends for all their support.

Aalborg, September, 2010
Saqib Sohail Toor

ABSTRACT

Application of biomass and waste, as a renewable and possibly sustainable energy source, has gained an important role in the world's future energy policy. The Danish government, for instance, has set a target for 2030, which states that 35% of the total energy consumption must be based on renewable sources. The EU has set itself the objective of increasing the proportion of renewable energies in its energy mix by 20% by 2020. In Denmark, biomass currently accounts for approximately 70% of renewable energy consumption, mostly in the form of straw, wood and renewable wastes.

An important fraction of the available biomass and waste streams has high moisture content. Wet streams cannot be converted economically by thermal conversion techniques like combustion, pyrolysis and gasification because of the large amount of energy required for evaporation of water. Over the last decades research activities worldwide have been devoted towards the development of new thermochemical processes, which can convert wet biomass efficiently and economically. One of the novel technologies for conversion of wet biomass and waste streams is hydrothermal liquefaction ($280<T<370$ ^{o}C, $10<P<25$ MPa). Bio-oil with a relatively high heating value, water-soluble substances and gases can be produced by this process that can be controlled by the process conditions and catalysis.

The research described in this thesis deals with the CatLiq® process; a hydrothermal liquefaction technology developed by the Danish company SCF Technologies A/S, which operates a continuous 20L/h capacity pilot plant in Copenhagen. This company uses organic matter as for instance DDGS (Dried Distillers Grains with Solubles) as a feedstock to produce bio-oil in the presence of a homogeneous (K_2CO_3) and a heterogeneous (Zirconia) catalyst at subcritical conditions (T = 280-350 ^{o}C, P = 22.5-25.0 MPa). The experimental work was conducted to analyze the liquid and gaseous product. The thermodynamic work was completed to understand the phase behavior of the system.

Prior to the experiments milled DDGS (0.5 mm) was mixed with water to slurries with 25% dry matter. K_2CO_3 corresponding to 2.5% of the slurry mass was added. The catalytic conversion was carried out in a fixed-bed reactor filled with zirconia-catalyst at process temperature of

350°C and the feed rate was 11L/h. Each trial was run for 6 h and the process was considered to be in steady-state after 4 h. The oil was separated from the water phase by a disc-stack centrifuge. The oil yield on dry matter in the feed is 34%. The oil contains more than 6 times less oxygen than the DDGS and thus the effective heat value is almost double, 35.8 MJ/kg. As much as 73.2% of the energy in the feed is recovered in the oil.

Two characterization studies, GC-MS and TGA analysis, were conducted to analyze the oil phase. In order to determine the distribution of compounds in the oil, a semi-quantitative study was made by means of the percentage of area of the chromatographic peaks. The compounds were identified by means of the NIST library of mass spectra. The oil contains a large fraction of long chain aliphatic acids.

The water phase was analyzed for short-chained alcohols and acids as well as acetone by GC analysis. The TOC (Total Organic Content) is 33.3 ± 0.8 g/L, corresponding to a carbon recovery to water-soluble compounds of 30%. The content of short-chained alcohols and acids as well as acetone is 8% of the TOC content. The gas phase contains about 95% CO_2 and 1.6% H_2, small amounts of N_2, CO and CH_4.

In the modeling work, the bubble point pressures of a selected model mixture (CO_2 + H_2O + Ethanol + Acetic acid + Octanoic acid) were measured to investigate phase boundaries of the CatLiq® process. The bubble points were measured in the JEFRI-DBR high pressure PVT phase behavior system. The experimental results were presented for the temperatures between 40 ^oC and 75 ^oC. The results were correlated by the PSRK (Predictive Soave-Redlich-Kwong) model using Huron-Vidal first-order mixing rule of Michelsen coupled with the modified UNIFAC model. The average absolute deviation between the experimental and predicted data is 8.7% in the selected model mixture.

The CatLiq® process has been demonstrated to be an effective technology for catalytic liquid conversion of DDGS, giving a high yield of bio-oil. Even though the oil is probably not directly suitable as transportation fuel it may well be used for direct green electricity production, as input for refineries or as marine diesel.

DEDICATION

To the memory of my younger sister; Tina

TABLE OF CONTENTS

Paper III.

List of Figures

List of Tables

NOMENCLATURE

Symbol	Description	Unit
a	Co-energy parameter	Pa m^6 mol^{-2}
b	Co-volume parameter	m^3 mol^{-1}
a_{nm}, b_{nm}, c_{nm}	Interaction parameters between each two groups	-
Bps	Bottom of piston	cm
Bpsm	Bottom of piston in highest position	cm
Cp	Constant pressure specific heat capacity	kJ kg^{-1} K^{-1}
c_1, c_2, c_3	Mathias-Copeman parameters	-
Dv	Dead volume	cc
G^E	Molar excess Gibbs free energy	Pa m^3 mol^{-1}
IP	Ionic product	K_w
K	Equilibrium constant	-
P	Pressure	bar or MPa
Qc	Capacity	cc cm^{-1}
Q_k	Surface area parameter of structural group k	-
q_l	EOS-empirical dependent parameter	-
q_i	Surface area parameter of component i	-
R	Universal gas constant	cm^3 MPa K^{-1} mol^{-1}
R_k	Volume parameter of structural group k	-
r_i	Volume parameter of component i	-
T	Temperature	^oC or K
v	Molar volume	m^3 mol^{-1}
Vt	Total volume	cc
x	Mole fraction	-
Z	Compressibility factor	-
z	Coordination number	-

Greek letters

Symbol	Description	Unit
Ψ	UNIFAC group interaction parameter	-
γ	Activity coefficient	-
ω	Acentric factor	-
η	Dynamic viscosity	mPas
ρ	Density	g cm^{-3}
ϵ	Dielectric constant	Fm^{-1}
Φ	Volume fraction	
Θ	Surface area fraction	
$\Gamma_k^{(i)}$	Pure component residual activity coefficient	-
Γ_k	Group residual activity coefficients	-
φ	Fugacity coefficient	-
$\nu_k^{(i)}$	Number of structural groups of type k in molecule of component i	-

Subscripts

Symbol	Description
k	Structural group in a molecule of a component
c	Critical properties
r	Reduced properties
i, j	Component
m	Mixture
m, n	Structural group in the set of different molecules of all components
cal.	Calculated
exp.	Experimental

Superscripts

Symbol	Description
E	Excess properties
C	Combinatorial
R	Residual
L	Liquid
V	Vapor
sat.	Saturated

List of abbreviations

AAD	Average Absolute Deviations
ASTM	American Society for Testing and Materials
AHG	Anhydrous Glucose
CHN	Carbon Hydrogen Nitrogen
daf	Dry Ash Free
db	Dry Basis
DDGS	Dried Distillers Grains with Solubles
DIAS	Danish Institute of Agricultural Sciences
EOS	Equation of State
EREC	European Renewable Energy Council
GC	Gas Chromatography
GC-MS	Gas Chromatography Mass Spectroscopy
HMF	Hydroxymethyl Furfural
HTU	Hydrothermal Upgrading
IEA	International Energy Agency
IEO	International Energy Outlook
IP	Ionic product
MHV1	Modified Huron-Vidal first-order
NIST	National Institute of Standards and Technology

OECD	Organization for Economic Cooperation and Development
PSRK	Predictive Soave-Redlich-Kwong
PVT	Pressure Volume Temperature
R&D	Research and Development
Rel. Dev.	Relative Deviation
RES	Renewable Energy Sources
RT	Retention Time
SCF	Supercritical Fluid
SRK	Soave-Redlich-Kwong
TGA	Thermo Gravimetric Analysis
TOC	Total Organic Content
UNIFAC	Universal Functional Activity Coefficient
WDGS	Wet Distillers Grains with Solubles
WSH	Water Soluble Hydrocarbons

1 OBJECTIVES, SUMMARY AND CONCLUSIONS

1.1 The aim of the work (PhD study)

The overall aim of this PhD study was to assess the potential of a hydrothermal liquefaction process in Denmark using DDGS (Dried Distillers Grains with Solubles), a byproduct in first generation ethanol production, available in large quantities. This aim was accomplished by meeting the following objectives:

- To characterize the bio-oil produced during the CatLiq® process quantitatively and by heating value.
- Conducting different analysis methods to investigate oil, water and gas phase of the system.
- Determining the experimental and predictive bubble point pressures of the selected model mixture to understand the phase behavior of the process.

1.2 Materials and methods used

DDGS was collected from the Agroethanol AB, Norrköping, Sweden and characterized prior to processing. CHN analysis and heat value was carried out at Karlshamns Kraft, Karlshamn, Sweden. DDGS was milled in a dry-mill to reduce particle size to 0.5mm. Prior to the experiments milled DDGS was mixed with water to slurries with 25% dry matter. K_2CO_3 (homogeneous catalyst) corresponding to 2.5% of the slurry mass was added.
The catalytic conversion of DDGS was performed in a continuous pilot plant (Figure 1.1) with a capacity of 10-20 L/h of wet biomass. The reaction was carried out in the presence of ZrO_2 (heterogeneous catalyst) at subcritical conditions (280-350 ^oC and 22.5-25.0 MPa) and the feed rate was 11L/h.

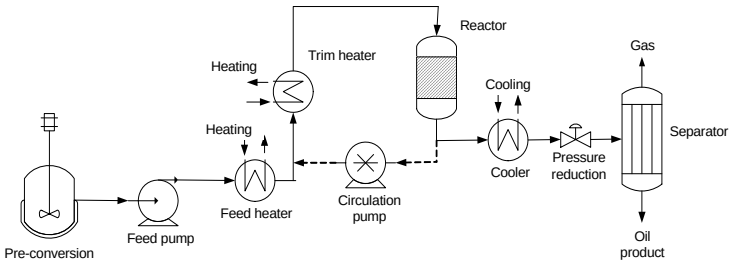

Figure 1.1 Schematic of the CatLiq® process

The conditioned feed from the feed tanks was pumped through a high pressure feed pump. The feed was then preheated in the feed heater. The feed entered in a recirculation loop, in which a recirculation pump ensured a high flow rate. The flow passed through a trim heater and a fixed-bed reactor filled with zirconia-catalyst. After the reactor a fraction of the product stream was withdrawn and passed through a cooler. After pressure reduction the oil is separated from the water phase by centrifugation or gravimetrical separation. The full product contained a bio-oil phase, a gas-phase and a water phase with soluble organic compounds.

Oil obtained from catalytic conversion of DDGS was analyzed by gas chromatograph equipped with a mass selective detector [GC-MS; Varian CP-3800; column, VF-5ms; (5% phenyl 95% dimethylpolysiloxane, 30m × 0.25mm × 0.25µm); temperature programmed: 75°C (hold 2 min.) → 325°C (20°C/min, hold 15 min.). The compounds were identified by means of the NIST (National Institute of Standards and Technology) library of mass spectra. To calculate the elementary composition, heat value, and Conradson number of bio-oil, all analysis were carried at Karlshamns Kraft, Karlshamn, Sweden. The water content was determined by Carl-Fischer titration performed with a TitraLab TIM 580 (Radiometer, France). Thermogravimetric analysis (TGA) was performed both in nitrogen and oxygen environment to characterize the evaporation, thermal decomposition and combustion properties of bio-oil.

The water phase was analyzed for short-chained alcohols and acids as well as acetone by GC (Varian 3800, column: fused silica, 25m × 0.32mm, temperature programmed: 50 °C hold 2 min. → 140 °C, 35 °C/min.). The total organic content (TOC) in the water phase was measured by using a kit (LCK 387) and a spectrophotometrical analysis

unit (DR 2800) from Hach & Lange, Germany. The gas phase was sent for analysis at Statens Provningsanstalt, Borås, Sweden.
To determine the bubble point pressures, a mixture of a limited number of well-defined components resembling the products from the CatLiq® process was used instead of a real fraction. This method allows a thorough experimental investigation that can be used to verify the prediction and adjust the description by equations of state. Table 1.1 shows the system studied, indicating the components and their compositions in weight percent.

Table 1.1 The investigated system and its composition

Component	(%, w/w)
CO_2	7.0
Water	84.8
Ethanol	0.1
Acetic acid	0.1
Octanoic acid	8.0

Experiments were carried out in a JEFRI-DBR high pressure PVT phase behavior system (Figure 1.2). The heart of the system was a high-pressure PVT cell consisting of a glass cylinder, secured between two full-length sight glass windows, inside a stainless steel frame. This design allowed for unimpaired visibility of the entire contents of the cell. Pressure was regulated through an automated, high pressure, positive displacement pump. The hydraulic fluid inside the pump was connected to a floating isolation piston located inside the PVT cell. The piston isolated the hydraulic fluid from the process side of the PVT cell. Controlled displacement of the isolation piston allowed for volume changes in the process chamber, thus providing an effective way to control pressure. The PVT cell was mounted inside a temperature-controlled air bath by means of a bracket, attached to a horizontal shaft.

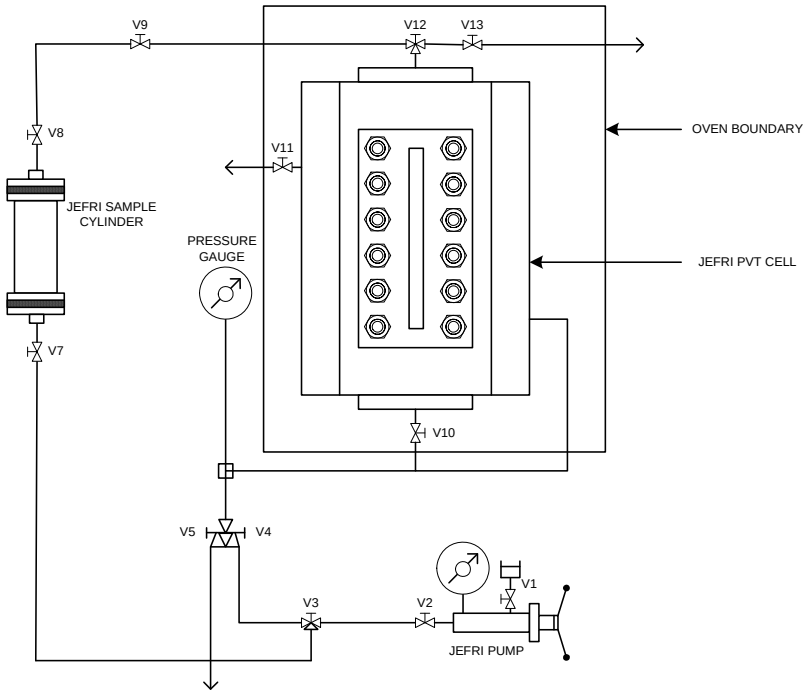

Figure 1.2 Schematic diagram of JEFRI-DBR PVT system

The bubble point pressures were determined at different constant temperatures (40 ^{o}C, 50 ^{o}C, 60 ^{o}C, and 75 ^{o}C) by observing the appearance of gas bubble through the cell window as the pressurized liquid sample was decompressed. As soon as the bubble point pressure reached the overall compressibility of the system increased. Small changes in pressure resulted the large changes in the total fluid volume in the PVT cell. This was manifested graphically by the change of the slope when the sample pressure was plotted against the sample volume.
The experimental results were correlated by the PSRK (predictive Soave-Redlich-Kwong) model, which is predictive Soave-Redlich-Kwong (SRK) equation of state with the modified Huron-Vidal first-order (MHV1) mixing rule coupled with the modified UNIFAC model.

1.3 Overall conclusions

There are several processes for thermal transformation of biomass to liquids with fuel properties such as pyrolysis, Catalytic depolymerization (CDP) and biomass gasification combined with Fischer-Tropsch synthesis (BG-FT). Many of these processes are not optimal for wet biomass. To remove the water by evaporation consumes a considerable amount of energy. Therefore direct liquefaction of biomass is an attractive process from the view point of energy consumption. The degradation pattern for the different biomass components (Carbohydrates, Lignin, Protein and Lipids) differs widely and so does the product. There is also most likely a synergy between the different biomass components. DDGS could be used directly to produce a liquid fuel in a thermal liquefaction process, such as the CatLiq® process. This would offer a more flexible process, which allows for adjustment of the product profile depending of the price of DDGS and crude oil. A fixed bed reactor at the CatLiq pilot plant facility was used in this study. The GC-MS analysis showed, the oil produced contained mainly long chain aliphatic acids. More importantly, 73% of the energy in the DDGS was recovered. The oil had an effective heat value of 36 MJ/kg, not far from that of commercial diesel. The water phase contained short-chained alcohols and acids as well as acetone. During the process more than 80% of the oxygen was removed, therefore gas contained about 95% CO_2.
The CatLiq® process has been demonstrated to be an effective technology for catalytic liquid conversion of DDGS, giving a high yield of bio-crude oil. Even though the oil due to the rather high viscosity, is not directly suitable as transportation fuel, it may well be used for direct green electricity production, as feed-stock for refineries or as marine diesel. The CatLiq technique offers an alternative use of WDGS and thus flexibility in terms of product spectrum.
Comparison of the percentages of error and average absolute deviation between the experimental and predictive data obtained from the bubble point pressure calculations showed that the capability of the PSRK model is reasonably good in predicting the phase behavior of such a model system for CatLiq process. This modelling work is useful for the CatLiq process design, development and optimization, which provides a general thermodynamic approach on how to model biomass conversion processes, and is, of course, applicable to other biomass conversion processes.

1.4 Summary and conclusions of the papers

Paper I.

This paper reviews the hydrothermal liquefaction of biomass in the presence of water. Thermochemical conversion can be subdivided into gasification, pyrolysis, and direct liquefaction. Direct liquefaction is attractive from the view point of energy consumption and it's a promising method for the biomass conversion. The carbonaceous materials are converted to liquefied products through a complex sequence of changes in physical structure and chemical bonds. Liquefaction process may become an important technology for converting wet biomass or organic waste into bio-oil or other types of fuels. Technical hurdles are not yet solved completely but significant progress has been made through experimentation.
Catalyst has a positive effect on the liquefaction process and can increase the yield of liquid product, as well as improve the quality of liquid product. With a catalyst, more bio-oil and less gas can be obtained than that without using a catalyst.
Among the available solutions, biomass liquefaction has been regarded as a long-term option and so might appear now as unimportant. Nonetheless, its potential does really exist, particularly for producing specific fuels. Research and development have to progress in order to solve the associated technological problems and integrate the product into existing markets.

Paper II.

In this paper, Catalytic liquid conversion of DDGS was performed in a 20L/h continuous pilot-plant at subcritical conditions (280-350^{o}C and 22.5-25.0 MPa) in the presence of homogeneous K_2CO_3 and heterogeneous ZrO_2 catalysts. The oil produced contained mainly long chain aliphatic acids and the oil yield on DDGS was 34% (w/w). More importantly, 73% of the energy in the DDGS was recovered in the oil. During the process more than 80% of the oxygen was removed. The oil had an effective heat value of 36 MJ/kg, not far from that of commercial

diesel (42 MJ/kg, effective), and significantly higher than that of ethanol (28MJ/kg, effective).
There are only few similar techniques for utilization of wet materials that have reached further than bench-scale. The most important is the HTU® (Hydrothermal Upgrading) process, which has been evaluated in a 20 kg/h pilot plant. Even though the CatLiq® and HTU® process are based on the same principles there are basic differences; firstly, the use of heterogeneous catalysts in the CatLiq® and secondly that the design of the internal recirculation system differs. The oil from the HTU-process in general has a low heating value (LHV) of 30-35 MJ/kg and an oxygen content of 12-21%. In a specific case sugar beet pulp was converted and the lower heating value was 33.3 MJ/kg and the energy recovery 79%. It is obvious that the CatLiq® process compares well to these results even though the raw materials were different. In addition the CatLiq oil from DDGS is stable during extended storage. Many pyrolysis oils and oils from similar processes often show poor stability.
Only compounds corresponding to about 20% of the TOC could be identified with GC and GC-MS. The number of compounds was obviously large and thus not all compounds could be identified. In the GC-MS analysis of water extract, the detected compounds accounted only for 35% of the total area. It is overall certain that the main components are short-chain alcohols and acids, amines and aliphatic acids and that the unidentified compounds are most likely derivates thereof.

Paper III.

In this paper, thermodynamic models and methods have been proposed for the description of the CatLiq process, which can give good predictions for the phase separation and phase properties. Bubble point pressures of a selected model mixture (CO_2 + H_2O + Ethanol + Acetic acid + Octanoic acid) were measured to investigate phase boundaries of the CatLiq process. The bubble points of this system were measured in a JEFRI-DBR high pressure PVT phase behavior system. The experimental results were presented for the temperatures (40 ^oC, 50 ^oC, 60 ^oC and 75 ^oC). The results were correlated by the PSRK model proposed by Holderbaum and Gmehling, which is predictive Soave-

Redlich-Kwong (SRK) equation of state (EOS) with the modified Huron-Vidal first-order (MHV1) mixing rule of Michelsen coupled with the modified UNIFAC model. The average absolute deviation between the experimental and predicted data was 8.7% in the selected model mixture.

1.5 Contribution to papers

Saqib Sohail Toor has contributed to the papers as follows:

Paper I and II.

Saqib Sohail Toor has written the paper-I under the proper guidance of Andreas Rudolf and Lasse Rosendahl. In the paper-II Saqib Sohail Toor has prepared the oil and water phase samples and performed all the experiments. Evaluation and analysis of the experimental results were performed in cooperation with Lasse Rosendahl, Mads Pagh Nielsen, Andreas Rudolf and Olofsson G.

Paper III.

Saqib Sohail Toor has prepared the model mixture and performed all the experiments. Evaluation and analysis of the experimental results were performed in cooperation with Lasse Rosendahl and Kristian P. Nøgaard. MatLab coding work was completed under the supervision of M.N. Baig, P.T. Robbins and R.C.D. Santos.

2 INTRODUCTION

The sun was the first energy source. It provided light and heat to the first humans. During the day, the people searched for food. They had no home. When it began to get dark, they looked for shelter. Once the sun went down, the world was dark and cold. The moon and stars gave the only light. People huddled together for warmth. Later, they learned how to start fires. They rubbed pieces of flint together to make sparks. They used fire to make stronger tools. They used fire to help them capture animals for food. They had an energy source that could do many things for them. It made life easier. The sun and wood gave man energy for a long time. It was only about 5,000 years ago that people started using other sources. People began using the wind to move from one place to another. They built boats with sails that captured the wind. Wind was the first energy source used for transportation.
Throughout history, energy has been a driver in humankind's progress. Its utilization brought comfort and an increasing standard of living throughout the years. Together with its growing utilization, the sources from which energy could be generated had evolved as well. From burning of wood to the burning of coal, from harnessing the inherent power of sunlight to generating energy from the fission of uranium, these are testaments to the ingenuity as well as the need of the human race to feed what has been sustaining them. Among these, fossil fuel became the most important source for nearly the past two centuries.

2.1 Current status of world energy

2.1.1 Supply and demand of energy

World energy consumption has been steadily increasing for a variety of reasons, which include enhancements in quality of life, population increase, industrialization, rapid economic growth of developing countries, increased transportation of people and goods, etc. There are many types of fuel available worldwide, the demand for which strongly depends on application and use, location and regional resources, cost,

"cleanness" and environmental impact factors, safety of generation and utilization, socioeconomic factors, global and regional policies, etc. the energy utilization cycle consists of three phases: generation, distribution, and consumption, all of which must be closely balanced for an ideal energy infrastructure (Lee 2007). Figure 2.1&2.2 illustrates the world total primary energy supply and total final consumption by fuel from 1971 to 2007 respectively (IEA, 2009). As can be seen from Figure 2.1, of all the fossil fuels, crude oil is the major source of energy in the world.

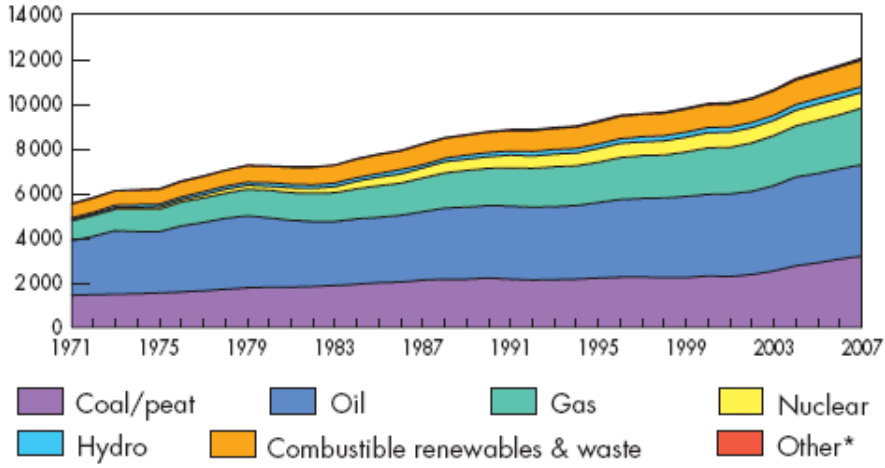

Figure 2.1 Evolution from 1971 to 2007 of world total primary energy supply by fuel (Mtoe) [IEA, 2009]

*Other includes geothermal, solar, wind, heat, etc.

According to IEA (2009), total primary energy supply in the world increased from almost 5500 Mtoe in 1971 to 12000 Mtoe in 2007 and total final consumption increased from almost 4200 Mtoe in 1971 to 8200 Mtoe in 2007 (Figure 2.1&2.2).

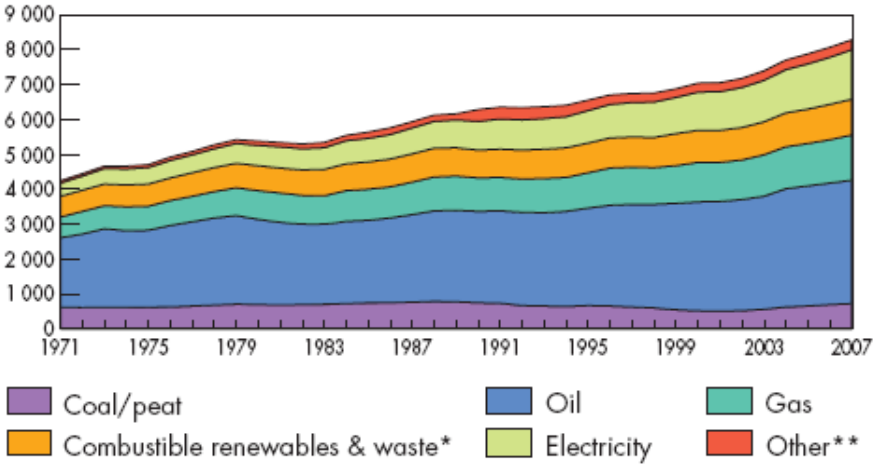

Figure 2.2 Evolution from 1971 to 2007 of world total final consumption by fuel (Mtoe)
IEA, 2009

*Prior to 1994 combustible renewables & waste final consumption has been estimated
**Other includes geothermal, solar, wind, heat, etc.

As shown in Figure 2.2, Coal/peat show the slowest increase in consumption for the period, whereas other includes geothermal, solar, wind, heat, etc have recorded the steepest increase, indicating that these are the emerging energy sources with the greatest future in the world energy market. The higher rates of growth for renewable energy consumption also show their strong potential as alternative fuels that ultimately will replace and supplement the conventional fuel types in a variety of applications and end uses.
In the IEO 2009 reference case - which reflects a scenario in which current laws and policies remain unchanged throughout the projection period - world marketed energy consumption is projected to grow by 44 percent over the 2006 to 2030 period. Total world energy use rises from 472 quadrillion Btu (4.979864×10^{17} kJ) in 2006 to 552 quadrillion Btu (5.823908×10^{17} kJ) in 2015 and then to 678 quadrillion Btu (7.153279×10^{17} kJ) in 2030 (Figure2.3).

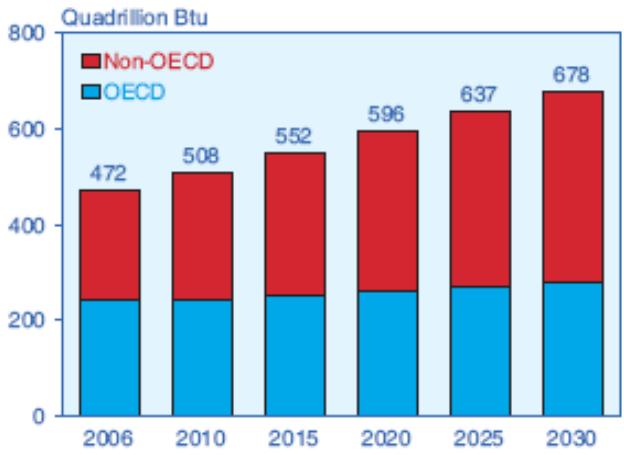

Figure 2.3 World marketed energy consumption, 2006-2030 [IEO, 2009]

World carbon dioxide emissions are projected to rise from 29.0 billion metric tons in 2006 to 33.1 billion metric tons in 2015 and 40.4 billion metric tons in 2030-an increase of 39 percent over the projection period (Figure 2.4).

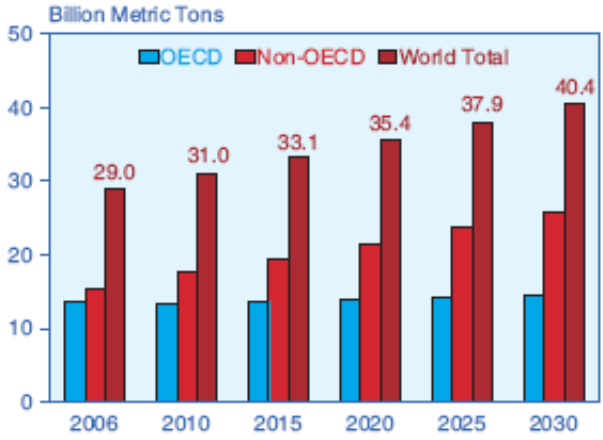

Figure 2.4 World carbon dioxide emissions, 2006-2030 [IEO, 2009]

With strong economic growth and continued heavy reliance on fossil fuels expected for most of the non-OECD economies, much of the increase in carbon dioxide emissions is projected to occur among the developing, non-OECD nations. In 2006, non-OECD emissions

exceeded OECD emissions by 14 percent. In 2030, however, non-OECD emissions are projected to exceed OECD emissions by 77 percent.

2.1.2 The issue of non-sustainability: Declining of oil reserves

Fossil fuels are generally considered as non-renewable resources. As of January 1, 2009, proved world oil reserves, as reported by the Oil & Gas Journal, were estimated at 1,342 billion barrels -10 billion barrels (about 1 percent) higher than the estimate for 2008 (IEO, 2009). According to the Oil & Gas Journal, 56 percent of the world's proved oil reserves are in the Middle East (Figure 2.5).

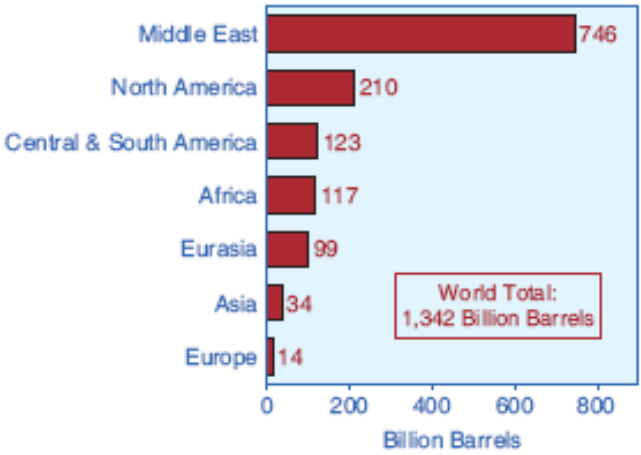

Figure 2.5 World proved oil reserves by geographic region as of January 1, 2009 [IEO, 2009]

Oil is the fossil fuel that is most in danger of running out. Figure 2.6 shows global oil production scenarios based on today's production (Demirbas, 2008). Over the years, concerns about the steady decline of the available petroleum in the face of ever-increasing demand for this valuable commodity have fueled researchers to look for possible alternative energy sources as well as chemical feedstock. Coupled with unrest in most nations where the majority of crude oil is sourced, the fear

of losing a steady supply of fuel gave impetus to renewed efforts in countries to being self-reliant.

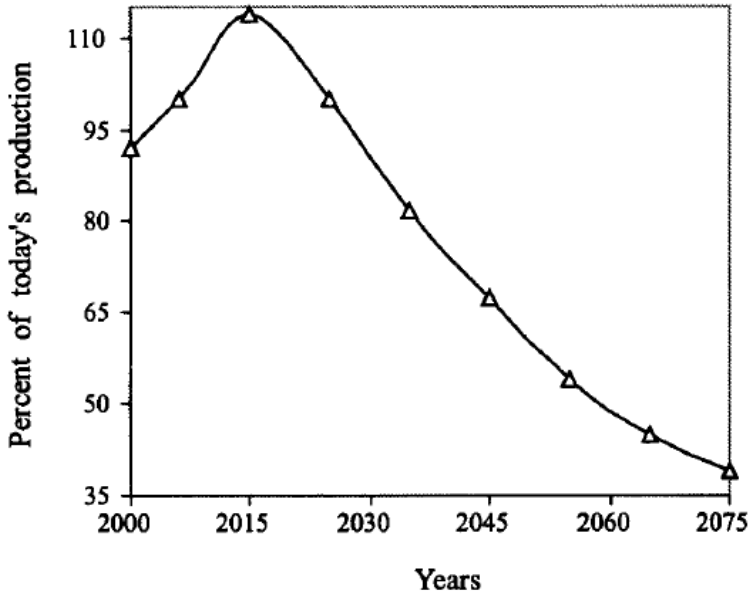

Figure 2.6 Global oil production scenarios based on current production Demirbas, 2008

Recently, most governments all over the world have turned their policies towards improving renewable and sustainable energy sources that are accessible in their own backyard.

2.1.3 Renewable sources

Renewable energy sources (RESs) are also often called alternative energy sources. RESs that use indigenous resources have the potential to provide energy services with zero or almost zero emissions of both air pollutants and greenhouse gases. Renewable energy technologies produce marketable energy by converting natural materials into useful form of energy. These technologies use the sun's energy and its direct and indirect effects on the earth (solar radiation, wind, falling water, and various plants, i.e., biomass), gravitational forces (tides), and the heat of

the earth's core (geothermal) as the resources from which energy is produced.

About 98% of carbon emissions result from fossil fuel combustion. Reducing the use of fossil fuels would considerably reduce the amount of carbon dioxide produced, as well as reducing the levels of the pollutants. Indeed, much of the variation in cost estimates to control carbon emissions revolves around the availability and cost of carbon-free technologies and carbon-reducing technologies, such as energy efficiency and energy conservation equipment. This can be achieved by either using less energy altogether or using alternative energy resources.

Figure 2.7 represents the main fuels in the world total primary energy supply (TPES)[1], with a disaggregation of the share of the main renewables categories. In 2004, renewables accounted for 13.1% of the 11059 Mtoe of world total primary energy supply. Combustible renewables and waste (97% of which is biomass, both commercial and non-commercial) represented 79.4% of total renewables followed by hydro (16.7%) (IEA, 2007).

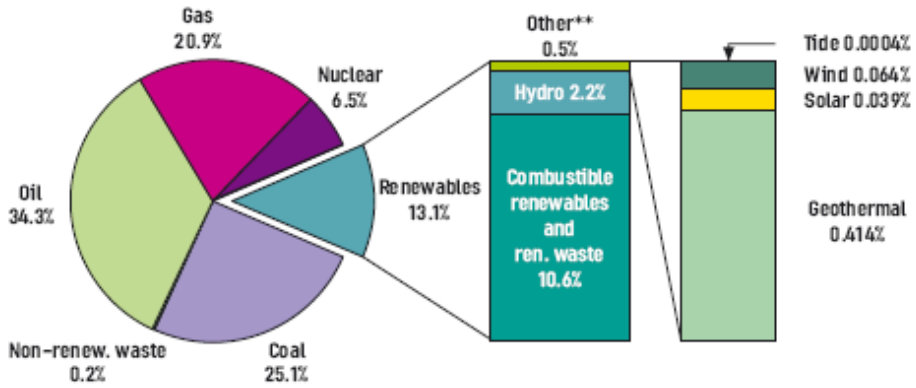

Figure 2.7 2004 fuel shares of world total primary energy supply IEA, 2007

***Geothermal, solar, wind, tide/wave/ocean.*

According to the European Renewable Energy Council (2006), approximately half of the global energy supply will come from RESs in 2040. Table 2.1 shows the global renewable energy scenario by 2040. The most significant developments in renewable energy production will

be observed in photovoltaics (from 0.2 to 784 Mtoe) and wind energy (from 4.7 to 688 Mtoe) between 2001 and 2040.

Table 2.1 Global renewable energy scenario by 2040 EREC, 2006

	2001	**2010**	**2020**	**2030**	**2040**
Total Consumption in (Mtoe)	10038.3	10549	11425	12352	13310
Biomass	1080	1313	1791	2483	3271
Large hydro	222.7	266	309	341	358
Small hydro	9.5	19	49	106	189
Wind	4.7	44	266	542	688
PV	0.2	2	24	221	784
Solar thermal	4.1	15	66	244	480
Solar thermal electricity	0.1	0.4	3	16	68
Geothermal	43.2	86	186	333	493
Marine (tidal/wave/ocean)	0.05	0.1	0.4	3	20
Total RES	1364.5	1745.5	2694.4	4289	6351
RES contribution	13.6	16.6	23.6	34.7	47.7

[1]TPES is calculated using the IEA conventions (physical energy content methodology). It includes international marine bunkers and excludes electricity/heat trade. The figure includes both commercial and non-commercial energy.

In early 2007, the European Commission (RE 2007) adopted new binding targets for 2020, including 20 percent of final energy and 10 percent of transport fuels (Figure 2.8).

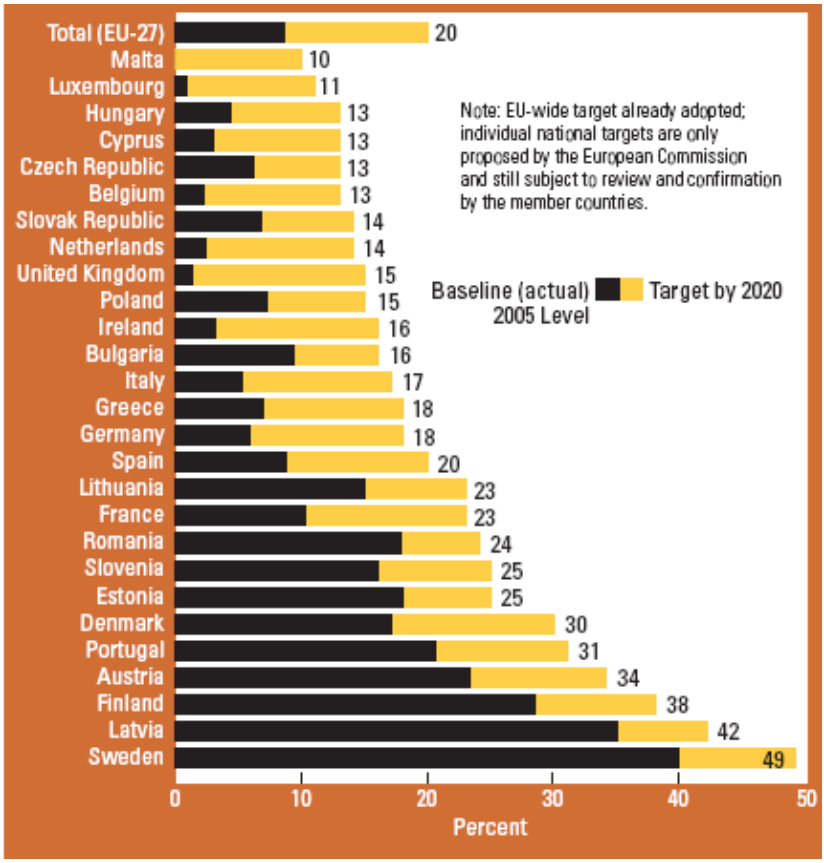

Figure 2.8 EU renewable energy targets-share of final energy by 2020 [RE, 2007]

The current Danish Energy Policy (DIAS 2003) is based on four political main targets:

- Stabilization of the annual energy consumption at 800 PJ
- Maintaining continued economic growth
- Reduce CO_2 emissions
  - 20% by year 2000
  - 50% by year 2030
- Sustainable development

Several means are in operation in order to fulfill the political targets within the planning period (2030) of which the most important in this context is a conversion from coal in the central power plants to natural

gas and renewables at a rate of 1% annually from a total of 8% in 1996 to approx. 30% in 2030. Table 2.2 shows the targeted shares of the different renewable energy sources within the planning period.

Table 2.2 Targets for the use of renewable energy in Denmark (PJ) [DIAS, 2003]

	1996	2000	2005	2010	2030
Wind power	4.4	9	14	23	60
Other	3.5	1	3	4	29
Biomass	61.4	77	85	96	146
-solid municipal waste	25.4	23	23	23	22
-straw	13.7	25	27	28	34
-Wood chips	20.3	24	26	27	24
-energy crops	0	0	0	5	46
-biogas	2.0	5	9	13	20
Total	69.3	87	102	123	235
% of total consumption	8	10-11	12-14	17-19	35

The Danish Council for Strategic Research (DCSR) programme committees have appropriated about DKK 320 million in total for energy projects (Energy 2009). The most highly prioritized technological focus areas are biofuels, hydrogen and fuel cells, energy systems and wind energy (Figure 2.9).

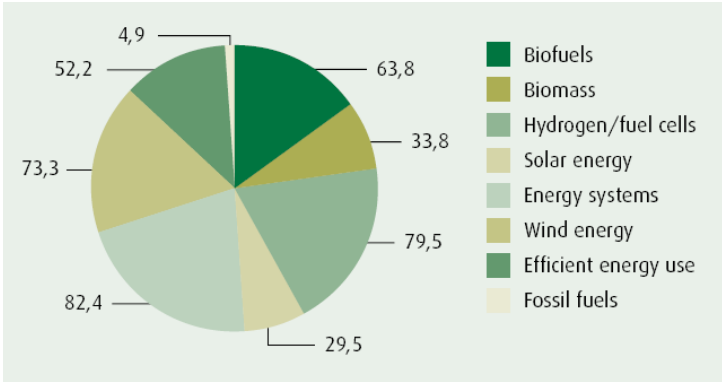

*Figure 2.9 DCSR energy: Funding 2004-2008 (DKK million)**

**Danish Agency for Science, Technology and Innovation.*

2.2 Energy from biomass

The term biomass refers to wood, short-rotation woody crops, agricultural wastes, short-rotation herbaceous species, wood wastes, bagasse, industrial residues, waste paper, municipal solid waste, saw dust, biosolids, grass, waste from wood processing, aquatic plants and algae animal wastes, and a host of other materials. Biomass is the name given to all the Earth's living matter. Biomass as solar energy stored in chemical form in plant and animal materials is among the most precious and versatile resources on Earth. It is a rather simple term for all organic materials that derive from plants, trees, crops, and algae. The components of biomass include cellulose, hemicelluloses, lignin, extractives, lipids, proteins, simple sugars, starches, water, ash and other compounds.

In the past decade or so, utilization of biomass has become of keener interest - not only as fuel but also as a source of chemicals which could potentially replaced petroleum-based feedstock. Why is biomass attractive? Because it is renewable, readily available and considered to give zero net emission of one of the most notorious greenhouse gases, carbon dioxide. Its utilization addresses the timely issues of sustainability, self-sufficiently and environmental consciousness. Biomass is a complex resource that can be processed in many ways leading to a variety of products. This is reviewed by (Chum *et al.* 2001) and in Figure 2.10. However, for renewable processing of biomass the cost of technologies still needs to be decreased through research, development, demonstration, and diffusion of commercialized new technologies. Valuing the environmental and social contributions that biomass inherently makes can also help to increase its use. Each route requires integrated efforts across multiple industrial sectors, academia, national laboratories, professional societies etc. In Denmark, biomass currently accounts for approximately 70% of renewable energy consumption, mostly in the form of straw, wood and renewable wastes (Danish Energy Agency).

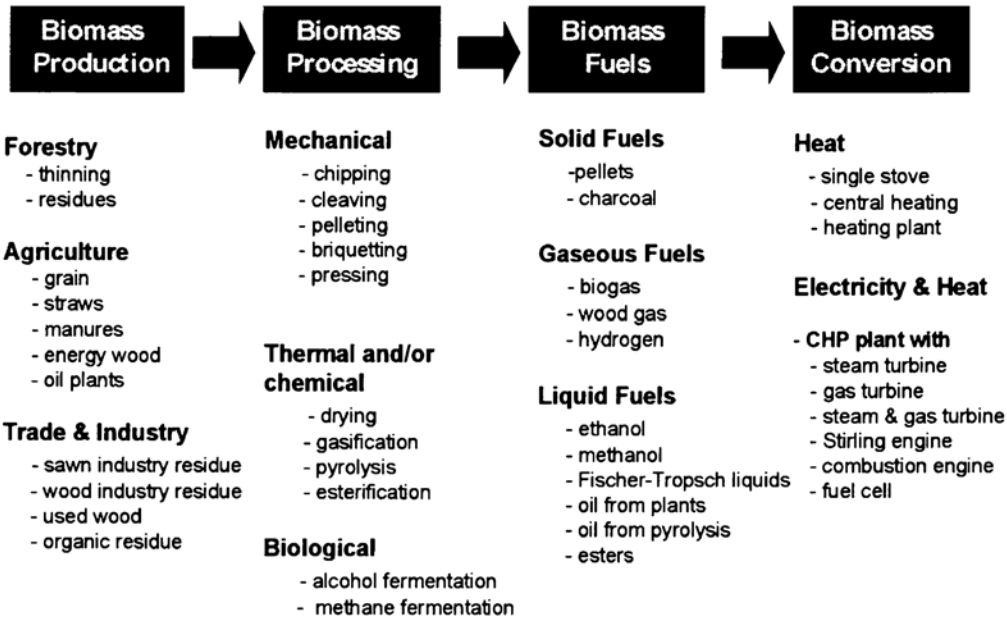

Figure 2.10 From multiple biomass resources to a variety of fuels & energy products
Chum et al. 2001

As we can see in Figure 2.10 and according to (Bridgwater *et al.* 1999) the biomass conversion technologies are mostly physical/chemical processing, thermo-chemical and biological.
There are several ways we consume energy. Basically, we need heat, electricity and fuel for transportation. Production of these services from biomass has to meet the possibilities. (Faaij 2001) has reviewed the different biomass applications and the different conversion technologies (Figure 2.11).

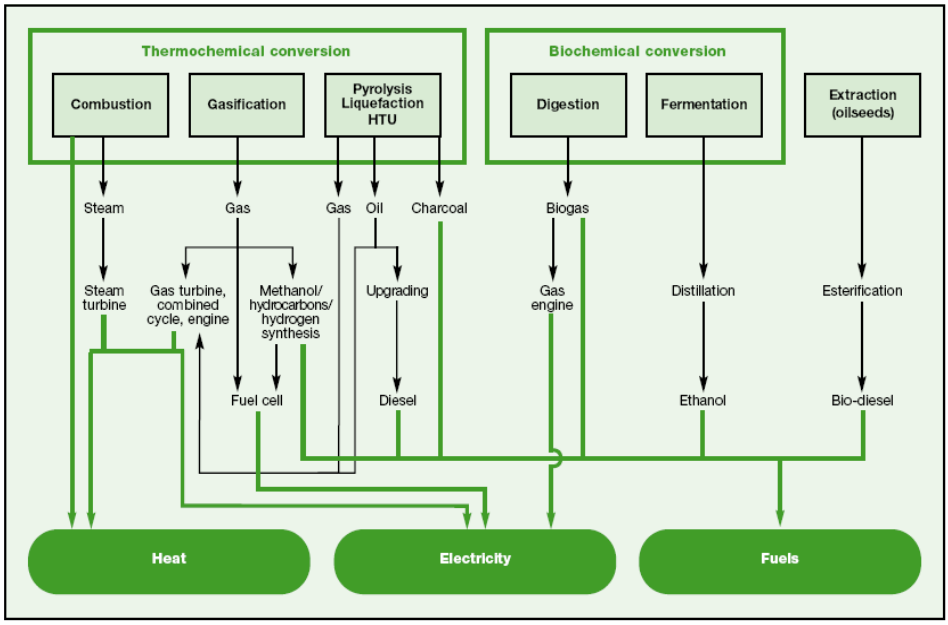

Figure 2.11 Main conversion options for biomass to secondary energy carriers Faaij, 2001

2.2.1 Biomass conversion technologies

Biomass can be converted into useful forms of energy using a number of different processes. Factors that influence the choice of conversion process are: the type and quantity of biomass feedstock; the desired form of the energy, i.e. end-use requirements; environmental standards; economic conditions; and project specific factors. In many situations it is the form in which the energy is required that determines the process route, followed by the available types and quantities of biomass. Biomass can be converted into three main products: two related to energy-power/heat generation and transportation fuels- and one as a chemical feedstock.

Conversion of biomass to energy is undertaken using two main process technologies: thermo-chemical and bio-chemical/biological. Mechanical extraction (with esterification) is the third technology for producing energy from biomass, e.g. rapeseed methyl ester (RME) bio-diesel. Within thermo-chemical conversion four process options are available: combustion, gasification, pyrolysis and hydrothermal liquefaction. Bio-

chemical conversion encompasses two process options: digestion (production of biogas, a mixture of mainly methane and carbon dioxide) and fermentation (production of ethanol). All these biomass process technologies are grouped as following:

- Mechanical extraction process
- Bio-chemical processes
    - Anaerobic digestion
    - Fermentation
- Thermo-chemical processes
    - Combustion
    - Gasification
    - Pyrolysis
    - Hydrothermal liquefaction

2.2.1.1 Mechanical extraction process

Extraction is a mechanical conversion process used to produce oil from the seeds of various biomass crops, such as oilseed rape, cotton and ground nuts. The process produces not only oil but also a residual solid or 'cake' which is suitable for animal fodder. Rapeseed oil can be processed further by reacting it with methyl alcohol using a process termed esterification to obtain rapeseed methyl ester (RME) or bio-diesel. RME is used in some European countries as a supplementary transport fuel (Faaij 2001).
Biodiesel from oil crops, waste cooking oil and animal fat cannot realistically satisfy even a small fraction of the existing demand for transport fuels. Microalgae appear to be the only source of renewable biodiesel that is capable of meeting the global demand for transport fuels. Like plants, microalgae use sunlight to produce oils but they do so more efficiently than crop plants. Photobioreactors are used for producing large quantities of microalgal biomass. Unlike other oil crops, microalgae grow extremely rapidly and many are exceedingly rich in oil. Microalgae commonly double their biomass within 24 h. Oil content in micro algae can exceed 80% by weight of dry biomass (Chisti 2007).

2.2.1.2 Bio-chemical processes

Anaerobic digestion

Anaerobic digestion is the conversion of organic material directly to a gas, termed biogas, a mixture of mainly methane and carbon dioxide. The biomass is converted by bacteria in an anaerobic environment, producing a gas with an energy content of about 20-40% of the lower heating value of the feedstock. Anaerobic digestion is a commercially proven technology and is widely used for treating high moisture content organic wastes, i.e. 80-90% moisture. Biogas can be used in gas turbines and can be upgraded to higher quality i.e. natural gas quality, by the removal of CO_2.

Fermentation

Fermentation is used commercially on a large scale in various countries to produce ethanol from sugar crops (e.g. sugar cane, sugar beet) and starch crops (e.g. maize, wheat), so called first generation bioethanol production. The biomass is ground down and the starch converted by enzymes to sugars, with yeast then converting the sugars to ethanol. Purification of ethanol by distillation is an energy-intensive step. The solid residue from the fermentation process can be used as cattle-feed and in the case of sugar cane, the bagasse can be used as fuel for boilers or for subsequent gasification. The conversion of lignocellulosic biomass such as wood, straw, and grasses, so called 2^{nd} generation technologies is more complex, due to the presence of longer-chain polysaccharide molecules and requires acid or enzymatic hydrolysis before the resulting sugars can be fermented to ethanol. As shown in Figure 2.12 (Lee 2007), in making grain alcohol, the distiller produces sugar solution from feedstock, ferments the sugar to ethanol, and then separates the ethanol from water through distillation.
In 2009, global production of bio-ethanol was 73.81553 billions of liters according to data assembled by F.O. Licht. The Global Renewable Fuels Alliance (GRFA) predicts global production will reach 85.92885 billions of liters in 2010 growing by 16.2 percent from 2009 production (Global Renewable Fuels Alliance). The largest producers are US, Brazil and European Union.

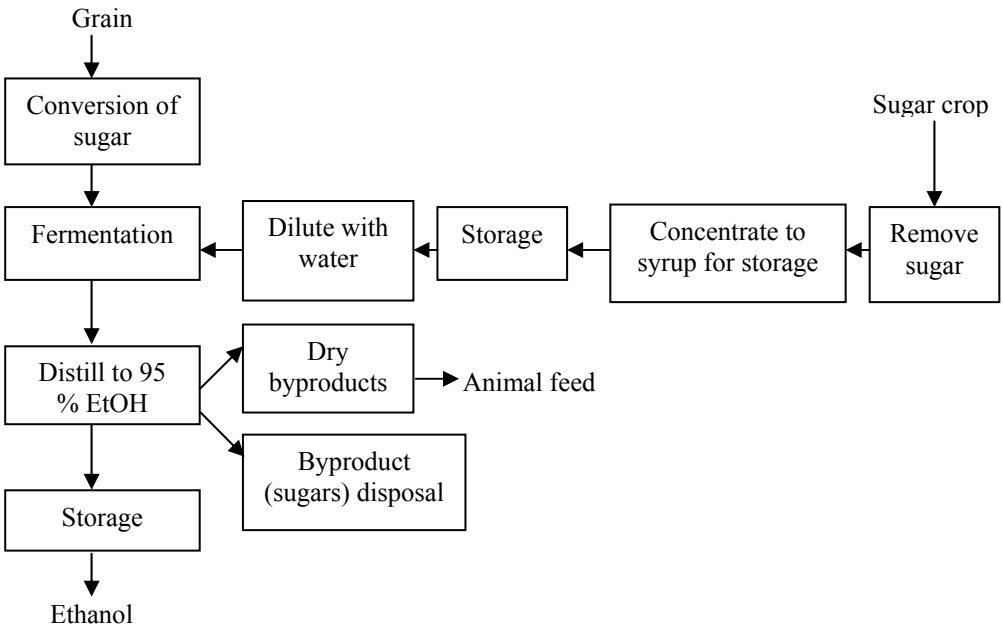

Figure 2.12 Synthesis of ethanol from grains and sugar crops [Lee, 2007]

2.2.1.3 Thermo-chemical processes

Combustion

The burning of biomass in air, i.e. combustion, is used over a wide range of outputs to convert the chemical energy stored in biomass into heat, mechanical power, or electricity using various items of process equipment, e.g. stoves, furnaces, boilers, steam turbines, turbo generators, etc. Combustion of biomass produces hot gases at temperatures around 800-1000 ^{o}C. It is possible to burn any type of biomass but in practice combustion is feasible only for biomass with a moisture content <50%, unless the biomass is pre-dried. High moisture content biomass is better suited to biological conversion processes.
The scale of combustion plant ranges from very small scale (e.g. for domestic heating) up to large-scale industrial plants in the range 100-3000 MWe. Net bio-energy conversion efficiencies for biomass combustion power plants range from 20% to 40%. The higher

efficiencies are obtained with systems over 100 MWe or when the biomass is co-combusted in coal-fired power plants (McKendry 2002).

Gasification

Gasification is the conversion of biomass into a combustible gas mixture by the partial oxidation of biomass at high temperatures, typically in the range 800-900 ^{o}C. The low calorific value (CV) gas produced (about 4-6 MJ/Nm^{3}) can be burnt directly or used as a fuel for gas engines and gas turbines. The product gas can be used as a feedstock (syngas) in the production of chemicals (e.g. methanol).
One promising concept is the biomass integrated gasification/combined cycle (BIG/CC), where gas turbines convert the gaseous fuel to electricity with a high overall conversion efficiency. The integration of gasification and combustion /heat recovery ensures a high conversion efficiency, producing net efficiencies of 40-50% (based on the lower heating value of the incoming gas for a plant of 30-60 MWe capacity. The production of syngas from biomass allows the production of methanol and hydrogen, each of which may have a future as fuels for transportation (McKendry 2002).

Pyrolysis

Pyrolysis is the conversion of biomass to liquid (termed bio-oil or bio-crude), solid and gaseous fractions, by heating the biomass in the absence of air to around 500 ^{o}C. Pyrolysis can be used to produce predominantly bio-oil if flash pyrolysis is used, enabling the conversion of biomass to bio-crude. The bio-oil can be used in engines and turbines and its use as feedstock for refineries is also being considered. Problems with the conversion process and subsequent use of the oil, such as its poor thermal stability and its corrosivity, still need to be overcome. Upgrading bio-oils by lowering the oxygen content and removing alkalis by means of hydrogenation and catalytic cracking of the oil may be required for certain applications.

2.3 Hydrothermal liquefaction

Conversion of wet biomass is often referred to as hydrothermal liquefaction. Hydrothermal liquefaction is generally carried out at 280 to 370 ^{o}C and between 10 and 25 MPa. At these conditions water is in a liquid state. The phase diagram of water can be seen in Fig. 2.13. In hydrothermal liquefaction, water is an important reactant and catalyst, and thus the biomass can be directly converted without an energy consuming drying step, such as in the case of flash pyrolysis (Bridgwater *et al.* 1999). The main products are bio-crude with a relatively high heating value, char, water-soluble substances and gas. Addition of various alkaline catalysts can suppress the char formation and thus improve the oil yield and quality. As the temperature is increased above the critical limit, gasification becomes the dominating process.

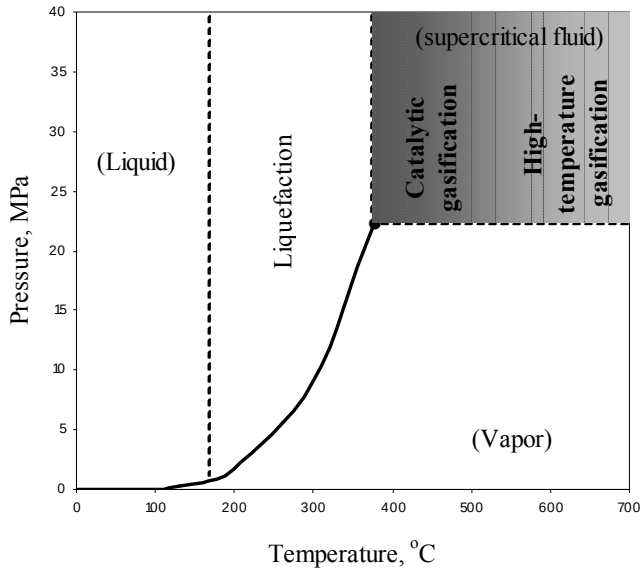

Figure 2.13 The phase diagram of water Peterson et al. 2008

Due to the severe process conditions, industrial application of these processes suffers from various challenges. Corrosion requires the use of expensive alloys and the high operation pressures put tough requirements on process components such as feed pumps. Most work on hydrothermal liquefaction has so far been carried out in lab- or bench-

scale, especially high investment costs is a considerable hurdle for commercialization. Nevertheless, a few pilot /demonstration processes do exist such as; HTU® (hydrothermal upgrading), LBL (Lawrence Berkeley Laboratory), CatLiq® (Catalytic Liquefaction) and the TDP process (Thermal Depolymerization) (Bridgwater 2001; Bouvier *et al.* 1988; Changing World Technologies, Inc.). The SlurrCarb™ process is a similar technique; however, the main product is a solid carbonaceous fuel (Kevin 2001). Other liquefaction processes, such as the PERC-process have utilized organic solvents instead of water (Bouvier *et al.* 1988).

In addition to hydrothermal liquefaction, a range of other hydrothermal conversion processes exist, however they usually are carried out at higher pressures and temperatures. Supercritical water oxidation (SCWO) utilizes temperatures above the critical temperature of water (374 ^{o}C) and oxidative conditions to produce thermal energy and a CO_2 rich gas phase (Cocero *et al.* 2002). The SCWO process has mainly been applied on industrial waste water and sludges. The major disadvantages with the SCWO process are salt precipitation, which occurs extensively at such high temperatures and corrosion due to high temperatures and oxidative conditions (Kritzer and Dinjus 2001). The SCWO process was extensively reviewed by (Bermejo and Cocero 2006a). Another hydrothermal process is SCWG (supercritical water gasification). Here the biomass is gasified to mainly CO_2, H_2, and CH_4 under supercritical but not oxidative conditions. Gasification of biomass in the presence of water has been extensively reviewed by (Matsumura *et al.* 2005). In temperatures up to 500 ^{o}C, effective reforming and gasification generally requires heterogeneous catalytic enhancement to achieve reasonable rates and selectivity (Peterson *et al.* 2008). At temperatures above 500 ^{o}C, homogeneous gasification is possible.

2.3.1 Properties of water

In hydrothermal liquefaction water is an active component as solvent, reactant and catalyst, and this make the process significantly different from pyrolysis. At conditions close to the critical point, water has several very interesting properties. Among them are low viscosity and high solubility of organic substances, which make sub and supercritical water an excellent medium for fast, homogeneous and efficient

reactions. (Franck 1968; Heger *et al.* 1980; Marshall and Franck 1981; Franck 1983; Franck and Weingärtner 1999; Kruse and Dinjus 2007a). Therefore, during the last decades, there have been strong research interests in using sub and super-critical water as a solvent and reaction medium for biomass conversion. Table 2.3 lists some properties of sub- and supercritical water (Bröll *et al.* 1999; Krammer and Vogel 2000; Kruse and Dinjus 2007a).

Table 2.3 Properties of water under various conditions Bröll *et al.* 1999; Krammer and Vogel 2000

	Ordinary Water T<150 ^{0}C P<0.4 MPa	**Subcritical water 150 ^{o}C < T <350 ^{o}C 0.4< P <20 MPa**		**Supercritical water T>370 ^{0}C**	
		5 MPa	**25 MPa**	**25 MPa**	**50 MPa**
Temp. (^{o}C)	25	250	350	400	400
Pressure, (MPa)	0.1	5	25	25	50
Density, ρ (g cm^{-3})	1	0.80	0.6	0.17	0.58
Dielectric constant, ϵ (Fm^{-1})	78.5	27.1	14.07	5.9	10.5
Ionic product, IP (K_w)	14.0	11.2	12	19.4	11.9
Heat capacity Cp (kJ kg^{-1} K^{-1})	4.22	4.86	10.1	13.0	6.8
Dynamic viscosity η (mPas)	0.89	0.11	0.064	0.03	0.07

Subcritical water has several properties that differ from those of water at room temperature as shown in Table 2.3. The dielectric constant decreases from 78 Fm^{-1}at 25 ^{o}C to 14.07 Fm^{-1}at 350 ^{o}C (Uematsu and Franck 1980). This decrease in dielectric constant gives rise to increase solubility otherwise hydrophobic organic compounds, for example free fatty acids are insoluble in water (Holliday *et al.* 1997; King *et al.* 1999). On the other hand the solubility of salts decreases. At supercritical conditions salts are almost insoluble, at subcritical conditions the solubility of most salts are much lower than at room temperature, however there are some important variations between different salts. So-called Type 1 salts such as NaCl still exhibit high solubility at subcritical conditions, whereas so-called Type 2 salts such as Na_2SO_4 have low solubility at these conditions (Hodes *et al.* 2004).
The low solubility might cause the formation of fine-crystalline, slimy "shock precipitate". The precipitating salts easily attaches to the walls of process components such as heat exchangers and reactor and thereby

causes fouling or even blockage. (Kritzer and Dinjus 2001; Marrone *et al.* 2004).

The ionic product of water (K_W) is relatively high in the subcritical range (10^{-12} compared to 10^{-14} at ambient conditions). The high levels of H^+ and OH^- at subcritical conditions means that many acid- or base catalyzed reactions, such as biomass hydrolysis, are accelerated. (Akiya and Savage 2002; Hunter *et al.* 2004).

The density of subcritical water is significantly lower than at ambient conditions but at the same time higher than at supercritical conditions. The compressibility is also lower than at supercritical conditions. The relatively high density combined with the high dissociation constant of subcritical water, favors ionic reactions, whereas at supercritical conditions with low densities radical reaction dominates. At subcritical conditions hot compressed water supports water eliminations from carbohydrates and alcohols and other reactions such as aldol splitting is enhanced by the special properties of subcritical water. Radical reactions at supercritical conditions first of all results in gas formation. (Kruse and Dinjus 2007b; Osada *et al.* 2006).

Although the properties of sub/supercritical water in many aspects are favorable, this also causes problems and limitations. Corrosion in the sub/supercritical water environment is a critical issue. In particular acid and oxidizing conditions can cause rapid corrosion. The corrosion can even be more severe at subcritical conditions than supercritical conditions due to the relatively dense and polar character of supercritical water. Main forms of corrosion are pitting corrosion, general corrosion, intercrystalline corrosion and stress corrosion cracking (Kritzer 2004). Pitting corrosion is a localized form of corrosion occurring in the passive state of the metal. High temperatures weaken the protective oxide film, and thus, pitting occurs much easier at high temperatures. In contrast to pitting corrosion, general corrosion attacks the entire surface of the metal. During the intercrystalline corrosion, either the grain boundaries or neighboring grain areas might be attacked. Stress cracking corrosion is an extremely dangerous form of corrosion and is observed along the grain boundaries or through the grains (Kritzer 2004). Several materials have been tested at these conditions, however only a few do have sufficient corrosion resistance. The most widely used in sub and supcritical applications are Ni alloys such as Inconel 625 and Hasteloy C-276. Furthermore, titanium alloys also have good resistance; however their mechanical strength is limited (Bermejo and Cocero 2006b; Kritzer and Dinjus 2001; Bröll *et al.* 1999).

As mentioned salt precipitation due to the unpolar properties of the water solvent poses a problem at conditions close to or above the critical point of water. Several approaches have been evaluated to alleviate the problem, among them on-line salt separation through specially designed separators and reactors (Schubert *et al.* 2010; Kritzer and Dinjus 2001; Marrone *et al.* 2004). One example is the transpiring wall reactor a modified reactor concept e.g. transpiring with an inner porous pipe, which is rinsed with water to prevent salt deposits at the wall (Bermejo and Cocero 2006b; Ahluwalia 1996, 1997). Dell'Orco et al (Dell'Orco *et al.* 1993) studied the used of hydrocyclons to eliminate particles with a known size distribution, under sub- and supercritical conditions. These devices proved to be effective in the elimination of particles of microscopic size and their efficiency is increased with temperature.
Another solution to avoid salt precipitation inside the reactor is to reduce the quantity of salt present in the feed. This can be achieved using solid-fluid separation methods. However, if the inorganic matter is bound the biomass matrix this cannot be easily carried out (Kritzer and Dinjus 2001).

Table 2.4 Corrosion resistance of nickel-based alloys & titanium against different media [Kritzer and Dinjus, 2001]

	$T<T_c$; high density		**$T>T_c$; low density**	
	Good resistance resistance	**Poor**	**Good resistance**	**Poor resistance**
Nickel-based alloys	H_3PO_4, HF	HCl, HBr	All acids	$[H_3PO_4]>0.1$mol/kg
	Alkaline solutions	H_2SO_4, HNO_3	-	NaOH
Titanium	All acids	F^{-1}	HCl	H_2SO_4, H_3PO_4

2.3.2 Reaction pathways for liquefaction

Biomass is a broad definition and includes a wide range of materials with varying compositions. The main biomass components are: carbohydrates, lignin, protein and lipids. The degradation pattern of these components in sub and supercritical water differs; however, the basic mechanisms can be described as (Demirbas 2000; Chornet and Overend 1985; Peterson *et al.* 2008):

- Hydrolysis of the biomass
- Depolymerization of the main components
- Chemical and thermal defragmentation, dehydration, decarboxylisation and deammination.
- Recombination of reactive fragments.

The degradation pattern for the different biomass components differs widely and so does the product.

2.3.3 Conversion of carbohydrates

The most abundant carbohydrates in biomass are the polysaccharides cellulose, hemicelluloses and starch. Under hydrothermal conditions carbohydrates undergo hydrolysis to form glucose and other monosaccharides. The hydrolysis is acid-catalyzed and the rate of hydrolysis varies between different carbohydrates. Hemicelluloses and starch are hydrolyzed much faster than cellulose, which to a large extent has a crystalline structure. The degradation of carbohydrates in sub and supercritical water has been thoroughly reviewed by several authors (Yu *et al.* 2008; Behrendt *et al.* 2008; Bobleter 1994).
Several attempts to describe a general degradation mechanism have been made. The models vary in detail however the over-all pattern is similar (Figure 2.14).
At supercritical conditions, the main products are gaseous ones, which are formed via defragmentation segments. At subcritical conditions the degradation of glucose proceeds via both isomerization to fructose, dehydration and defragmentation. Furans, defragmentation products and phenols are major products; however the distribution is dependent on pH and temperature. Glucose reversibly isomerizes into fructose via the LBAE (Lobry de Bruyn, Alberda van Ekenstein) transformation (Peterson *et al.* 2008; Antal and Mok 1990). The LBAE transformation has been well-studied and proof of its occurrence is supported well by deuterium exchange reactions of glucose (Speck, 1953).

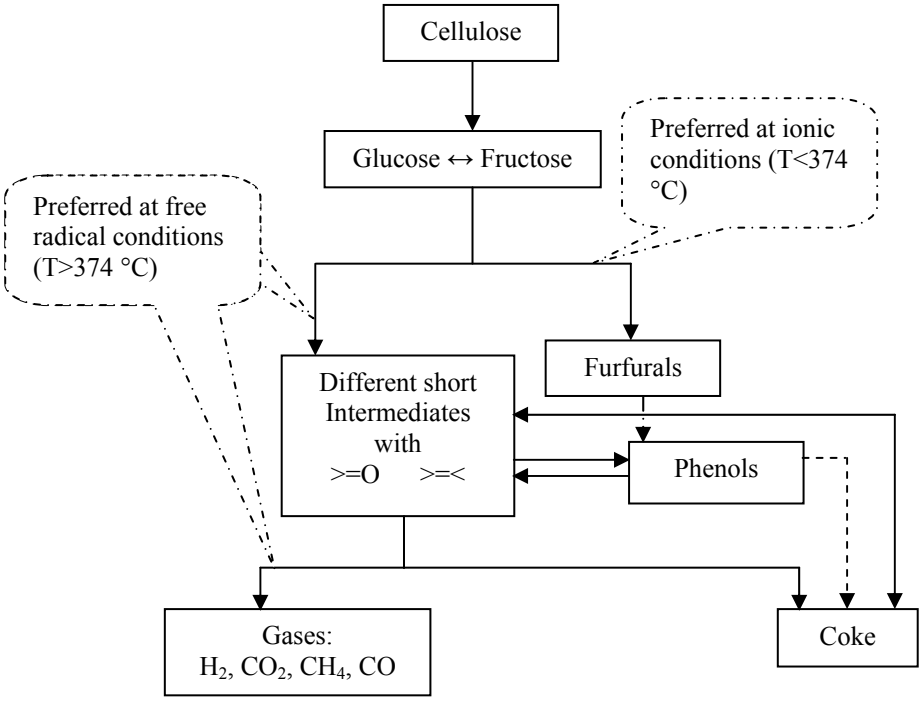

Figure 2.14 A simplified reaction mechanism for biomass degradation at supercritical conditions Kruse et al. 2007c; Kruse and Gawlik, 2003

Watanabe (Watanabe *et al.* 2005b) studied the effect of reaction conditions and additives on glucose and fructose reactions with 5 min. residence time (Figure 2.15). The primary reactions of glucose were found to be as follows: (1) glucose isomerization into fructose via keto-enol tautomerization, (2) glucose dehydration into 1, 6-anhydroglucose, and (3) glucose decomposition into aldehyde and ketone via retro-aldol condensation. Further, (4) dehydration of tautomerization intermediate and fructose produce 5-HMF.

It has been shown that the contribution of retro-aldol condensation is predominant at higher temperatures (400-500 ^{o}C), whereas that of the dehydration reaction is significant at lower temperatures (250-350 ^{o}C) (Yang and Montgomery 1996; Kabyemela *et al.* 1997b; Moreau *et al.* 2000; Sasaki *et al.* 2002; Watanabe *et al.* 2005b).

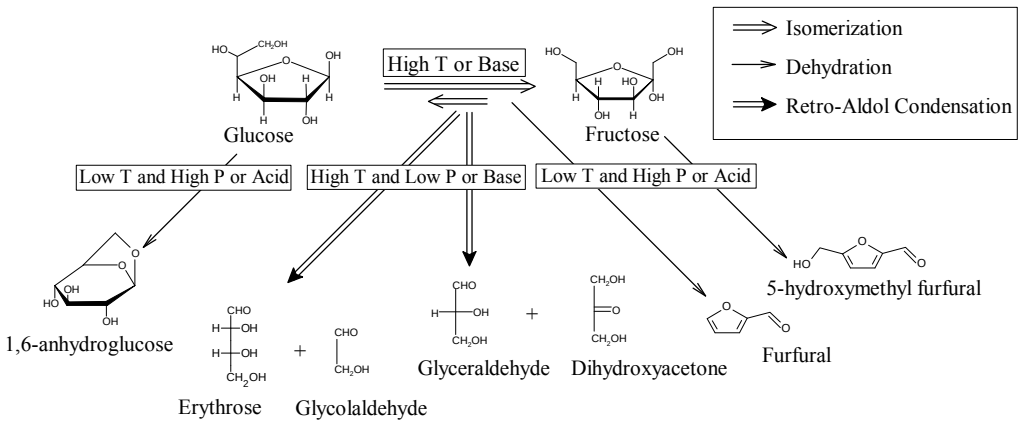

Figure 2.15 Effect of reaction conditions and additives on glucose and fructose reactions Watanabe et al. 2005b

The formation of aromatic compounds during hydrothermal treatment of glucose has been reported.

Luijkx (Luijkx *et al.* 1993) reported that the aromatic compound 1, 2, 4-benzenetriol could be formed in significant yields from the glucose degradation product, 5-HMF at 27.5 MPa and 290-400 ^{o}C. At neutral conditions, a yield of 46% was attained. The addition of HCl (0.01M) also resulted in complete HMF conversion at 330 ^{o}C with residence time ranging from 1-5 min. Under these conditions, the normal product of HMF degradation was 4-oxopentanoic acid but formation of 1, 2, 4-benzenetriol was still substantial.

Table 2.5 summarizes research performed with biomass and model compounds.

Table 2.5 Summary of conversion of biomass and model compound

Substrate	Conditions	Compounds	Reference
Glucose	300-400 ^{o}C 25-40 Mpa 0.02-2s (neutral pH)	Fructose Dihydroxyacetone Glyceraldehyde Erythrose Glycolaldehyde Pyruvaldehyde 1,6 anhydroglucose Acetic, formic acid 5-HMF	(Kabyemela *et al.* 1997a; Kabyemela *et al.* 1997b) Kabyemela *et al.* 1999;
D-glucose and other monosaccharides	340 ^{o}C 27.5 Mpa 25-204s (acid and base catalyzed)	5-HMF Glycolaldehyde Glyceraldehyde formic acid, acetic acid, lactic acid, acrylic acid, 2-furaldehyde 1, 2, 4-benzenetriol	(Srokol *et al.* 2004)
D-fructose	200-320 ^{o}C 120s pH range (1.5-5)	5-HMF Formic acid Levulinic acid	(Asghari and Yoshida 2006)
Microcrystalline cellulose	320-400 ^{o}C 25MPa 0.05-10.0s (neutral pH)	1, 6-anhydroglucose Erythrose Glycolaldehyde Glyceraldehyde Pyruvaldehyde Dihydroxyacetone Furfural 5-HMF	(Sasaki *et al.* 2000)
5-HMF	290-400 ^{o}C 27.5 MPa 0.107-0.308min^{-1}	1,2,4-benzenetriol 4-oxopentanoic acid (330 ^{o}C, 1-5 min., acidic media)	(Luijkx *et al.* 1993)
Cellulose	250-407 ^{o}C Alkaline environment	o-,m-or p-Xylene Ethylbenzene n-Propylbenzene 1 -Methyl-2-ethylbenzene 1 -Methyl-3-ethylbenzene Phenol o-, m-,p-Cresol 2-Phenoxyethanol	(Russell *et al.* 1983)

Russell (Russell *et al.* 1983) detected many aromatic compounds from the oily product obtained after liquefaction of cellulose with aqueous Na_2CO_3 at 250-470 ^oC. The most abundant were substituted benzenes, phenols and cresols. They proposed that, under liquefaction conditions, the cellulose degrades to low molecular weight aldehydes and ketones, as been previously mentioned for glucose. These aldehydes and ketones may then form aromatic compounds by condensation and dehydration.

2.3.4 Conversion of lignin

Lignin is together with cellulose and hemicellulose major part of plant materials. It is an aromatic heteropolymer consisting of p-hydroxyphenylpropanoid units held together by C-C or C-O-C bonds. The three basic building blocks are trans-p-coumaryl alcohol, coniferyl alcohol and sinapyl alcohol. Lignin is relatively resistant to chemical or enzymatic degradation (Bobleter 1994). During hydrothermal degradation various phenol derivates are formed by hydrolysis of ether-bonds. The lignin hydrolysis is catalyzed by alkaline pH.
Hydrothermal treatment process of Kraft pine and organosolv lignin was conducted at 374 ^oC and 22MPa for 10 min. The liquid yields were between 57.8 and 79.1 % and the solid residue yields were between 12.1 and 37.6%. The product profile differed between the two substrates, but in general the major lignin hydrolysis products were: guaiacol, 4-ethylguaiacol, 4-ethyl phenol and 2-Methoxy-4-propy-phenol (Zhang *et al.* 2008).
Liu *et al* (Liu *et al.* 2006) studied hydrothermal processing of walnut shell by both acid- (HCl) and base-catalyzed (KOH, Na_2CO_3) at reaction temperature of (200-300 ^oC), corresponding to a pressure range of (1.5-8.6 MPa) for 1h. Several phenol derivates such as 2-methoxy phenol, 3, 4-dimethoxy phenol and 1, 2-benzenediol most likely were produced by base-catalyzed lignin hydrolysis followed by hydrolysis of methoxy groups.
Karagöz *et al* (Karagöz *et al.* 2005b) also obtained phenolic compounds (2-methoxy phenol, 1, 2-benzenediol, 4-methyl-1,2-benzenediol, 3-methyl-1,2-benzenediol and phenol) from hydrothermal treatment (280 ^oC for 15 min.) of lignin.

2.3.5 Conversion of lipids

Fats and oils are non-polar compounds with mainly aliphatic character, which are insoluble in water at normal conditions. As shown in Table. 2.3, the dielectric constant of water decreases drastically under subcritical and supercritical conditions, allowing greater miscibility. (Peterson *et al.* 2008; Khuwijitjaru *et al.* 2002).
Fats and oils in biological systems are typically in the form of triacylglycerides (TAGs), which consist of three fatty acids bound to a glycerol backbone. Hot compressed water is one of the candidates for treating the fats/oils to produce long chain hydrocarbons because of its capability to hydrolyze TAGs into free fatty acid and glycerol without catalyst. On the other hand, free fatty acids are relatively stable in subcritical water (Holliday *et al.* 1997; King *et al.* 1999). A higher rapid hydrolysis of soybean oil was achieved in liquid water, at temperatures of 330 to 340 ^{o}C, P = 13.1 MPa, and water-to-oil ratios of 2.5 to 5.0 : 1, giving 90 to 100% yields of free fatty acids in 10 to 15 minutes. Using an optically accessible reactor, the phase behavior was found to be extremely important. King *et al* noted that the reaction quickly went to completion when the mixture became a single phase at 339 ^{o}C (King *et al.* 1999).

Fatty acids

Fatty acids can be degraded in hydrothermal systems to produce long-chained hydrocarbons. The reaction is however slow at subcritical conditions. Stearic acid ($C_{17}H_{35}COOH$) was decomposed at temperature of 400 ^{o}C and pressure of 25 MPa in a batch reactor at a fixed density of 0.17 gcm^{-3} for 30 min. At uncatalyzed conditions the alkane yield was only a few percent. However, addition of KOH accelerated the decomposition and a yield of 32% was achieved. At alkaline conditions, the major decomposition mechanism was decarboxylization of the fatty acid producing the corresponding alkane. The reaction in a hydrothermal system was compared to pyrolysis of water-free stearic acid. Degradation tests were also carried out at water-free conditions and this revealed that supercritical water stabilized the fatty acid and suppressed the degradation (Watanabe *et al.* 2006).

2.3.6 Conversion of proteins

Proteins are a major biomass component in particular in animal, plant and microbial biomass. Proteins are made up from one or several peptide-chains. The smallest buildings-blocks are the amino acids. The structural bond that links amino acids together into protein is the peptide bond, which is an amide bond between carboxyl and amine groups of the amino acids. Hydrolysis rates of various biopolymers, strongly depend on the type of bond. Peptide bonds in the proteins are much more stable than the glycosidic bonds in cellulose and starch, and only slow hydrolysis occurs below 230 ^{o}C (Brunner 2009; Rogalinski *et al.* 2008). In addition, yields of amino acids are generally significantly lower than by conventional acid hydrolysis since the degradation rate of amino acids at hydrothermal conditions is much higher than for example glucose (Peterson *et al.* 2008).

Some researchers have reported ways to enhance hydrolysis yields. Rogalinski *et al* (Rogalinski *et al.* 2008) reported that the yield of amino acids quadrupled with the addition of CO_2 due to acceleration of acid hydrolyzed catalysis steps: at 250 ^{o}C, 25MPa and 300 s residence time total amino acid yield increased from 3.7 to 15 wt%. It was also observed that the catalytic influence of carbon dioxide decreases with increasing temperature. Xian *et al* (Xian *et al.* 2008) investigated the hydrolysis and reaction kinetics for amino acids production from fish proteins in subcritical water reactor without catalyst at 180-320 ^{o}C, 5-26 MPa and residence time from 5-60 min. It was found that the hydrolysis rate increased five-fold between 220 and 260 ^{o}C. Another phenomenon described was that the stability of the various amino acids differed markedly and that both process temperature as well as process gas had an influence. Rogalinski *et al* (Rogalinski *et al.* 2005) observed production of amino acids from bovine serum albumin (BSA) by continuous subcritical water hydrolysis. The highest amino acid yield in subcritical water was obtained at 290 ^{o}C and 65s. For a residence time of 30s the optimum temperature was found to be 310 ^{o}C and yield was 32 mg/g BSA.

Amino acids

The monomeric components of proteins are amino acids. All 21 different amino acids contain an amine group, a carboxylic acid group and a side chain. The side chains vary significantly between different amino acids, there hydrophilic, hydrophobic, aromatic, charged ones etc. Due to the differences in the chemical structure the individual amino acids have somewhat different degradation patterns. However, all amino acids have the same peptide backbone, and undergo similar decarboxylation and deamination reactions resulting mainly in hydrocarbons, amines, aldehydes and acids (Peterson *et al.* 2008).
Klinger (Klinger *et al.* 2007) recently studied glycine and alanine, two of the simplest amino acids. Similarly, they found that the primary mechanisms of degradation of these amino acids to be decarboxylation and deamination (Figure 2.16). About 50% of their starting material was degraded in 5-15 s in 350 ^{o}C water at 34 MPa. Klinger found no effect of pressure on the decomposition rate between 24 and 34 MPa at 300- 350 ^{o}C. Major compounds were acetaldehyde, acetaldehyde-hydrate, diketopiperazine, ethylamine, methylamine, formaldehydes, lactic acid and propionic acid. Table 2.6 summarizes research performed with different amino acids.

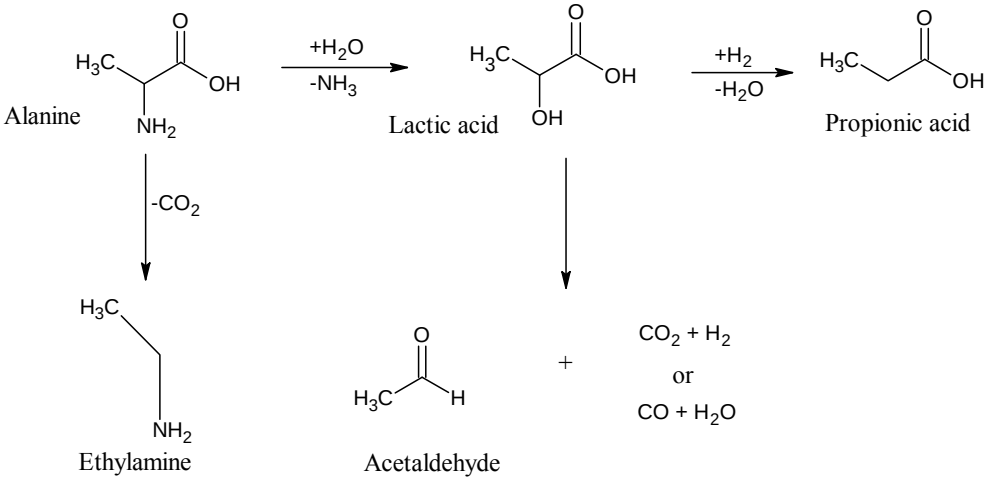

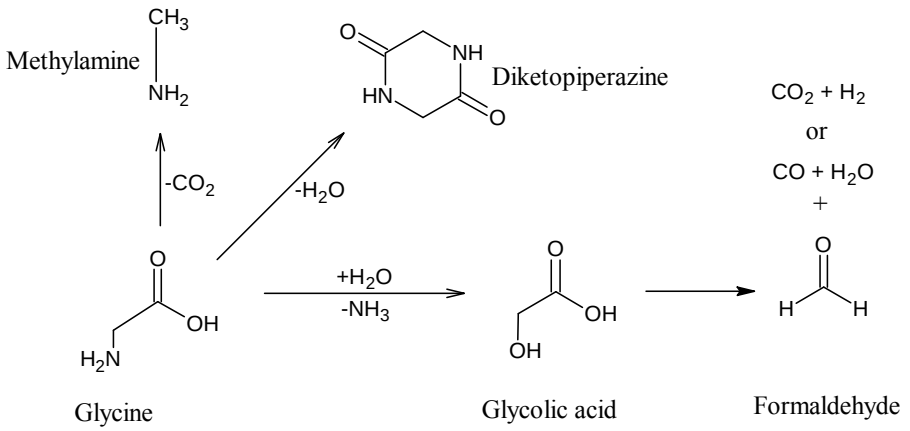

Figure 2.16 Reaction networks of hydrothermal alanine and glycine decomposition
Klinger et al. 2007

Table 2.6 Summary of conversion of amino acids

Substrate	Conditions	Compounds	Reference
Valine, Leucine and Isoleucine	at 220 ^{0}C and above under non-oxidative conditions	NH_3, CO_2 and CO propane, butane, isobutane,isopentane, 3-methyl-1-butene, 2-methyl-1-butene, Propene, butane, isobutylene Acetone, Iso-butylamine	(Lien *et al.* 1974)
glycine and alanine	350 ^{0}C 34 MPa 5-15s	acetaldehyde, acetaldehyde-hydrate diketopiperazine, ethylamine, methylamine, formaldehydes, lactic acid, Propionic acid.	(Klinger *et al.* 2007)
alanine	300 ^{0}C 20 MPa	NH_3, carbonic acid, lactic acid, pyruvic acid, acrylic acid, acetic acid, propionic acid, formic acid	(Sato *et al.* 2004)
bovine serum albumin (BSA)	310 ^{o}C 25 MPa 30s	CO_2, CO, H_2, and CH_4 acetic acid, propanoic acid, n-butyric acid, iso-butyric acid, Iso-valeric acid	(Rogalinski *et al.* 2005)

During hydrolysis of biomass both amino acids and sugars are formed and these can react via the so-called Maillard reaction (Fig. 2.17). These types of reactions lead to the formation of nitrogen containing cyclic organic compounds, which are more or less strong free radical scavengers and inhibit free radical chain reactions that are highly relevant for gas formation (Kruse *et al.* 2007c).

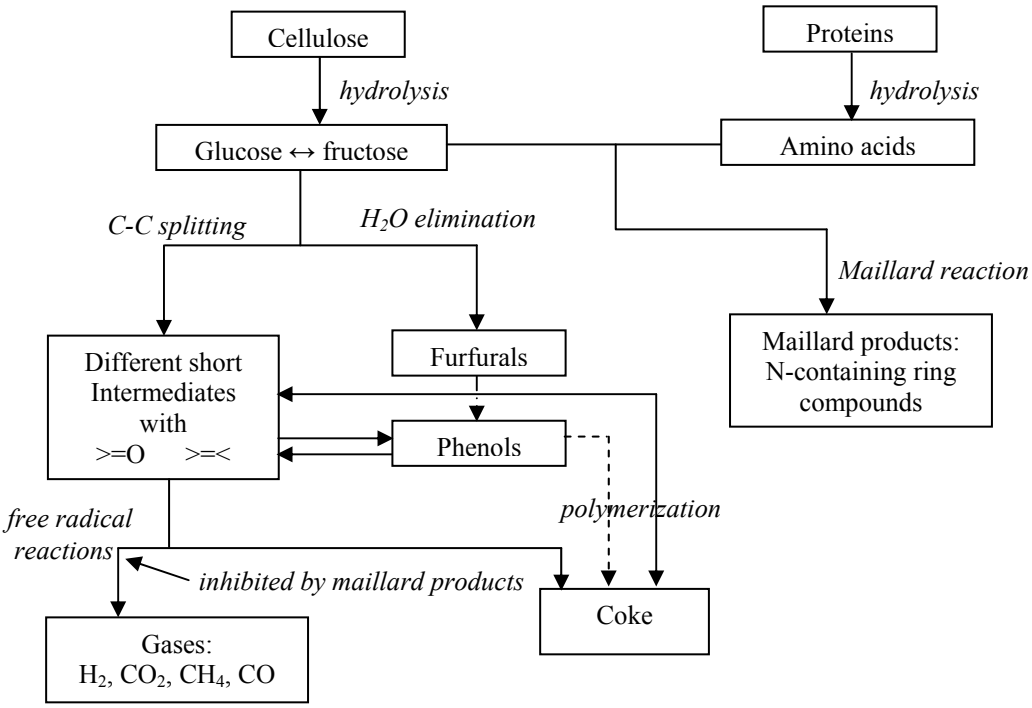

Figure 2.17 Reaction pathways of hydrothermal biomass degradation in the presence of proteins Kruse et al. 2007c

2.3.7 Effect of catalysts

Catalysts are important in hydrothermal liquefaction processes and are used for improving gasification efficiency, suppress tar and char formation etc. Homogeneous catalysts in forms of alkali salts have been frequently used, whereas heterogeneous catalysts such as various form for Ni-catalysts has been less frequently utilized in hydrothermal

liquefaction. On the other hand, heterogeneous catalysts are widely used in low-temperature water gasification of biomass.

Homogeneous catalysts

It is well-known that the addition of alkali salts has a positive influence on hydrothermal processes. It improves gasification, accelerates the water-gas shift, suppresses tar and char formation and increases liquid yields. It was reported that the addition of alkali promoted the yield of fructose and inhibited the yield of anhydrous glucose (AHG) by isomerization reaction of glucose, whereas the addition of acid promoted the dehydration reaction of glucose by providing anhydrous glucose and hydroxymethyl furfural (HMF) (Watanabe *et al.* 2005a; Yang and Montgomery 1996; Mok *et al.* 1992; Watanabe *et al.* 2003).
Song (Song *et al.* 2004) investigated the effect of Na_2CO_3 on the liquefaction of corn stalk and concluded that the catalyst has a positive effect on the liquefaction process and can increase the yield of liquid products, as well as increase the quality of liquid product. With a catalyst, more bio-oil and less gas could be obtained than without using a catalyst. The catalyst mainly improved the yield of bio-oil, from 33.4% without a catalyst, increasing to 47.2% with 1.0 wt% of Na_2CO_3. Alkali also favors the so-called water gas shift and thus favors H_2 and CO_2 formation at the expense of CO.
Karagöze (Karagöze *et al.* 2006; Karagöze *et al.* 2005a) performed catalytic hydrothermal treatment of wood biomass at 280 ^oC for 15 min. in the presence of K_2CO_3 with different concentration. They found that the concentrations of base solutions have an important effect on the degradation of wood biomass in terms of both oil yield and conversion. Their study showed that the use of alkali catalyst during the hydrothermal treatment of biomass inhibits the char formation, and subsequent increase in oil yields. They concluded that the concentration of base solutions has an important effect on the inhibition of char (solid residue) formation. Decreasing the concentration of base solutions decreased the water-soluble hydrocarbons (WSH). They concluded that alkaline salts are more effective than the hydroxides and ranked the order of catalysts activity as follows: $K_2CO_3 > KOH > Na_2CO_3 > NaOH$. This may come from one possible reason, which is alkaline salts react with water and form their bases and bicarbonates and act as secondary catalyst.

Minowa (Minowa *et al.* 1998) tested the catalytic action of Na_2CO_3 during hydrothermal conversion of cellulose. Above 300°C the catalyst decreased secondary tar formation from the oil product and catalyzed the gasification of the aqueous organics. Watanabe (Watanabe *et al.* 2006) enhanced the conversion of C_{17}-acid (fatty acid) decomposition from 2% to 32 % with the addition of KOH catalyst by promoting the decarboxylation of C_{17}-acid.

Heterogeneous catalysts

Heterogeneous catalysts have so far mostly been used in gasification processes, where they are reported to have a significant positive effect on low-temperature processes. In hydrothermal liquefaction, where the main purpose is to produce liquid products, though, the number of studies is limited. Watanabe and co-workers (Watanabe *et al.* 2002) studied the influence of heterogeneous acid and base additives, such as metal oxides, on the glucose reactions. They found that the addition of ZrO_2 also promotes isomerization of glucose and fructose, and thus, ZrO_2 can be considered to be a base catalyst for glucose.
Minowa (Minowa and Ogi 1998b; Minowa *et al.* 1998c; Minowa and Inoue 1999) conducted gasification of cellulose over nickel, palladium, and platinum catalysts with a batch-type reactor at reaction conditions 350 ^{o}C, 25 MPa, and 10 to 180 min reaction time. They reported that methane and carbon dioxide were mainly produced over supported nickel catalysts, whereas hydrogen and carbon dioxide were obtained over supported palladium and platinum catalysts.
Elliott (Elliott *et al.* 1993, 1994a, 1994b) examined the activities of supported ruthenium and nickel catalysts for the gasification with a bench-scale flow type reactor at 350 ^{0}C and 21 MPa. Various wastewaters such as manure grain and brewer's spent grain were completely gasified to methane and carbon dioxide. They also reported that ruthenium was more stable catalyst than nickel at these conditions.
Watanabe (Watanabe *et al.* 2006) studied effect of metal oxide (ZrO_2) on stearic acid ($C_{17}H_{35}COOH$) decomposition at 400 ^{o}C and 25 MPa for 30 min. They observed metal oxide (ZrO_2) enhanced the decarboxylation of C_{17}-acid and the main products were CO_2 and C_{16} alkene.
Various other heterogeneous catalysts have been tested in hydrothermal conversion processes; however the main focus has been to improve

gasification, not the liquid yields. Examples of these catalysts are Ni/Al_2O_3, Ru/TiO_2 and ZrO_2. Catalysis of gasification at conditions below 400 ^oC was extensively reviewed by (Peterson *et al.* 2008).

2.3.8 Hydrothermal liquefaction of various biomasses

A large amount of studies on hydrothermal liquefaction on various biomasses have been carried out. In general an oily phase, aqueous organics and a CO_2 rich gas phase are formed. However, the yields, oil characteristics and char formation varies widely between different biomasses. In general the energy density in these oils is 30-37 MJ/kg i.e. almost 50% higher than in the biomass itself (Peterson *et al.* 2008).
Waste materials from the fishing industry and slaughter houses are rich in protein and triglycerides can be converted into water-insoluble bio-oils. Yoshida *et al* (Yoshida *et al.* 1999) liquefied raw fish meat under subcritical conditions. Aqueous phase and solids were formed as the reaction products at 200 ^oC (1.52 MPa) in 5 min. Amino acids such as cystine, alanine, glycine, and leucine were produced at the optimum conditions of 270 ^oC (5.51 MPa). At 300 ^oC (8.4 MPa), the amount of solids decreased, and water-insoluble phase was formed above the aqueous phase. This water-insoluble phase contains oil and fat-like solids, and the oil with 0.922 g/cm^3 density could be extracted with hexane. When the temperature was further increased to 350 ^oC (16.1 MPa), the solids disappeared, and the amount of water-insoluble phase decreased. This behavior can be explained as follows; the solids formed at low temperature were unconverted substrate and the water-insoluble phase was produced from a part of the solids as the reaction temperature increased. At higher temperature, the water-insoluble phase was increasingly degraded to other organic compounds. Their preliminary analysis with GC/MS showed that the oil extracted with hexane contains useful fatty acids such as arachidonic acid, eicosapentanoic acid (EPA), and docosahexianoic acid (DHA). The total organic carbon (TOC) of the aqueous phase increased from 0.2 at 200 ^oC and reached 0.58 above 300 ^oC, indicating that about 60% of the organic carbon in the raw fish meat was recovered in the aqueous phase. Organic acids produced in the aqueous phase were lactic acid, pyroglutamic acid, phosphoric acid, and acetic acid. Formation of gaseous products such as CO_2 and NH_3 was not significant under the employed reaction conditions.

Cellulose and lignin rich materials represent a large pool of abundant and cheap raw materials. These include not only wood products but also household and agricultural wastes. At the University of Illinois, He and co-workers (He *et al.* 2000) have worked to convert swine manure into oil via conversion at temperatures of 275-350 ^{o}C and pressures of 5.5-18 MPa. Carbon monoxide was used as a reducing agent. The process was carried out on a bench scale thermochemical conversion (TCC) reactor operated in a batch mode. Retention time varied from 5 to 180 min. for different operating conditions. The produced oil was found to have heating values of approximately 35 MJ/kg and to be made up of 71% carbon, 14.2% oxygen, 8.9% hydrogen, 4.1% nitrogen, and 0.21 ppm of sulfur. CO_2 was the sole detected gaseous by-product. In another study the liquefaction of garbage was studied (Minowa *et al.* 1995), generally at conditions of 340 ^{o}C, 18 MPa with Na_2CO_3 catalyst and 0.5h residence time. The oil was obtained in the highest yield of 27.6% with heating value of 36 MJ/kg.

In another study on liquefaction of Indonesian biomass residue, heavy oil was produced in the presence of Na_2CO_3 as the catalyst at 300 ^{o}C and around 10MPa in 30 min. The oil yield was between 21-36 wt%, the calorific value around 30MJ/kg and the viscosity>10^5 mPa.s (Minowa *et al.* 1998a).

Karagöz *et al* (Karagöz *et al.* 2005b) conducted hydrothermal liquefaction of wood (saw dust) and non-wood biomass (rice husk), and major biomass components (lignin and cellulose) at 280 ^{o}C for 15 min. Total oil yield was 3.9% from lignin and highest solid residue of 60%. The major hydrocarbons from hydrothermal liquefaction of lignin were 2-methoxy-phenol and 1, 2-benzenediol derivatives. They concluded decomposition of lignin in water (280 ^{o}C, 15 min.) was comparatively less than other samples.

Demirbaş (Demirbaş *et al.* 2005) obtained the highest heavy oil yield of 28% from beech wood at liquefaction temperature around 376 ^{o}C in 25 min. The oil was found to have heating values of approximately 34.9 MJ/kg.

Table 2.7 Summary of conversion of various biomasses

Substrate	Conditions	Compounds	Reference
Raw fish meat	350 °C 16.1 MPa 5 min. Without oxidants	NH_3, CO_2 lactic acid, pyroglutamic acid phosphoric acid, acetic acid citric acid, malic acid sussinic acid formic acid Arachidonic acid Eicosapentanoic acid (EPA) Docosahexianoic acid (DHA)	(Yoshida *et al.* 1999)
Swine manure	275-350 °C 5.5-18 MPa 5 to 180 min.	Raw oil Average yield = 53.8% heating value = 35MJ/kg	(He *et al.* 2000)
Garbage	340 °C , 18 MPa, 0.5 h Na_2CO_3 as catalyst	Oil Highest yield = 27.6% calorific value = 36 MJ/kg	(Minowa et al., 1995)
Indonesian biomass residues	300 °C 10MPa, 30min. Na_2CO_3 as catalyst	Heavy oil yields between 21-36% calorific value = 30MJ/kg	(Minowa *et al.* 1998a)
Saw dust, rice husk lignin and cellulose	280 °C 15 min.	2-methoxy-phenol 4-methyl phenol Hexadecanoic acid Octadecanoic acid 1, 2-benzenediol derivatives	(Karagöz *et al.* 2005b)
Beech wood	376 °C 25 min.	Heavy oil yields =28% heating value = 34.9MJ/kg	(Demirbas *et al.* 2005)

2.3.9 Existing processes

This section contains a brief detail of historic and ongoing approaches to the liquefaction process. Table 2.8 shows an overview of direct liquefaction processes of different biomass materials.

Pioneering liquefaction work was done by Appell and coworkers at the Pittsburgh Energy Research Center in the 1970s, which was later demonstrated at a pilot plant in Albany, Oregon. This process differed from most modern processes in that the high-pressure reaction took

place in an oil-rich phase (anthracene oil), rather than a water-rich phase. In their continuous process wood flour was heated to about 330 to 370 ^{o}C and a pressure of 20 MPa in the presence of ~5 % Na_2CO_3 catalyst and water at a ratio of about 2.8 kg water per kg wood for residence time of 10 to 30 min. They obtained heavy oil with heating value of 34.52 MJ/kg on dry basis. Later on, researchers at Lawrence Berkeley Laboratory pointed out that the high-pressure liquefaction could take place in a water-rich phase, rather than an oil-rich phase, which eliminated the need for recycle but employed subsequent alkaline and acid treatments (Bouvier *et al.* 1988; Stevens 1994). Both processes were demonstrated at the Albany, Oregon facility starting from the late 1970s, but research was halted by the US Department of Energy in the early 1980s as the price of petroleum began to drop and national interests shifted to fuel additives, such as ethanol.

Table 2.8 Overview of direct liquefaction processes

Process Name	**Developer/Supplier of the Process**	**Raw Material**	**Temperature, ^{0}C**	**Pressure, MPa**
PERC-Process	Pittsburg Energy Research Center (USA)	Wood Chips	330-370	20
LBL-Process	Lawrence Berkeley Laboratory (USA)	Wood Chips	330-360	10-24
HTU-Process	Shell Research Institute (NL)	All types of biomass, domestic, agricultural, and industrial residues, wood	300-350	12-18
DoS-Process	HAW (GER)	Lignocellulosic biomass (e.g. wood, straw)	350-500	8.0
CatLiq-Process	SCF Technologies A/S (DK)	DDGS	280-350	22.5-25

The HTU® process has been investigated in 1981-1988 at Shell Laboratory in Amsterdam, as a reaction to the two oil crisis of 1973 and

1980. Due to the commercial circumstances in the late eighties, the research on the promising HTU® technology was discontinued after only a few hundred hours of continuous bench scale operation. On November 1st, 1997, with support from the Dutch Government, a consortium with Shell Netherlands and Stork Engineers & Contractors as the main partners started a R&D program that ran till the end of 2000.
Its purpose was a validated process on pilot plant scale for the generation of data for the reliable design of the first commercial applications. Based on the results of R&D project, including the process design studies, a technical and economic feasibility study was carried out for a first commercial demonstration plant at a scale of 25000 tons biomass (dry basis)/year for the conversion of the wet organic fraction of domestic waste. This feasibility study intends to establish the potential for a first commercial demonstration of the HTU® process.
In the Hydrothermal Upgrading process a number of different biomass (also with high moisture content) can be liquefied under high pressure (Naber and Goudriaan 2005; Feng *et al.* 2004). The biomass is suspended and pumped into the reactor using a high pressure pump. At temperatures of 300 to 350 ^{o}C, pressure between 12 and 18 MPa and a residence time of 5 to 20 min. a bio-crude is produced. The oxygen in the biomass is removed by water and CO_2. The product consists of 45 % bio-crude (wt% of input material, dry and without ash), 25% gas (>90% CO_2), 20% H_2O and 10% dissolved organic materials (e.g. acetic acid, ethanol). Bio-crude is a heavy organic fluid that becomes solid at 80 ^{o}C. The heating value is 30-35 MJ/kg, the H/C ratio is 1:1 and the oxygen content is between 10 to 18%. The thermal efficiency for one variant of this process amounts to 74.9% (theoretically a maximum of 78.6% could be reached) (Behrendt *et al.* 2008).
HAW (Hochschule für Angewandte Wissenschaften Hamburg, Germany) developed the DoS process which is a direct one-step liquefaction process for lignocellulosic biomass (e.g. wood, straw). It works under a pressure of about 8.0 MPa and at temperatures between 350 and 500 ^{o}C. The conversion of hackled and dried biomass is carried out in a bottom phase reactor under high-pressure using hydrogen to produce oil, water, coal and gas. The thermal efficiency of the whole system is around 70% (Behrendt *et al.* 2008).
The Danish company SCF Technologies has developed the CatLiq technology and operates a 20 L/h capacity pilot plant in Copenhagen, Denmark. In the CatLiq® process the organic fraction of DDGS (Dried Distillers Grains with Solubles), is converted to oil in the presence of a

homogeneous (K_2CO_3) and a heterogeneous (Zirconia) catalyst, at subcritical conditions (280-350 ^oC and 22.5-25.0 MPa). The full product consists of a top-phase of bio-oil, a gas-phase mainly consisting of CO_2, a water phase with soluble organic compounds (e.g. ethanol, acetic acid.) and a bottom-phase mainly consisting of inorganic salts.

The CatLiq® process has been demonstrated to be an effective technology for catalytic liquid conversion of DDGS, giving a high yield 34% of bio-crude oil. The oil contained more than 6 times less oxygen than the DDGS and thus the effective heat value was almost double, 35.8 MJ/kg. As much as 73.2% of the energy in the feed was recovered in the oil. Even though the oil is not directly suitable as transportation fuel it may well be used for direct green electricity production, as input for refineries or as marine diesel. The CatLiq® technique offers an alternative use of WDGS and thus flexibility in terms of product spectrum. In addition a CatLiq® process based on WDGS process with optimized energy integration will consume less energy than a drying process for DDGS production, since the CatLiq® process is carried out in the liquid state.

EPA's Water Engineering Research Laboratory, Cincinnati, OH developed a prototype sludge-to-oil reactor system (STORS) capable of processing undigested municipal sewage sludge with 20% solids at a rate of 30L/hr. Approximately 73% of the energy content of the feedstock was recovered as combustible products (oil and char), suitable for use as a boiler fuel. The oil product had a heating value of 80 to 90% that of diesel fuel. Sludge liquefaction occurred rapidly above 265 ^oC. The feedstock conversion was completely achieved at 300 ^oC with nominal 1.5h residence time (Molton *et al.* 1986).

3 PRODUCTION AND EVALUATION OF BIO-OIL FROM DDGS

3.1 Bio-oil production

Most of the thermal processes are not optimal for wet biomass. However, many biomass based materials contain a large fraction of water. To remove the water by evaporation consumes a considerable amount of energy. In hydrothermal liquefaction processes aqueous biomass is directly converted to oil, water soluble substances and gas at subcritical conditions (Srokol *et al.* 2004; Karagöz *et al.* 2006; Elliott *et al.* 1991; Sealock *et al.* 1993; He *et al.* 2000). Most of these processes such as Hydrothermal upgrading (HTU®) operates at pressures and temperatures in the range of 300-350 ^{o}C and 10-20 MPa respectively, and alkaline catalysts such as NaOH, Na_2CO_3, KOH and K_2CO_3 are often added (Zhong *et al.* 2002; Feng *et al.* 2004; Karagöz *et al.* 2005). The CatLiq® process is similar to these processes, but the use of heterogeneous catalyst, as well as several process features, is unique. In particular, the heat-up of the feed to process temperature is carried out within seconds. This rapid heat-up is important to optimize oil yields and prevent tar and coke formation (Zhang *et al.* 2008).
The aim of the current work was to carry out an initial study of the conversion of DDGS to bio oil in the CatLiq pilot plant. It was demonstrated that DDGS could be converted to bio oil with a heat value of 35.8 MJ/kg, comparable to that of gasoline. High oil yield 33.9 % and energy recovery of 73.2 % was obtained.

3.1.1 The CatLiq® process

The Danish company SCF Technologies has developed the CatLiq technology and operates a continuous 20 L/h capacity pilot plant in Copenhagen, Denmark. The study described in this chapter was carried out in the pilot plant. In the CatLiq® process the organic fraction of the feed stream is converted to oil in the presence of a homogeneous (K_2CO_3) and a heterogeneous (Zirconia) catalyst, at subcritical conditions (280-350^{o}C and 22.5-25.0 MPa). The full product consists of

a top-phase of bio-oil, a gas-phase mainly consisting of CO_2, a water phase with soluble organic compounds and a bottom-phase mainly consisting of inorganic salts. The conditioned feed from the feed tanks is pumped through a high pressure feed pump. The feed is then preheated in the feed heater. The feed enters a recirculation loop, in which a recirculation pump ensures a high flow rate. This design ensures instantaneous heat up in the mixing point. The flow passes through a trim heater and a fixed-bed reactor filled with zirconia-catalyst. After the reactor a fraction of the product stream is withdrawn and passed through a cooler. After pressure reduction the oil is separated from the water by centrifugation or gravimetrical separation. A schematic flow sheet is shown in Fig. 1.1.

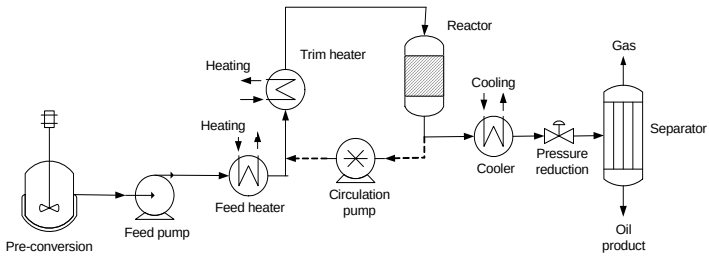

Figure 1.1 Schematic of the CatLiq® process

3.1.2 Feed material and liquid separation

DDGS and WDGS are the major co-products of first generation ethanol production. The main components of DDGS are crude protein and crude fat but it also contains crude fiber (Kim *et al.* 2008). The content of the elements C, N and H were determined according to ASTM D 5291 and sulfur according to ASTM D 1552 (Table 3.1). The oxygen content was calculated from these results. The heating value of the DDGS was 18.8 MJ/kg and was determined according to ASTM D 240. Analysis of elementary composition and heat value was carried out at Karlshamns Kraft, Karlshamn, Sweden. The DDGS used in the current work comes from Agroetanol AB, Norrköping, Sweden. Due to storage reasons DDGS was used instead of WDGS. The DDGS was milled in a dry-mill to reduce particle size to 0.5 mm. Prior to the experiments milled DDGS was mixed with water to slurries with 25% dry matter.

Table 3.1 The composition of the DDGS used in the experiments

Elementary composition, daf *(wt %)	
C	45.50
H	7.0
N	8.10
S	0.79
O	38.7
Major components wt%	
Protein	35
Moisture	6.0
Fibers	47
Fat	5.5
Ash contents (db)	4.0
Starch	1.7

*daf, dry ash free; db, dry basis.

K_2CO_3 (homogeneous catalyst) corresponding to 2.5% of the slurry mass was added. The heterogeneous catalyst in the reactor was zirconia (ZrO_2). The catalytic conversion of DDGS was carried out at process temperature of 350°C and the feed rate was 11L/h. Each trial was run for 6 h and the process was considered to be in steady-state after 4 h. Each oil yield measurement was based on the oil production during 1 h at steady-state. The oil was separated from the water phase by a disc-stack centrifuge (Alfa-Laval, Sweden).

3.2 Oil phase analysis

3.2.1 Oil properties

To evaluate the bio-oil quality, density, viscosity, heat value and elemental composition were determined. The heat value was determined according to ASTM D 240 and the elementary composition according to ASTM D 5291 and 1552. The oxygen content was calculated from these results. The Conradson number, a measure of the oil stability, was measured according to ASTM D 189. The analyses mentioned above were carried out at Karlshamn Kraft, Karlshamn, Sweden. The water content was determined by Karl-Fischer titration performed with a TitraLab TIM 580 (Radiometer, France). The over-all results are given

in table 3.2 and 3.3, expressed as average values with 95% confidence intervals. The values are based on five separate trials.

Table 3.2 Over-all results of the experiments, values are given with 95% confidence intervals

Oil yield on dry biomass (%)	33.9 ± 1.8
Energy recovery in oil (%)	73.2 ± 3.9
Carbon recovery from biomass to oil (%)	57.8 ± 2.8
Low heat value of oil* (MJ/kg)	35.8 ± 0.2
Elementary composition of oil (%)*	
C	78.3 ± 0.3
H	9.3 ± 0.1
O	5.1 ± 0.4
N	6.4± 0.4
S	0.4± 0.1

*corrected for the water content

Table 3.3 Properties of the bio-oil, representative sample

Viscosity at 40 °C, (cP)	499 ± 52
Viscosity at 60 °C, (cP)	116 ± 10
Viscosity at 80 °C, (cP)	39 ± 3
Water content in oil (%)	7.2 ± 0.9
Ash content in oil (%)*	0.6 ± 0.1
Conradson number	13± 1

*Water-free

The oil yield on dry matter in the feed was 34%. The oil contained more than 6 times less oxygen than the DDGS and thus the effective heat value was almost double, 35.8 MJ/kg. As much as 73.2% of the energy in the feed was recovered in the oil. The viscosity of the produced oil was high but decreased significantly with temperature and the rheological behavior was Newtonian. The oil contained some water that could be removed by a second centrifugation. The ash content in the oil was relatively low. The stability of the oil was checked by measuring the change in viscosity, elementary composition and heat value after 4 months of storage at ambient conditions. In addition, there was no change in elementary composition and heat value after 8 months of storage.

3.2.2 Analysis of oil phase by GC-MS and TGA

Oil obtained from catalytic conversion of DDGS was analyzed by gas chromatograph equipped with a mass selective detector [GC-MS; Varian CP-3800; column, VF-5ms; (5% phenyl 95% dimethylpolysiloxane, 30m × 0.25mm × 0.25µm); temperature programmed: 75°C (hold 2 min.) → 325°C (20°C/min, hold 15 min.). The compounds were identified by means of the NIST (National Institute of Standards and Technology) library of mass spectra.

The identified compounds in the oil are presented in Table 3.4 and Fig. 3.1. The oil contained a large fraction of long chain aliphatic acids such as: tetradecanoic acid, hexadecanoic acid and octadecanoic acid.

In order to determine the distribution of compounds in the oil, a semi-quantitative study was made by means of the percentage of area of the chromatographic peaks. This type of qualitative analysis in which the concentrations of the components is related to the total area has also been used by other researchers (Karagöz *et al.* 2005; Aguado *et al.* 2000; Domínguez *et al.* 2003). The deviation from 100% represents the area of unidentified compounds.

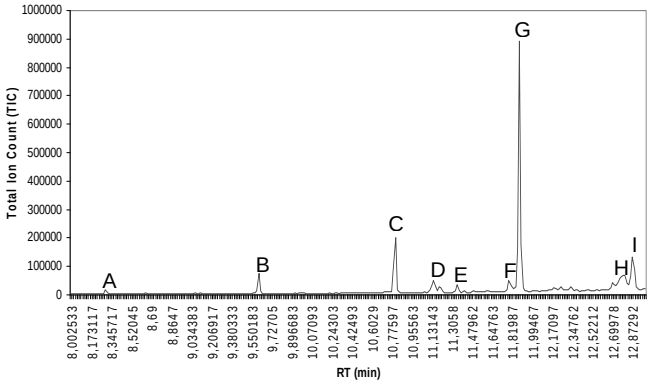

Fig. 3.1 GC-MS spectrum of bio-oil with peak identification. A=decanoic acid; B=dodecanoic acid; C=tetradecanoic acid; D=tridecanoic acid; E=n-pentadecanoic acid; F=palmitelaidic acid; G=hexadecanoic acid; H=11-cis-octadecenoic acid; I=octadecanoic acid

Table 3.4 Identification of compounds in oil phase

RT(min)	Compound	Area (%)
8.299	Decanoic acid	0.571
9.616	Dodecanoic acid	3.039
10.809	Tetradecanoic acid	9.431
11.147	Tridecanoic acid	2.772
11.352	n-Pentadecanoic acid	1.216
11.790	Palmitelaidic acid	2.416
11.885	Hexadecanoic acid	37.376
12.793	11-cis-Octadecenoic acid	7.006
12.873	Octadecanoic acid	8.071
Σ Area		**71.898**

Thermogravimetric analysis (TGA) was performed in TGA/SDTA 851 Mettler Toledo equipment to characterize the evaporation, thermal decomposition and combustion properties of CatLiq bio-oil. The experiment was performed with the amount of 6.0 mg oil sample in the presence of nitrogen and oxygen with a heating rate of 10 ^{o}C/min. The experimental data of the weight loss (TG) and weight loss rates (DTG) of the bio-oil are presented in Figure 3.2 & 3.3. At temperature higher than 300 ^{o}C, the TG curve of the bio-oil sample heated in nitrogen corresponds to the evaporation of light volatiles in the bio-oil. The DTG curve of the bio-oil heated in O_2 shows clear peaks at 55 ^{o}C, 72 ^{o}C, 145 ^{o}C, (350 ^{o}C -390 ^{o}C) and 460 ^{o}C. The first three peaks are attributed to the evaporation of light volatiles, and the peaks at (350 ^{o}C -390 ^{o}C) and 460 ^{o}C are characteristic to the burning of char residue.

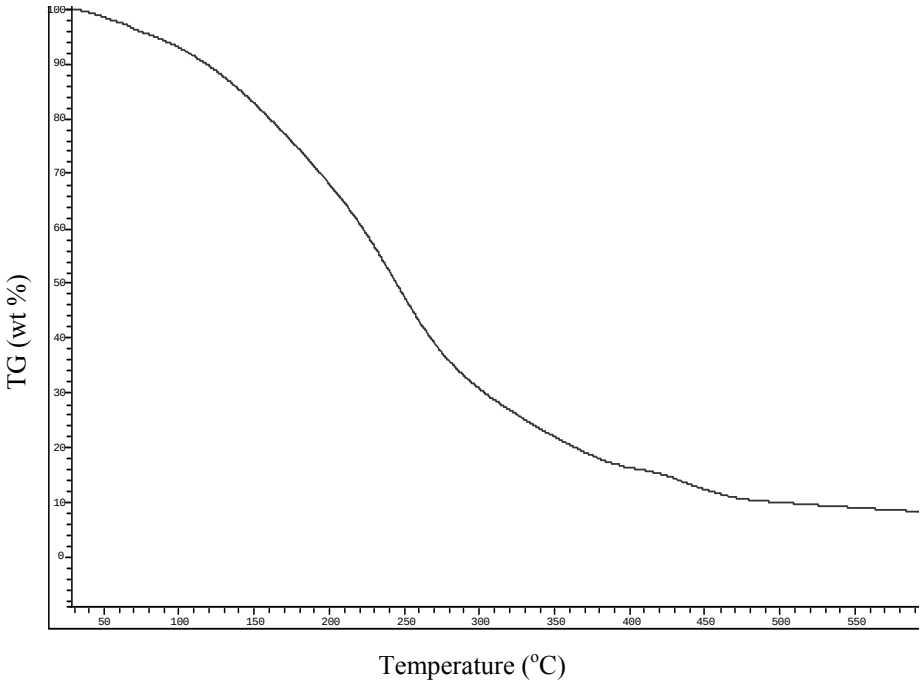

Fig. 3.2 TG curve of the CatLiq bio-oil heated in N_2

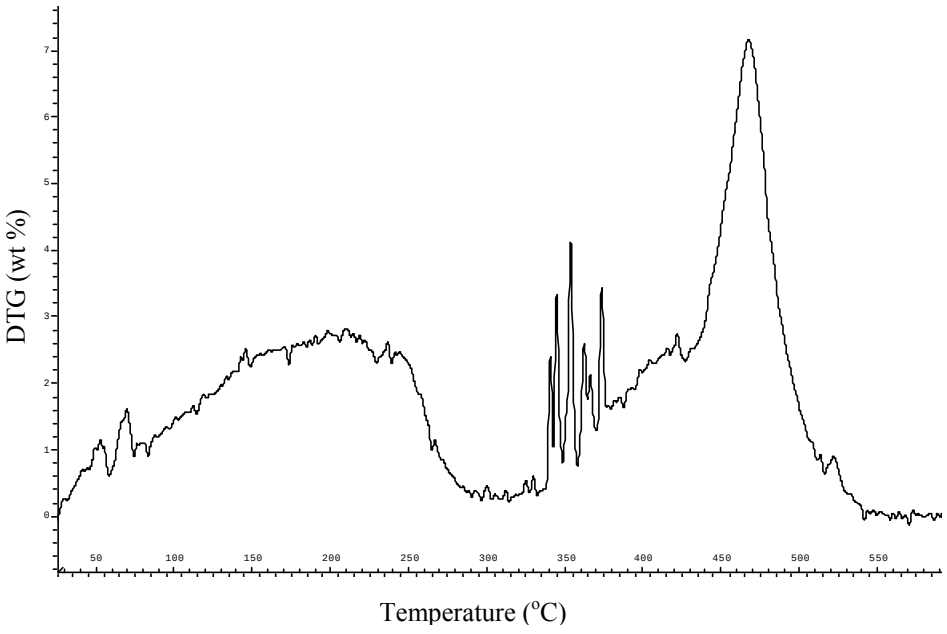

Fig. 3.3 DTG curve of the CatLiq bio-oil heated in O_2

3.3 Water phase analysis

3.3.1 Analysis of water phase by GC analysis

The water phase was analyzed for short-chained alcohols and acids as well as acetone by GC (Varian 3800, column: fused silica, 25m × 0.32mm, temperature programmed: 50 ^{o}C hold 2 min. → 140 ^{o}C, 35 ^{o}C/min.). To detect other compounds such as amines and fatty acids, 24 mL of water-phase was acidified by addition of concentrated hydrochloric acid (2 mL). This made the water phase cloudy, indicating the presence of acidic organic compounds. The cloudy water phase was extracted using dichloromethane and the combined organic phases dried ($MgSO_4$) and evaporated *in vacuo* to give a colorless residue (240 mg, 1.0 wt%). The isolated residue was analyzed by GC-MS at the University of Copenhagen. The total organic content (TOC) in the water phase was measured by using a kit (LCK 387) and a spectrophotometrical analysis unit (DR 2800) from Hach & Lange, Germany.
The TOC (Total Organic Content) was 33.3 ± 0.8 g/L, corresponding to a carbon recovery to water-soluble compounds of 30%. A quantitative composition of the water is shown in Table 3.5 and Figure 3.4 & 3.5. It can be seen that the content of short-chained alcohols and acids as well as acetone is 8% of the TOC content. The analysis of water-phase extract showed rather high levels of piperidone, benzamine, cyclopentenone derivates and heptanoic acid, however only enough to account for about 10% of the TOC.

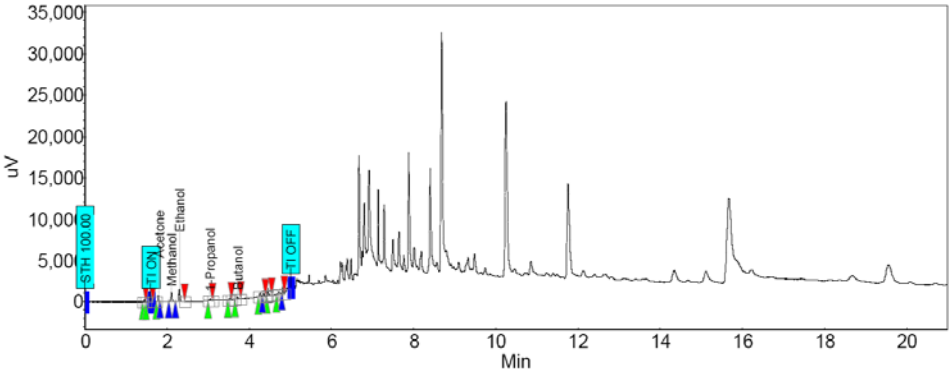

Fig. 3.4 GC spectrum of water phase with alcohols identification

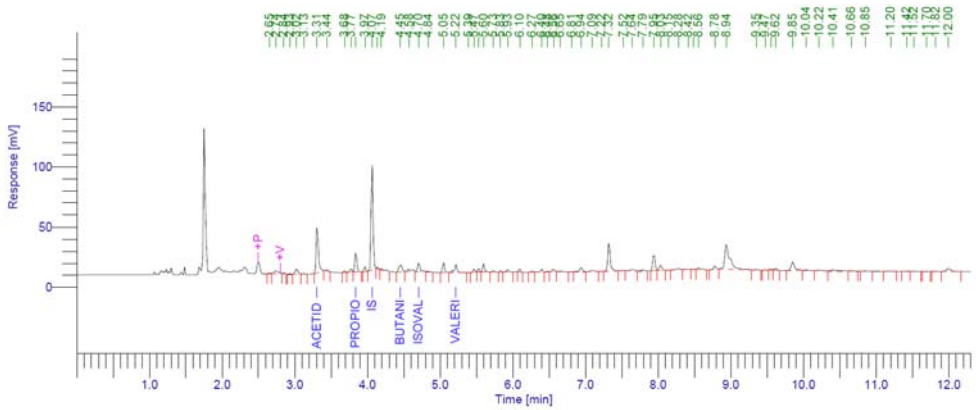

Fig. 3.5 GC spectrum of water phase with acids identification

Table 3.5 Concentration of short-chained alcohols and acids in water phase

Compound	Quantity (mg/L)
Methanol	252
Ethanol	290
1-Propanol	40
Butanol	40
Acetone	110
Acetic acid	3320
Propionic acid	727
Butanic acid	305
Valeric acid	230
Isovaleric acid	241.23

3.4 Gas phase analysis

The gas phase was sent for analysis at Statens Provningsanstalt, Borås, Sweden. The gas contained about 95% CO_2 and 1.6% H_2, small amounts of N_2, CO and CH_4 as well as traces of short-chain alkanes and alkenes. The product gas flow was about 350-410 L/h corresponding to a carbon recovery from biomass to gas of about 12%.

4 THERMODYNAMIC MODELING OF CATLIQ® PROCESS

4.1 Choice of thermodynamic model

Modeling of a physical system rests on the knowledge of pure component and binary properties. These properties serve as a basis for the determination of the thermodynamic properties, transfer properties and fluid phase equilibria. The results accuracy is thus directly linked to the pure components and binary properties and to the thermodynamic model that has been chosen to represent the thermodynamic behavior of the system. The choice of the thermodynamic model is lead by a concern of rigor, reliability and validity in the considered operating range. Similar to other chemical processes, biomass conversion processes require thermodynamic properties, models and analysis method for process development, design and optimization. Due to the complexity of the biomass structure and the chemical reactions occurred in biomass conversion, the phase behavior and the thermodynamic properties involved in this kind of processes are rather complex, which require special considerations in the thermodynamic modeling. To meet this demand a systematic thermodynamic study has been carried out for the CatLiq® process.

4.2 The PSRK model

The products from CatLiq® process are bio-oil, gases, and organic compounds such as alcohols and acids, and water. These products make the CatLiq® process a highly non-ideal, asymmetric system containing polar and non-polar substances. The selected model should accommodate all this. The PSRK model proposed by Holderbaum and Gmehling (Holderbaum and Gmehling 1991) was selected as the thermodynamic model to describe the phase behavior of the system. The PSRK model is predictive Soave-Redlich-Kwong (SRK) equation of state (EOS) with the modified Huron-Vidal first-order (MHV1) mixing

rule of Michelsen (Michelsen 1990) coupled with the modified UNIFAC model.

The PSRK model is a combination of the following thermodynamic models:

- Mathias-Copeman modification of the SRK equation of state
- MHV1 mixing rule
- UNIFAC group contribution method

The PSRK method extends the applicability of the original UNIFAC (Fredenslund *et al.* 1975) in order to predict thermodynamic properties over a large temperature and pressure range. Details of the individual models are described in the following sections.

4.2.1 The Mathias-Copeman-SRK equation of state

The Soave-Redlich-Kwong (SRK) equation of state (Soave 1972) has the form:

$$P = \frac{RT}{v-b} - \frac{a}{v(v+b)} \qquad (1)$$

Where a and b are the EOS energy and size parameters, respectively.

Two modifications are necessary to obtain an equation of state for predicting vapor-liquid-equilibria of polar as well as non-polar mixtures. The first modification concerns the temperature dependence of pure component parameter a, which was originally expressed by Soave in terms of the acentric factor ω.

$$a_i = 0.42748 \frac{R^2 T_{ci}^2}{P_{ci}} f(T) \qquad (2)$$

$$b_i = 0.08664 \frac{RT_{ci}}{P_{ci}} \quad (3)$$

$$f(T) = \left[1 + c_1\left(1 - T_r^{0.5}\right)\right]^2 \quad (4)$$

$$c_1 = 0.48508 + 1.5517\omega + 0.15613\omega^2 \quad (5)$$

This temperature dependence yields sufficiently accurate vapor pressure data for non-polar substances, but improvements are still necessary for polar components. Therefore, the expression proposed by Mathias and Copeman (Mathias and Copeman 1983) is used in the PSRK equation.

$$f(T) = \left[1 + c_1\left(1 - T_r^{0.5}\right) + c_2\left(1 - T_r^{0.5}\right)^2 + c_3\left(1 - T_r^{0.5}\right)^3\right]^2, T_r < 1 \quad (6)$$

$$f(T) = \left[1 + c_1\left(1 - T_r^{0.5}\right)\right]^2, T_r > 1 \quad (7)$$

The use of the three adjustable parameters especially improves the description of the pure component vapor pressures for polar components. This is of course important when a reliable prediction of the real behavior of polar mixtures is required.

4.2.2 The MHV1 Mixing rule

The second modification concerns the mixing rule for the parameter a. The modified Huron-Vidal first-order (MHV1) mixing rule (Michelsen 1990) relates the mixture parameters a and b of a cubic equation of state to an activity coefficient model.

$$\frac{a_m}{b_m} = \sum_i x_i \frac{a_i}{b_i} + 1/q_1 \left[G^E + RT \sum_i x_i \ln\left(b_m / b_i\right) \right] \qquad (8)$$

$$b_m = \sum x_i b_i \qquad (9)$$

Where a_m and b_m are the mixture co-energy and co-volume parameters, respectively and G^E is the molar excess Gibbs free energy, which can be calculated from the UNIFAC group contribution method. The q_1 is an empirical parameter and is set to be -0.64663 in the PSRK model (Holderbaum and Gmehling 1991) for better results at higher pressures.

4.2.3 The UNIFAC group contribution method

Any appropriate model for excess Gibbs free energy can be used in connection with the present mixing rules. The system involved in the CatLiq® process is highly asymmetric system. Therefore, modified UNIFAC model (Zhong *et al.* 1996, Kikic *et al.* 1980) was adopted as the required G^E model in the PSRK model, which reduces to the original UNIFAC model (Fredenslund *et al.* 1975) for symmetric or slightly asymmetric systems.

$$G^E = RT \sum x_i \ln \gamma_i \qquad (10)$$

Where x_i is the mole fraction of component i

$$\ln \gamma_i = \ln \gamma_i^C + \ln \gamma_i^R \qquad (11)$$

Where the residual part $\ln \gamma_i^R$ is identical to the original UNIFAC model and combinatorial part $\ln \gamma_i^C$ is modified as follows:

$$\ln \gamma_i^C = \ln\left(\frac{\Phi'_i}{x_i}\right) + 1 - \left(\frac{\Phi'_i}{x_i}\right) - \left(\frac{z}{2}\right) q_i \left[\ln\left(\frac{\Phi_i}{\theta_i}\right) + 1 - \left(\frac{\Phi_i}{\theta_i}\right) \right] \quad (12)$$

with

$$\Phi_i = \frac{x_i r_i}{\sum_j x_j r_j} \qquad \theta_i = \frac{x_i q_i}{\sum_j x_j q_j} \quad (13)$$

and

$$\Phi'_i = \frac{x_i r'_i}{\sum_j x_j r'_j} \quad (14)$$

with

$r_i' = 0.6583\ r_i$, for large molecules (15)

$r_i' = r_i$, for small molecules (16)

Φ = volume fraction r'_i = volume parameter of component

θ = surface area fraction q_i = surface area parameter of component i

z = coordination number, 10 (Zhong *et al.* 2002)
xi = mole fraction of component i

The pure component parameters ri and qi are calculated as the sum of the group volume and group area parameters R_k and Q_k by the Bondi method:

$$r_i = \sum_k v_k^{(i)} R_k \qquad q_i = \sum_k v_k^{(i)} Q_k \quad (17)$$

$v_k^{(i)}$ = number of groups of type k in molecule of component i

The residual part is identical to the original UNIFAC model and can be written as:

$$\ln \gamma_i^R = \sum_k v_k^{(i)} \left(\ln \Gamma_k - \ln \Gamma_k^{(i)} \right) \tag{18}$$

$\Gamma_k^{(i)}$ and Γ_k are pure component and group residual activity coefficients respectively.

Γ_k is calculated by the following expression:

$$\ln \Gamma_k = Q_k \left[1 - \ln \left(\sum_m \theta_m \Psi_{mk} \right) - \sum_m \left(\frac{\theta_m \Psi_{km}}{\sum_n \theta_n \Psi_{nm}} \right) \right] \tag{19}$$

Ψ_{nm} are group interaction parameters, however for the interaction parameters of gas-containing group pairs temperature dependent interaction parameters are used, and the UNIFAC expression

$$\Psi_{nm} = \exp\left(-\frac{a_{nm}}{T} \right)$$

is replaced by

$$\Psi_{nm} = \exp - \frac{a_{nm} + b_{nm} T + c_{nm} T^2}{T}$$

a_{nm}, b_{nm} and c_{nm} are interaction parameters between each two groups.

The current status of the PSRK group interaction parameter matrix is shown in Figure 4.1 (Horstmann *et al.* 2005).

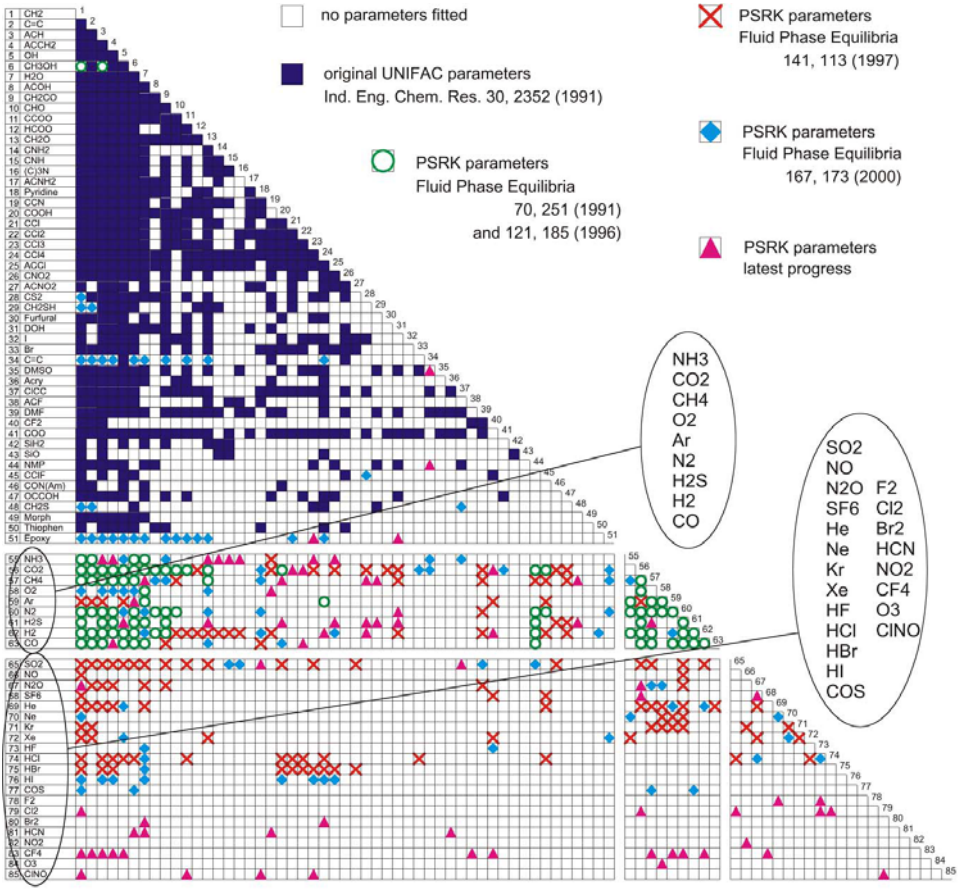

Fig. 4.1 PSRK group interaction parameter matrix Horstmann *et al.* 2005

4.3 Numerical modeling of the system

4.3.1 Algorithm for bubble point pressures

The general solution to vapor-liquid equilibria including high-pressure applications may be advantageously obtained using an equation of state by iteration methods. The proposed algorithm (Sandler and Orbey 1998) for bubble pressure calculations is shown in Figure. 4.2. In this algorithm, y is iterated for convergence to a constant value $\sum y_i' = 1$ at a given *P*, which is iterated in the outer loop until the equilibrium conditions are satisfied.

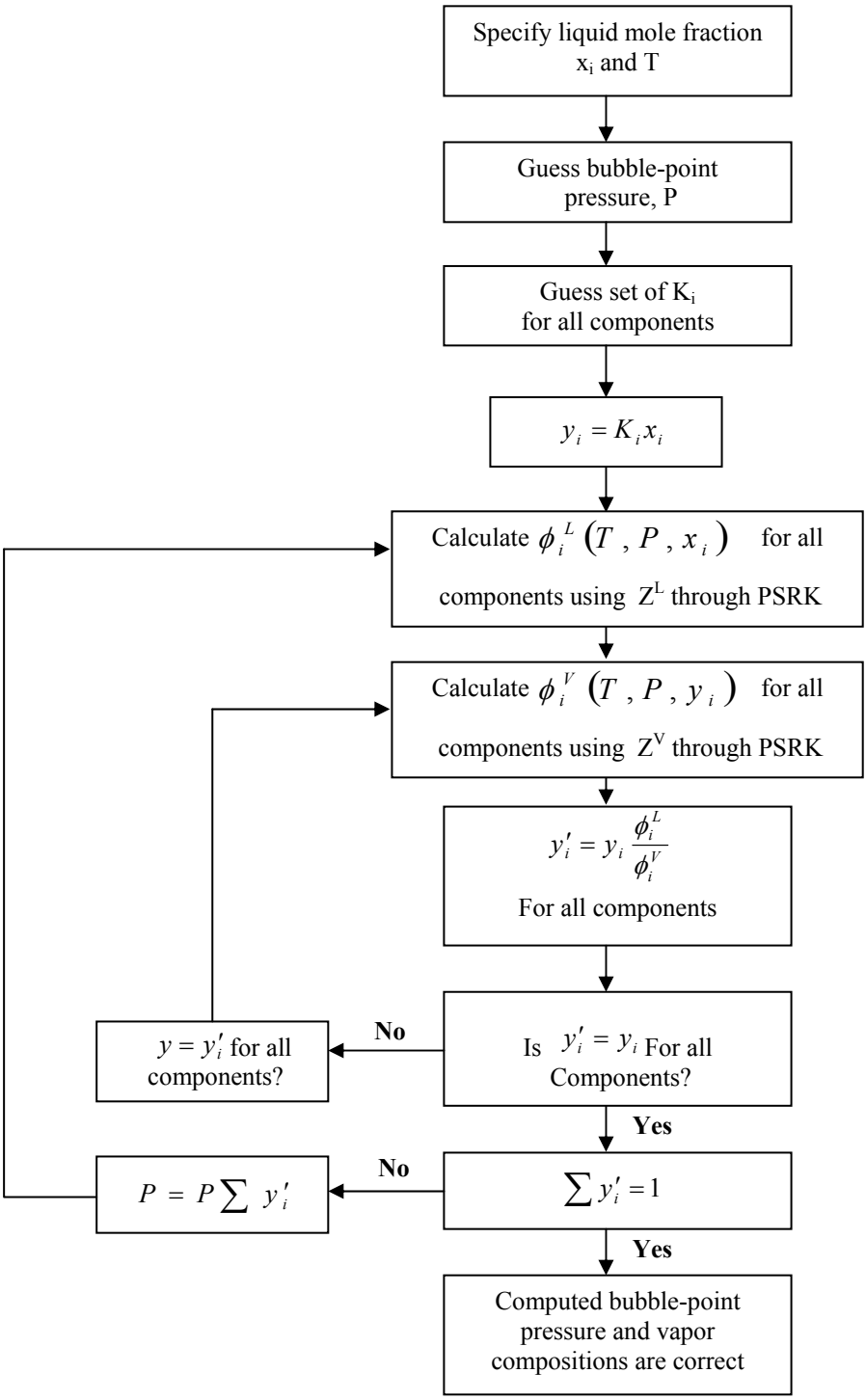

Fig. 4.2 Flow chart for bubble P calculation

Where the *K*-value is defined by

$$K_i = \frac{\phi_i^L(T,P,x)}{\phi_i^V(T,P,y)} \tag{20}$$

$$y_i = K_i x_i \tag{21}$$

Here, ϕi are fugacity coefficients of different phases, for the evaluation of which EOS are solved.

Proper guess is very important in efficient computations. A good guess for the pressure may be obtained by the following equation:

$$P = \sum x_i P_i^{sat}(T) \tag{22}$$

A vapor composition is calculated by using guessed *K*-values obtained by:

$$K_i = \frac{P_i^{Sat}(T)}{P} \tag{23}$$

4.3.2 Selected model mixture

The full product of CatLiq® process consists of a top-phase of bio-oil, a gas-phase and a water phase with soluble organic compounds. The analysis of all these phases showed that the oil contained a large fraction of long chain aliphatic acids such as: tetradecanoic acid, hexadecanoic acid and octadecanoic acid, the gas consisting of 95 %CO_2 and some combustible gases. The water-phase contained short-chained alcohols and acids. Therefore a mixture of a limited number of well-defined components resembling the products from the CatLiq® process was used instead of a real fraction. This method allows a thorough experimental

investigation that can be used to verify the prediction and adjust the description by equations of state. Therefore bubble point pressures of a selected model mixture (CO_2 + H_2O + Ethanol + Acetic acid + Octanoic acid) were determined.

4.3.3 Pure component parameters using ASPEN PLUS

For nonpolar substances (CO_2 and Octanoic acid) and the substance like acetic acid whose c_1, c_2, and c_3 cannot be obtained, Eq. (4) is good enough (Soave1972), however, for polar substances (H_2O and Ethanol) Eqs. (6) and (7) proposed by Mathias and Copeman (Mathias and Copeman 1983) are much more accurate. Critical properties and acentric factors are required in the phase equilibria calculations. However, they cannot be measured for large molecules like Octanoic acid due to decomposition. Therefore, suitable estimation methods have to be selected. The group contribution method of Joback (Reid et al 1987) and that of Constantinou and Gani (Constantinou and Gani 1994) were adopted for the estimation of critical properties, and the acentric factor was estimated with the Lee-Kesler method (Reid et al 1987) and that of Constantinou and Gani (Constantinou and Gani 1995). All these properties were estimated in Aspen Plus software.

Table 4.1 Pure component properties used in the mixing rule

Substance	T_c (^oC)	P_c(bar)	ω	c_1	c_2	c_3
Carbon dioxide	31.04[a]	73.8[a]	0.228[a]			
Water	374.15[a]	220.5[a]	0.344[a]	1.0783[b]	-0.5832[b]	0.5462[b]
Ethanol	243.01[a]	63.8[a]	0.637[a]	1.3327[b]	0.9695[b]	-3.1879[b]
Acetic acid	319.56[a]	57.86[a]	0.462[a]			
Octanoic acid	442.86[c]	27.35[c]	0.7653[c]			

[a] *Yaw's (2003)*
[b] *Holderbaum and Gmehling (1991)*
[c] *Estimated by Aspen Plus*

4.4 Apparatus and methodology for the study of phase equilibria

4.4.1 Introduction

In the design and development of biomass conversion processes, the importance of accurate correlation and prediction of phase behavior should never be underestimated. In particular, accurate prediction depends on both a powerful model and high-quality experimental data.

4.4.2 JEFRI-DBR PVT apparatus

The experimental work was carried out in a high-pressure JEFRI-DBR phase behavior system. In this apparatus, pressures up to approximately 700 bar can be handled and the temperature can be range from 0 ^{o}C to 200 ^{o}C. An advantage of this apparatus is that the phase transitions can be observed visually. An actual photograph and schematic diagram of the JEFRI-DBR PVT system is shown in Figure. 4.3 (a and b).

Fig. 4.3(a and b) An Actual photograph and Schematic diagram of JEFRI-DBR PVT system

The heart of the system was a high-pressure PVT cell consisting of a glass cylinder, secured between two full-length sight glass windows, inside a stainless steel frame. This design allowed for unimpaired visibility of the entire contents of the cell. Pressure was regulated through an automated, high pressure, positive displacement pump. The hydraulic fluid inside the pump was connected to a floating isolation piston located inside the PVT cell. The piston isolated the hydraulic fluid from the process side of the PVT cell. Controlled displacement of the isolation piston allowed for volume changes in the process chamber, thus providing an effective way to control pressure. The PVT cell was mounted inside a temperature-controlled air bath by means of a bracket, attached to a horizontal shaft. The applications of the JEFRI-DBR phase behavior system have also been described by (Bruusgaard *et al.* 2008) and (Beltrán *et al.* 2008).

(b)

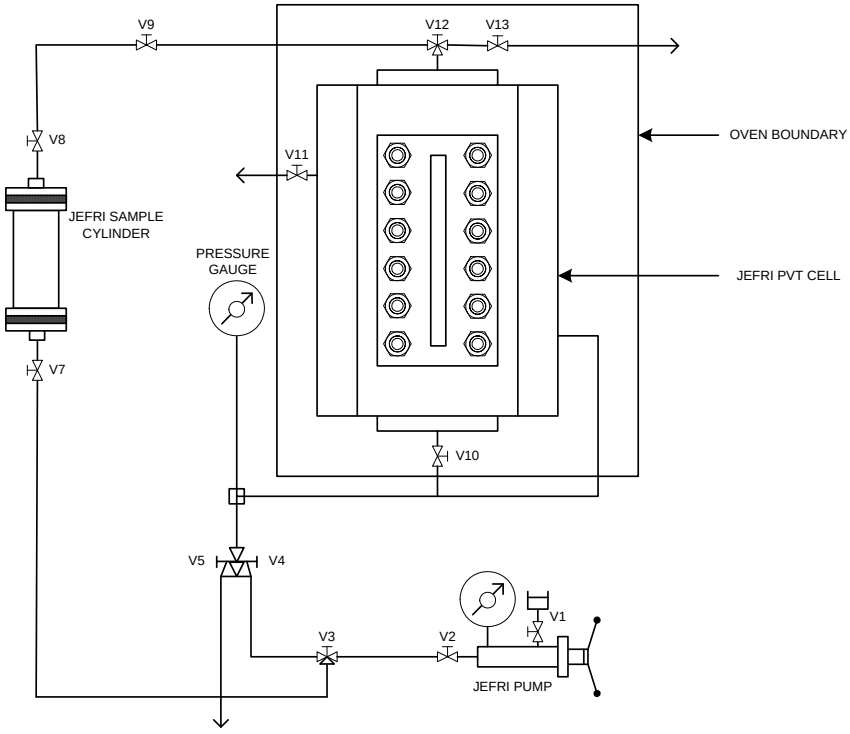

4.4.3 Determination of bubble point pressures

The bubble point pressures of selected model mixture (pH = 8.0, adjusted with 5% NaOH solution) were determined at different constant temperatures (40 ^{o}C, 50 ^{o}C, 60 ^{o}C, and 75 ^{o}C) by observing the appearance of gas bubble through the cell window as the pressurized liquid sample was decompressed. When the bubble point pressure reached the overall compressibility of the system increased. Small changes in pressure resulted the large changes in the total fluid volume in the PVT cell. This was manifested graphically by the change of the slope when the sample pressure was plotted against the sample volume. Table 4.3 summarizes the composition of the selected model mixture.

Table 4.2 Suppliers and purities of the substances used in this work

Substance	(%, w/w)	Supplier	Purity (mass %)
Carbon dioxide	7.0	Yara praxair	>99.95
Water	84.8	Sigma-Aldrich	>99
Ethanol	0.1	Sigma-Aldrich	>99
Acetic acid	0.1	Sigma-Aldrich	>99
Octanoic acid	8.0	Sigma-Aldrich	>99

4.4.4 Experimental results

Total volume of the mixture in the cell = 85 ml

Table 4.3 Volume of the components in the cell

Substance	Volume, ml
Water	72.08
Ethanol	0.085
Acetic acid	0.085
Octanoic acid	6.8
Total volume without CO_2	79.05

Amount of CO_2 in the cell

Bottom of piston in highest position (Bpsm) = 32.75 cm

Bottom of piston after CO_2 (Bps) = 22.72 cm

Dead volume (Dv) = 0.270 cc

Capacity (Qc) = 7.90 cc/cm

$$\text{Volume of } CO_2 = \left(Bpsm + \frac{D_v}{Q_c} - Bps \right) Q_c$$

$$= \left(32.75 + \frac{0.270}{7.90} - 22.72 \right) 7.90 \quad = 79.50 \text{ cc}$$

P= 478 psi = 32.95 bar
T = 293 K

R = 8.314 m^3 PaK^{-1} mol^{-1}

Z = 0.7968 (From PVT simulator)

n = PV/ZRT

$$n = \frac{\left(32.95 \times 10^{2}\right)\left(79.50 \times 10^{-6}\right)}{\left(0.7968\right)\left(8.314\right)\left(293\right)} = 1.3493 \times 10^{-4}$$

m = n × M

m = (1.3493 × 10^{-4}) × 44.01

m = 5.938 × 10^{-3} Kg

m = 5.938 gm

Total volume with CO_2 = 79.05 + 5.938 = 84.988 ml

Tables (4.4-4.7) indicate the motion of the pump cell piston at different pressures for the calculation of total sample volume at constant temperature. Figures 4.4 (a-d) shows the total sample volume verses pump cell pressure. The intersection of the two best fitted straight lines gives the bubble point pressure at constant temperature.

Table 4.4 Bubble point measurement at 40 ^{o}C

Pressure (bar)	Bottom piston, Bps (cm)	Total Volume, Vt (cc)
136.3265	22.541	80.92049
157.1429	22.555	80.80989
165.9864	22.559	80.77829
170.4082	22.564	80.73879
179.7959	22.572	80.67559
190.8844	22.578	80.62819
204.1497	22.579	80.62029
234.1497	22.585	80.57289

Table 4.5 Bubble point measurement at 50 ^{o}C

Pressure (bar)	Bottom piston, Bps (cm)	Total Volume, Vt (cc)
96.32653	22.576	80.64399
112.6531	22.581	80.60449
122.8571	22.585	80.57289
129.6599	22.589	80.54129
136.3946	22.591	80.52549
146.7347	22.605	80.41489
156.7347	22.622	80.28059
164.3537	22.623	80.27269
175.1701	22.63	80.21739
207.2109	22.635	80.17789

Table 4.6 Bubble point measurement at 60 ^{o}C

Pressure (bar)	Bottom piston, Bps (cm)	Total Volume, Vt (cc)
156.7347	22.396	82.06599
184.4218	22.414	81.92379
204.7619	22.424	81.84479
218.5034	22.438	81.73419
231.4286	22.455	81.59989
241.2925	22.461	81.55249
248.0952	22.476	81.43399
258.9796	22.495	81.28389
272.1088	22.499	81.25229
313.1293	22.516	81.11799

Table 4.7 Bubble point measurement at 75 ^{o}C

Pressure (bar)	Bottom piston, Bps (cm)	Total Volume, Vt (cc)
139.4558	22.442	81.70259
163.9456	22.462	81.54459
183.8776	22.481	81.39449
196.8027	22.501	81.23649
210.8844	22.521	81.07849
217.415	22.531	80.99949
224.4898	22.545	80.88889
231.0884	22.547	80.87309
237.8912	22.553	80.82569
247.9592	22.559	80.77829
261.2925	22.567	80.71509
288.6395	22.572	80.67559

(a)

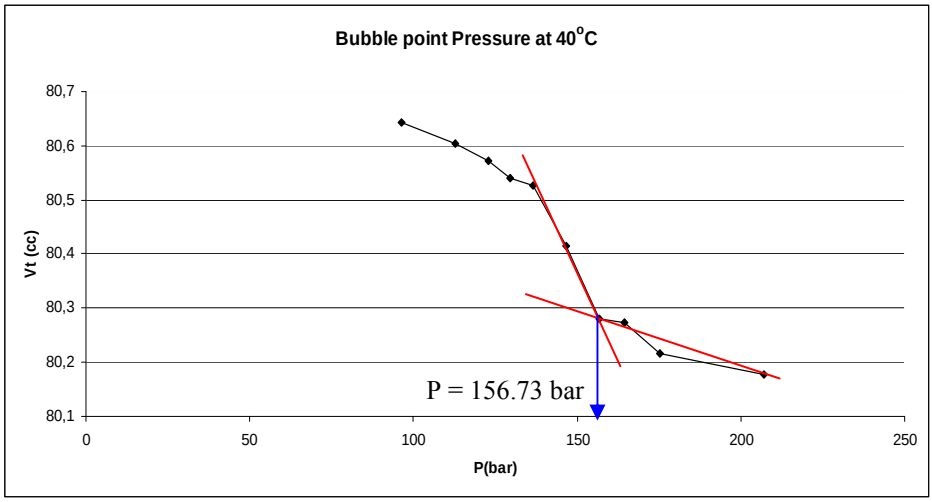
Bubble point Pressure at 40°C
Vt (cc)
80,7
80,6
80,5
80,4
80,3
80,2
80,1
0
50
100
150
200
250
P(bar)
P = 156.73 bar

(b)

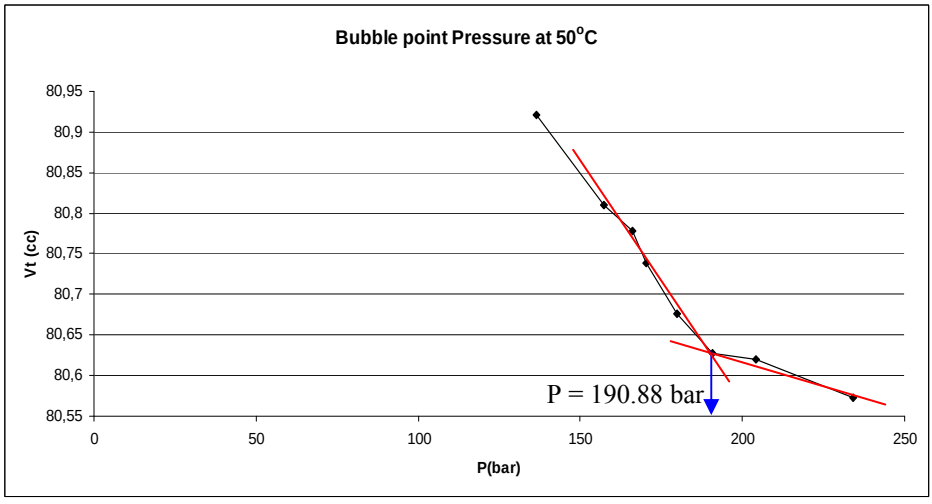
Bubble point Pressure at 50°C
Vt (cc)
80,95
80,9
80,85
80,8
80,75
80,7
80,65
80,6
80,55
0
50
100
150
200
250
P(bar)
P = 190.88 bar

(c)

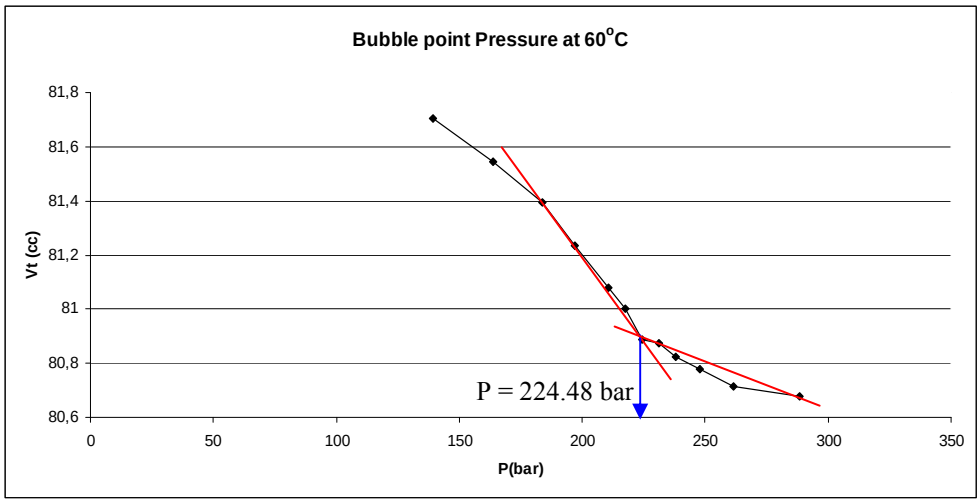

d)

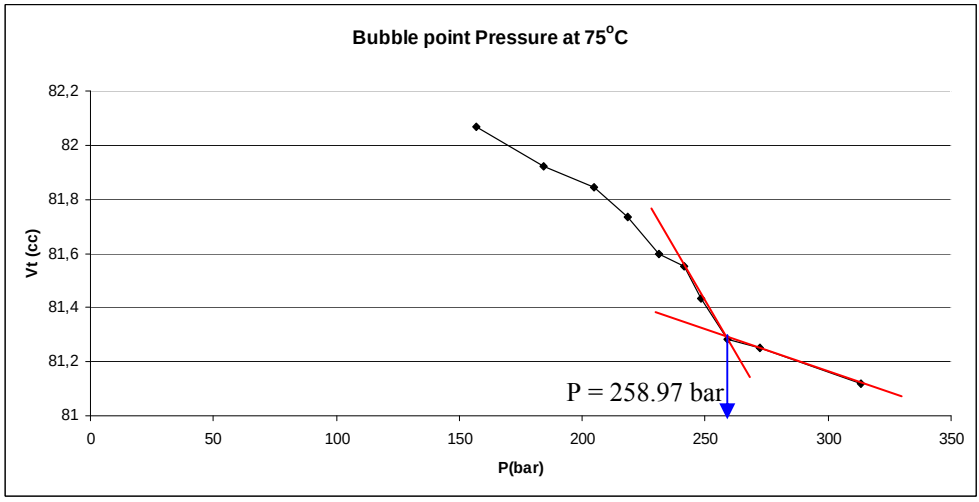

Fig. 4.4 Bubble point pressures at (a) 40 °C, (b) 50 °C, (c) 60 °C, and (d) 75 °C

4.4.5 Correlating experimental and PSRK model results

The experimental bubble point pressures for the selected model system and the predicted values by the PSRK model are given in Table 4.8, and Figure 4.5. For each measured point, the relative error between experimental and predictive values is given in the table and average

absolute deviation of the system is determined. It can be seen that average absolute deviations (AAD %) are less than 10% or equal to 8.7%.

Table 4.8 Experimental ($P_{exp.}$) and PSRK-Estimated ($P_{calc.}$) bubble point Pressures

T/^{o}C	P_{exp}/bar	P_{cal}/bar	Rel. Dev. (%)[a]
40	156.73	138.53	11.6123
50	190.88	169.22	11.3474
60	224.48	202.08	9.9786
75	258.97	253.85	1.9770
		AAD %[b]	**8.728863**

[a]Relative Deviation (%) = ($P_{exp.}$- $P_{calc.}$)/ $P_{exp.}$ ×100
[b]AAD % = (∑ | error % |) / number of data points

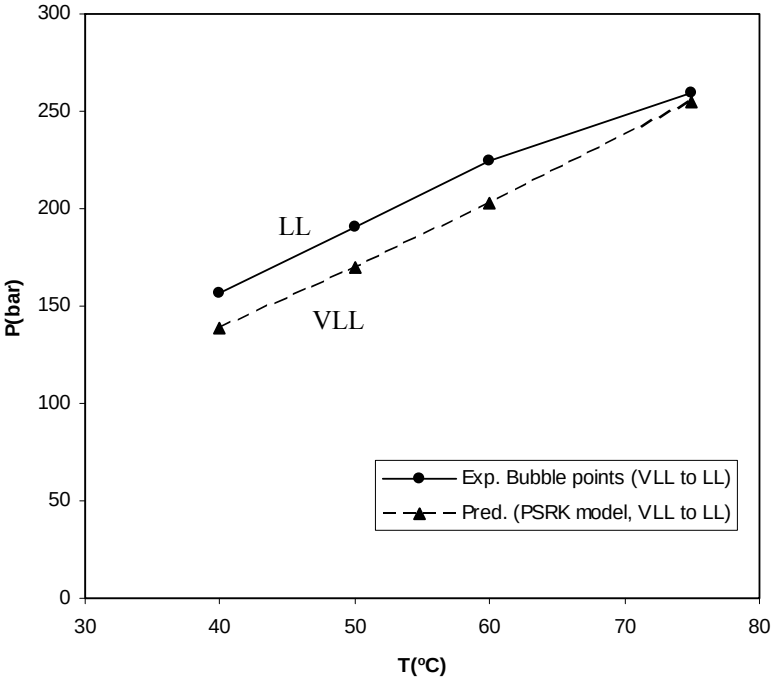

Fig. 4.5 Measured and predicted phase boundaries for the selected model system

5 SUGGESTIONS FOR FURTHER WORK

The further work in this research can be seen to take three different directions:

I. Typically, large pilot plants (PERC, HTU®, and CatLiq®) have been used for hydrothermal liquefaction processes but have as disadvantages that operation, modifications, cleaning and reparations are very costly and time consuming. Besides, the experimental cycle (time from beginning of one experiment to the beginning of the next one) is very long (sometimes days/weeks). For these reasons, for research purposes, we propose downsizing a continuous plant for CatLiq® to a flexible, cheap and safe bench scale setup. The setup should allow relatively short experimental cycles (several experiments per day). It should be suitable for the study and demonstration of various issues, such as, testing of various feedstocks and process conditions (effect of reaction temperature, reaction time, biomass/water ratio, and catalyst). In the future work the CatLiq® process should be carried out in (250ml-1L) stainless steel autoclave with magnetic stirrer, which allows fast, safe, cheap and efficient experimentation. Detailed description of the technique has been presented by (Zhong and Wei 2004; Qu *et al.* 2003; Qian *et al.* 2007).

II. A heat exchange network should be constructed through Pinch technology (Ebrahim and Kawari 2000) in order to heat up the feedstock stream to a temperature as high as possible by recovering the available process heat as much as possible. The feedstock can be heated by exchanging the heat between the liquid-liquid mixture from the reactor output stream and the feedstock stream. The water can be recycled into pre-conversion step after the separation of bio-oil and removal of dissolved organics from it.

III. Many potential product applications can be identified. For the short term especially the co-combustion in a power station is considered for heat and power. Flash experiments should be performed for the possibility to separate the CatLiq® bio-oil in a

clean top product for high grade applications and a residue for replacing coal in power stations to raise green electricity.

APPENDIX: MatLab coding work

```
%this program is a set of linked function m-files into
this central m-file
%It is currently set to calculate phase equilibria for a
five component
%mixture
%pos 1 corresponds to CO2
%pos 2 corresponds to H2O
%pos 3 corresponds to EtOH
%pos 4 corresponds to ActA
%pos 5 corresponds to Hdec

%housekeeping
clear; close all; clc; format short g

%Initial mol fractions
x=[0.06 0.9556 0.00044 0.0033 0.01125];
%check
c1=sum(x);

if c1==1
else
    disp('Initial Mol fractions do NOT add to 1 doh!')
    disp(' ')
    disp('-----------------------------------------')
    disp(' ')
    disp('Press any key to continue, ctrl <c>, quits')
    pause
    disp(' ')
    disp('-----------------------------------------')
end

%useful constants
R= 8.314; % R = 8.314 cm3.MPa/mol.K
Tref=313.15; %reference temperature in K
Tcr = [304.2 647.3 516.2 592.71 716.01];  % Temp =
Critical Temp K.
Pcr = [7.38 22.05 6.38 5.786 2.735];  % Pressure =
Critical Pressure MPa.
w = [0.228 0.462 0.7653];  % Acentric Factors.
C_1 = [1.0783 1.3327]; % Mathias Copeman Constants.
C_2 = [-0.5832 0.9695];
C_3 = [0.5462 -3.1879];
A = [22.3652 23.4416 23.6238 21.6472 17.5659]; % Antoine
Equation Constants.
B = [1984.41 3968.82 3828.00 3054.72 4274.24];
```

```
C = [-1.267 -40.074 -35.019 -89.237 -111.329];
%find vapour pressure via antoine
Pvap=fantoine(A,B,C,Tref);
Pvap_MPA=Pvap*1e-6;

%find ai and bi values for EOS
[ai, bi]=faibi(Tref,Tcr,Pcr,C_1,C_2,C_3,R,w);
%find bm corrections
bmL=fbm(x,bi);

%liquid fugacity data from UNIFAC model
z=10; %co-ordination number

tolerance = 1;
sum_y_prime = 1;
while (tolerance >= 0.1)
[FL, y_est, P_Bub, Gamma_L,
G_EL]=funifac_liquid_v2(x,Tref,z,R,ai,bi,bmL,Pvap_MPA,sum_
y_prime);

% To show the valuse of LIQUID.
FL = FL
Gamma_L = Gamma_L
G_EL = G_EL


%Vapour fugactiy data from UNIFAC model
bmV=fbm(y_est,bi);
[FV, Gamma_V,
G_EV]=funifac_vapour(y_est,x,Tref,R,ai,bi,bmV,P_Bub);

% To show the valuse of VAPOUR.
FV = FV
Gamma_V = Gamma_V
G_EV = G_EV

y_1=y_est;

y_prime=y_est.*FL./FV

y_2=y_prime/sum(y_prime);

current_error=sum(abs(y_2-y_1))

abs_tol=0.1
i=0;
```

```
while current_error >= abs_tol
    if i>=2

        disp('iteration limit reached without making
tolerance')
        disp(' ')
        disp('press <ctrl> c to quit, press enter to
continue (will use current value of y)')
        pause
        current_error
        current_error=0;
    else
        y_1= y_prime;
        bmV=fbm(y_1,bi);
        FV=funifac_vapour(y_1,x,Tref,R,ai,bi,bmV,P_Bub)
        y_prime=y_1.*FL./FV
        y_2=y_prime/sum(y_prime);
        current_error=sum(abs(y_2-y_1));
        i=i+1;
    end
end

sum_y_prime = sum(y_prime);
if (sum_y_prime)== 1;
    final_result=sum_y_prime
else
    mid_result = sum_y_prime
    final_P_Bub = P_Bub
    tolerance = abs(1-sum_y_prime)
end
end
```

```
function P_vap=fantoine(A,B,C,Tref)

P_vap=exp(A - (B./(C+Tref)));
```

```
function [ai, bi]=faibi(Tref,Tcrit,Pcrit,C_1,C_2,C_3,R,w)

Tr=Tref./Tcrit;

j = 1;
t1= 0.48508 + 1.5517*w - 0.15613*w.^2;
for i= 1:5
    if(i == 1 || i == 4 || i == 5)
        fT(i)=(1 + t1(j).*(1 - sqrt(Tr(i)))).^2;
%finds f(Ti) using simple form
        j=j+1;
    else
        %finds fTi for compounds 1 to Length(C_1) using
more complex data fit
        fT(i)=(1 + C_1(i-1)*(1 - sqrt(Tr(i)))+C_2(i-1)*(1
- sqrt(Tr(i))).^2+C_3(i-1)*(1 - sqrt(Tr(i))).^3).^2;
    end
end

%finds ai
ai = 0.42748 * ((R.^2 * Tcrit.^2)./Pcrit).* fT;

%finds bi
bi= 0.08664 * (R * Tcrit)./Pcrit;
```

```
function y=fbm(x,bi)

y=sum(x.*bi);
```

```
function [FL, y, P_Bub, Gamma_L,
G_EL]=funifac_liquid_v2(x,T,z,R,ai,bi,bmL,Pvap_MPA,yprime_
sum)

r = [1.300 0.9200 2.5755 2.2024 6.2488]; % Molecular Van
der Walls Volume parameter by Bondi Method
r_prime = [1.300 0.9200 2.5755 2.2024 4.1135]; % Molecular
Van der Walls Volume parameter by Bondi Method for large
molecule
q = [0.982 1.4 2.588 2.072 5.312]; % Molecular Van der
Walls Surface area parameter by Bondi Method
q1 = -0.64663; % Mixing Rule Constant by Michelsen for
PSRK EoS


%%%%%%%%%%%%%%%% Finding Combinatorial term gamma of
UNIFAC %%%%%%%%%%%%%%%%

% Initializations for theta Phi Prime & Phi from
Combinatorial Term of UNIFAC

Phi_i=x.*r./(sum(x.*r));

Phi_ip=x.*r_prime./(sum(x.*r_prime));

Theta_i=x.*q./(sum(x.*q));

t1=Phi_ip./x;
t2=Phi_i./Theta_i;
ln_gemaCL=log(t1)+1-t1-(z/2)*(q.*(log(t2)+1-t2));

%%%%%%%%%%%%%%%% Finding Residual term gamma of UNIFAC
%%%%%%%%%%%%%%%%

%%%%%%%%%%%%%%%% Interaction Parameters CO2=56, H2O=7,
CH2=1, OH=5, COOH=20 %%%%%%%%%%%%%%%%

a56_7 = 1720.6000; b56_7 = -4.3437; c56_7 = 0.001310;
a7_56 = -1163.5000; b7_56 = 5.4765; c7_56 = -0.002603;
a56_1 = -38.672; b56_1 = 0.86149; c56_1 = 1791;
a1_56 = 919.80; b1_56 = -3.9132; c1_56 = 4631;
a56_5 = 148.1600; a5_56 = 510.6400;
a56_20 = 50.3490; a20_56 = 73.8590;

a7_1 = 300.0; a1_7 = 1318;
a7_5 = -229.1; a5_7 = 353.5;
```

```
a7_20 = -14.09; a20_7 = -66.17;

a1_5 = 986.5; a5_1 = 156.4;
a1_20 = 663.5; a20_1 = 315.3;

a5_20 = 199.0; a20_5 = -151.0;

%%%%%%%%%%%%%%%% Final values for parameters
%%%%%%%%%%%%%%%%

psi56_7 = exp(-((a56_7 + (b56_7 * T) + (c56_7 *
T.^2))/T)); psi7_56 = exp(-((a7_56 + (b7_56 * T) + (c7_56
* T.^2))/T));
psi56_1 = exp(-((a56_1 + (b56_1 * T) + (c56_1 *
T.^2))/T)); psi1_56 = exp(-((a1_56 + (b1_56 * T) + (c1_56
* T.^2))/T));

psi56_5 = exp(-(a56_5/T)); psi5_56 = exp(-(a5_56/T));
psi56_20 = exp(-(a56_20/T)); psi20_56 = exp(-(a20_56/T));

psi7_1 = exp(-(a7_1/T)); psi1_7 = exp(-(a1_7/T));
psi7_5 = exp(-(a7_5/T)); psi5_7 = exp(-(a5_7/T));
psi7_20 = exp(-(a7_20/T)); psi20_7 = exp(-(a20_7/T));

psi1_5 = exp(-(a1_5/T)); psi5_1 = exp(-(a5_1/T));
psi1_20 = exp(-(a1_20/T)); psi20_1 = exp(-(a20_1/T));

psi5_20 = exp(-(a5_20/T)); psi20_5 = exp(-(a20_5/T));

%%%%%%%%%%%%%%%% Pure compound Residual Activity
%%%%%%%%%%%%%%%%%%%%%%%%%%%%%%%%
%%%%%% Molecular Van der Walls Surface area parameter
Q_56 = 0.982;    Q_7 = 1.4; Q_1A = 0.8480; Q_1B = 0.540;
Q_5 = 1.2; Q_20 = 1.224;

X56_CO2_struc = 1/1; X56_CO2 = 1;

X7_H2O_struc = 1/1; X7_H2O = 1;

X1A_EtOH_struc = 1/3; X1A_EtOH = 1/3; X1B_EtOH = 1/3;
X5_EtOH = 1/3;

X1A_ActA_struc = 1/2; X1A_ActA = 0.5; X20_ActA = 0.5;

X1A_Hdec_struc = 1/3; X1A_Hdec = 0.333; X1B_Hdec = 6/3;
X20_Hdec = 0.333;
```

```
Theta56_CO2 = (Q_56 * X56_CO2)/(Q_56 * X56_CO2);

Theta7_H2O = (Q_7 * X7_H2O)/(Q_7 * X7_H2O);

Theta1A_EtOH = (Q_1A * X1A_EtOH)/((Q_1A * X1A_EtOH)+(Q_1B
* X1B_EtOH)+(Q_5 * X5_EtOH));
Theta1B_EtOH = (Q_1B * X1B_EtOH)/((Q_1A * X1A_EtOH)+(Q_1B
* X1B_EtOH)+(Q_5 * X5_EtOH));
Theta5_EtOH = (Q_5 * X5_EtOH)/((Q_1A * X1A_EtOH)+(Q_1B *
X1B_EtOH)+(Q_5 * X5_EtOH));

Theta1A_ActA = (Q_1A * X1A_ActA)/((Q_1A * X1A_ActA)+(Q_20
* X20_ActA));
Theta20_ActA = (Q_20 * X20_ActA)/((Q_1A * X1A_ActA)+(Q_20
* X20_ActA));

Theta1A_Hdec = (Q_1A * X1A_Hdec)/((Q_1A * X1A_Hdec)+(Q_1B
* X1B_Hdec)+(Q_20 * X20_Hdec));
Theta1B_Hdec = (Q_1B * X1B_Hdec)/((Q_1A * X1A_Hdec)+(Q_1B
* X1B_Hdec)+(Q_20 * X20_Hdec));
Theta20_Hdec = (Q_20 * X20_Hdec)/((Q_1A * X1A_Hdec)+(Q_1B
* X1B_Hdec)+(Q_20 * X20_Hdec));

ln_TA56_CO2 = Q_56*(-log(Theta56_CO2));

ln_TA7_H2O = Q_7*(-log(Theta7_H2O));

ln_TA1A_EtOH = Q_1A*(1-log(Theta1A_EtOH + (Theta5_EtOH *
psi5_1))-...
    (Theta1A_EtOH/(Theta1A_EtOH + (Theta5_EtOH * psi5_1))
+...
    (Theta5_EtOH * psi1_5)/((Theta1A_EtOH * psi1_5) +
Theta5_EtOH)));
ln_TA1B_EtOH = Q_1B*(1-log(Theta1B_EtOH + (Theta5_EtOH *
psi5_1))-...
    (Theta1B_EtOH/(Theta1B_EtOH + (Theta5_EtOH * psi5_1))
+ ...
    (Theta5_EtOH * psi1_5)/((Theta1B_EtOH * psi1_5) +
Theta5_EtOH)));
ln_TA5_EtOH = Q_5*(1-log((Theta1A_EtOH * psi1_5)+
(Theta1B_EtOH * psi1_5)...
    + Theta5_EtOH)-((Theta1A_EtOH * psi5_1) + ...
    (Theta1B_EtOH * psi5_1)/(Theta1A_EtOH + (Theta5_EtOH *
psi5_1)) + ...
    (Theta1B_EtOH + (Theta5_EtOH * psi5_1)) +
(Theta5_EtOH)/((Theta1A_EtOH * psi1_5) + ...
```

```
    (Theta1B_EtOH * psi1_5) + Theta5_EtOH)));

ln_TA1A_ActA = Q_1A*(1-log(Theta1A_ActA + (Theta20_ActA *
psi20_1))-...
    (Theta1A_ActA/(Theta1A_ActA + (Theta20_ActA *
psi20_1)) + ...
    (Theta20_ActA * psi1_20)/((Theta1A_ActA * psi1_20) +
Theta20_ActA)));
ln_TA20_ActA = Q_20*(1-log((Theta1A_ActA * psi1_20) +
Theta20_ActA )-...
    ((Theta1A_ActA * psi20_1)/(Theta1A_ActA +
(Theta20_ActA * psi20_1)) + ...
    (Theta20_ActA)/((Theta1A_ActA * psi1_20) +
Theta20_ActA)));

ln_TA1A_Hdec = Q_1A*(1-log(Theta1A_Hdec + (Theta20_Hdec *
psi20_1))-...
    (Theta1A_Hdec/(Theta1A_Hdec + (Theta20_Hdec *
psi20_1)) + ...
    (Theta20_Hdec * psi1_20)/((Theta1A_Hdec * psi1_20) +
Theta20_Hdec)));
ln_TA1B_Hdec = Q_1B*(1-log(Theta1B_Hdec + (Theta20_Hdec *
psi20_1))-...
    (Theta1B_Hdec/(Theta1B_Hdec + (Theta20_Hdec *
psi20_1)) + ...
    (Theta20_Hdec * psi1_20)/((Theta1B_Hdec * psi1_20) +
Theta20_Hdec)));
ln_TA20_Hdec = Q_20*(1-log((Theta1A_Hdec * psi1_20)+
(Theta1B_Hdec * psi1_20)...
    + Theta20_Hdec)-((Theta1A_Hdec * psi20_1) + ...
    (Theta1B_Hdec * psi20_1)/(Theta1A_Hdec + (Theta20_Hdec
* psi20_1)) + ...
    (Theta1B_Hdec + (Theta20_Hdec * psi20_1)) +
(Theta20_Hdec)/((Theta1A_Hdec * psi1_20)...
    + (Theta1B_Hdec * psi1_20) + Theta20_Hdec)));

%%%%%%%%%%%%%%% Group Residual Activity
%%%%%%%%%%%%%%%%%%%%%%%%%%%%%%%%%%%%%%%%%%%%%%%%

v_i = [1 1 3 2 8]; % Number of Structural Groups
% Types of Structural Groups
v_56 = 1;  v_7 = 1; v_1A = 1; v_1B = 6; v_5 = 1; v_20 = 1;

denominator_X = sum(x.*v_i);

X_56 = v_56 * 0.06 / denominator_X;
```

```
X_7 = v_7 * 0.9556 / denominator_X;

X_1A = (v_1A * 0.00044)+(v_1A * 0.00033)+(v_1A * 0.01125)
/ denominator_X;

X_1B = (v_1A * 0.00044)+(v_1B * 0.01125) / denominator_X;

X_5 = v_5 * 0.00044 / denominator_X;

X_20 = (v_20 * 0.00033)+(v_20 * 0.01125) / denominator_X;

Q_X = (Q_56 * X_56)+(Q_7 * X_7)+(Q_1A * X_1A)+(Q_1B *
X_1B)+(Q_5 * X_5)+(Q_20 * X_20);

Theta_56 = (Q_56 * X_56)/Q_X;

Theta_7 = (Q_7 * X_7)/Q_X;

Theta_1A = (Q_1A * X_1A)/Q_X;

Theta_1B = (Q_1B * X_1B)/Q_X;

Theta_5 = (Q_5 * X_5)/Q_X;

Theta_20 = (Q_20 * X_20)/Q_X;

ln_TA56 = Q_56*(1-
log(Theta_56+(Theta_7*psi7_56)+(Theta_1A*psi1_56)+...

(Theta_1B*psi1_56)+(Theta_5*psi5_56)+(Theta_20*psi20_56))-
...

((Theta_56/(Theta_56+(Theta_7*psi7_56)+(Theta_1A*psi1_56)+
...

(Theta_1B*psi1_56)+(Theta_5*psi5_56)+(Theta_20*psi20_56)))
+...

((Theta_7*psi56_7)+(Theta_1A*psi56_1)+(Theta_1B*psi56_1)+(
Theta_5*psi56_5)+...
    (Theta_20*psi56_20)/((Theta_56 * psi56_7) +
Theta_7)+((Theta_56 * psi56_1) + Theta_1A)+...
    ((Theta_56 * psi56_1) + Theta_1B)+((Theta_56 *
psi56_5) + Theta_5)+((Theta_56 * psi56_20) + Theta_20))));
```

```
ln_TA7 = Q_7*(1-
log(Theta_7+(Theta_56*psi56_7)+(Theta_1A*psi1_7)+(Theta_1B
*psi1_7)+(Theta_5*psi5_7)+...
    (Theta_20*psi20_7))-
((Theta_7/(Theta_7+(Theta_56*psi56_7)+(Theta_1A*psi1_7)+(T
heta_1B*psi1_7)+...

(Theta_5*psi5_7)+(Theta_20*psi20_7)))+((Theta_56*psi7_56)+
(Theta_1A*psi7_1)+(Theta_1B*psi7_1)+...
    (Theta_5*psi7_5)+(Theta_20*psi7_20)/((Theta_7 *
psi7_56) + Theta_56)+((Theta_7 * psi7_1) + Theta_1A)...
    +((Theta_7 * psi7_1) + Theta_1B)+((Theta_7 * psi7_5) +
Theta_5)+((Theta_7 * psi7_20) + Theta_20))));

ln_TA1AEt = Q_1A*(1-
log(Theta_1A+(Theta_56*psi56_1)+(Theta_7*psi7_1)+(Theta_5*
psi5_1)+(Theta_20*psi20_1))...
    -
((Theta_1A/(Theta_1A+(Theta_56*psi56_1)+(Theta_7*psi7_1)+(
Theta_5*psi5_1)+(Theta_20*psi20_1)))+...

((Theta_56*psi1_56)+(Theta_7*psi1_7)+(Theta_5*psi1_5)+(The
ta_20*psi1_20)/((Theta_1A * psi1_56) + Theta_56)...
    +((Theta_1A * psi1_7) + Theta_7)+((Theta_1A * psi1_5)
+ Theta_5)+((Theta_1A * psi1_20) + Theta_20))));
ln_TA1BEt = Q_1B*(1-
log(Theta_1B+(Theta_56*psi56_1)+(Theta_7*psi7_1)+(Theta_5*
psi5_1)+(Theta_20*psi20_1))...
    -
((Theta_1B/(Theta_1B+(Theta_56*psi56_1)+(Theta_7*psi7_1)+(
Theta_5*psi5_1)+(Theta_20*psi20_1)))+...

((Theta_56*psi1_56)+(Theta_7*psi1_7)+(Theta_5*psi1_5)+(The
ta_20*psi1_20)/((Theta_1B * psi1_56) + Theta_56)...
    +((Theta_1B * psi1_7) + Theta_7)+((Theta_1B * psi1_5)
+ Theta_5)+((Theta_1B * psi1_20) + Theta_20))));
ln_TA5Et = Q_5*(1-
log(Theta_5+(Theta_56*psi56_5)+(Theta_7*psi7_5)+((Theta_1A
+Theta_1B)*psi1_5)+...
    (Theta_20*psi20_5))-
(((Theta_56*psi5_56)+(Theta_7*psi5_7)+((Theta_1A+Theta_1B)
*psi5_1)+(Theta_20*psi5_20)...

/(Theta_1A+(Theta_56*psi56_1)+(Theta_7*psi7_1)+(Theta_5*ps
i5_1)+(Theta_20*psi20_1)))+...
    ((Theta_5)/((Theta_1A * psi1_56) +
Theta_56)+((Theta_1A * psi1_7) + Theta_7)+((Theta_1A *
psi1_5) + Theta_5)...
```

```
    +((Theta_1A * psi1_20) + Theta_20))));

ln_TA1AAc = ln_TA1AEt;
ln_TA20Ac = Q_20*(1-
log(Theta_20+(Theta_56*psi56_20)+(Theta_7*psi7_20)+((Theta
_1A+Theta_1B)*psi1_20)+...
    (Theta_5*psi5_20))-
(((Theta_56*psi20_56)+(Theta_7*psi20_7)+((Theta_1A+Theta_1
B)*psi20_1)+(Theta_5*psi20_5)...

/(Theta_1A+(Theta_56*psi56_1)+(Theta_7*psi7_1)+(Theta_5*ps
i5_1)+(Theta_20*psi20_1)))+((Theta_20)...
    /((Theta_1A * psi1_56) + Theta_56)+((Theta_1A *
psi1_7) + Theta_7)+((Theta_1A * psi1_5) + Theta_5)...
    +((Theta_1A * psi1_20) + Theta_20))));

ln_TA1AHd = ln_TA1AEt;
ln_TA1BHd = ln_TA1BEt;
ln_TA20Hd = ln_TA20Ac;

%%%%%%%%%%%%%%% Total Residual Activity
%%%%%%%%%%%%%%%%%%%%%%%%%%%%%%%%%%%%%%%%%%%%%%%%%%%

ln_gammaR_CO2 = 1* (ln_TA56 - ln_TA56_CO2);
ln_gammaR_H2O = 1* (ln_TA7 - ln_TA7_H2O);
ln_gammaR_EtOH = 1* (ln_TA1AEt - ln_TA1A_EtOH)+1*
(ln_TA1BEt - ln_TA1B_EtOH)+1* (ln_TA5Et - ln_TA5_EtOH);
ln_gammaR_ActA = 1* (ln_TA1AAc - ln_TA1A_ActA)+1*
(ln_TA20Ac - ln_TA20_ActA);
ln_gammaR_Hdec = 1* (ln_TA1AHd - ln_TA1A_Hdec)+14*
(ln_TA1BHd - ln_TA1B_Hdec)+1* (ln_TA20Hd - ln_TA20_Hdec);

ln_gammaR_L=[ln_gammaR_CO2 ln_gammaR_H2O ln_gammaR_EtOH
ln_gammaR_ActA ln_gammaR_Hdec];

%%%%%%%%%%%%%%% Final Activity
%%%%%%%%%%%%%%%%%%%%%%%%%%%%%%%%%%%%%%%%%%%%%%%%%%%
Gamma_L=(ln_gemaCL+ln_gammaR_L);

%%%%%%%%%%%%%%% Excess Gibbs Free Energy
%%%%%%%%%%%%%%%%%%%%%%%%%%%%%%

G_EL = R*T*sum(x.*Gamma_L);

%%%%%%%%%%%%%% START OF FUGACITY F_L FOR LIQUID PHASE
THROUGH PSRK EoS %%%%%%%%%%%%%%
```

```
part_1 = sum(x.*ai./bi);
part_2 = R*T*sum(x.*log(bmL./bi));

%%%%%%%%%%%%%%%% Finding mixture co-energy parameter am
%%%%%%%%%%%%%%%

am_equ_L = bmL*( part_1 + (1/q1*(G_EL + part_2)));

%%%%%%%%%%%%%%%%%%%%%%%%%%%%%%%%%%%%%%%%%%%%%%%%%%%%

P_Bub = (sum(x.*Pvap_MPA))*yprime_sum;
K=Pvap_MPA/P_Bub;
y=K.*x;
A = (P_Bub * am_equ_L) / (R^2 * T^2);
B = (P_Bub * bmL) / (R * T);

Zi = B*1.03;
abs_tol=1e-8; %required tolerance for iteration loop to
find Z
Z(1)=Zi;
f_Z = (Z.^3) - (Z.^2) + Z*(A - B - (B.^2)) - (A*B);
f_der_Z = 3*Z.^2 - 2*Z + (A - B- B.^2);
Z(2)=Z(1)-f_Z/f_der_Z;
cur_err=abs(Z(2)-Z(1));
i=0;
while cur_err>abs_tol
    if i>=100
        disp('iteration limit reached without making
tolerance')
        disp(' ')
        disp('press <ctrl> c to quit, press enter to
continue (will use current value of Z)')
        pause
        cur_err
        cur_err=0;
    else
    Z(1)=Z(2);
    f_Z = (Z(1).^3) - (Z(1).^2) + Z(1)*(A - B - (B.^2)) -
(A*B);
    f_der_Z = 3*Z(1).^2 - 2*Z(1) + (A - B- B.^2);
    Z(2)=Z(1)-f_Z/f_der_Z;
    cur_err=abs(Z(2)-Z(1));
    i=i+1;
    end
end
Z=Z(2);
```

```
alpha_L = am_equ_L/((bmL)*R*T);

alpha = ai./(bi*R*T);

Part_L=(1/q1)*(   (alpha*q1)+ Gamma_L+(log(bmL./bi)) +
(bi/bmL) - 1) ;

%%%%%%%%%%%%%%%% Fugacity Coefficient for Liquid Phase
%%%%%%%%%%%%%%%%%%%%%%%%%%%%%%%%

t1=Z-B; t2=P_Bub/(R*T); t3=alpha_L*t2; t4=Z+B; t5=t4/Z;

Fc_L =  (1/t1).* ( exp( bi.*(  (t2/t1) - (t3/t4) )) ) ./
exp( Part_L.*log(t5));

%%%%%%%%%%%%%%%% Fugacity for Liquid Phase
%%%%%%%%%%%%%%%%%%%%%%%%%%%%%%%%%%%%%%%%%%%%%%%%%%%%%%%
FL=x.*Fc_L.*P_Bub;
```

```
function [FV, Gamma_V,
G_EV]=funifac_vapour(y,x,T,R,ai,bi,bmV,P_Bub)
z =10;    % Coordination number
r = [1.300 0.9200 2.5755 2.2024 6.2488]; % Molecular Van
der Walls Volume parameter by Bondi Method
r_prime = [1.300 0.9200 2.5755 2.2024 4.1135]; % Molecular
Van der Walls Volume parameter by Bondi Method for large
molecule
q = [0.982 1.4 2.588 2.072 5.312]; % Molecular Van der
Walls Surface area parameter by Bondi Method
q1 = -0.64663; % Mixing Rule Constant by Michelsen for
PSRK EoS

%%%%%%%%%%%%%%%% Finding Combinatorial term gamma of
UNIFAC %%%%%%%%%%%%%%%%
% Initializations for theta Phi Prime & Phi from
Combinatorial Term of UNIFAC

Phi_Prime_V=y.*r_prime./sum(y.*r_prime);

Phi_V=y.*r./sum(y.*r);

Theta_V=y.*q./sum(y.*q);

ln_gemaCV = log(Phi_Prime_V./y) + 1 - (Phi_Prime_V./y) -
(z/2)*(q.*((log(Phi_V./Theta_V)) + 1 - (Phi_V./Theta_V)));



%%%%%%%%%%%%%%%% Finding Residual term gamma of UNIFAC
%%%%%%%%%%%%%%%%

%%%%%%%%%%%%%%%% Interaction Parameters CO2=56, H2O=7,
CH2=1, OH=5, COOH=20 %%%%%%%%%%%%%%%%

a56_7 = 1720.6000; b56_7 = -4.3437; c56_7 = 0.001310;
a7_56 = -1163.5000; b7_56 = 5.4765; c7_56 = -0.002603;
a56_1 = -38.672; b56_1 = 0.86149; c56_1 = 1791;
a1_56 = 919.80; b1_56 = -3.9132; c1_56 = 4631;
a56_5 = 148.1600; a5_56 = 510.6400;
a56_20 = 50.3490; a20_56 = 73.8590;

a7_1 = 300.0; a1_7 = 1318;
a7_5 = -229.1; a5_7 = 353.5;
a7_20 = -14.09; a20_7 = -66.17;

a1_5 = 986.5; a5_1 = 156.4;
```

```
a1_20 = 663.5; a20_1 = 315.3;

a5_20 = 199.0; a20_5 = -151.0;

%%%%%%%%%%%%%%%% Final values for parameters
%%%%%%%%%%%%%%%

psi56_7 = exp(-((a56_7 + (b56_7 * T) + (c56_7 *
T.^2))/T)); psi7_56 = exp(-((a7_56 + (b7_56 * T) + (c7_56
* T.^2))/T));
psi56_1 = exp(-((a56_1 + (b56_1 * T) + (c56_1 *
T.^2))/T)); psi1_56 = exp(-((a1_56 + (b1_56 * T) + (c1_56
* T.^2))/T));

psi56_5 = exp(-(a56_5/T)); psi5_56 = exp(-(a5_56/T));
psi56_20 = exp(-(a56_20/T)); psi20_56 = exp(-(a20_56/T));

psi7_1 = exp(-(a7_1/T)); psi1_7 = exp(-(a1_7/T));
psi7_5 = exp(-(a7_5/T)); psi5_7 = exp(-(a5_7/T));
psi7_20 = exp(-(a7_20/T)); psi20_7 = exp(-(a20_7/T));

psi1_5 = exp(-(a1_5/T)); psi5_1 = exp(-(a5_1/T));
psi1_20 = exp(-(a1_20/T)); psi20_1 = exp(-(a20_1/T));

psi5_20 = exp(-(a5_20/T)); psi20_5 = exp(-(a20_5/T));

%%%%%%%%%%%%%%%% Pure compound Residual Activity
%%%%%%%%%%%%%%%%%%%%%%%%%%%%%%%%%%
% Molecular Van der Walls Surface area parameter
Q_56 = 0.982;  Q_7 = 1.4; Q_1A = 0.8480; Q_1B = 0.540; Q_5
= 1.2; Q_20 = 1.224;

X56_CO2_struc = 1/1; X56_CO2 = 1;

X7_H2O_struc = 1/1; X7_H2O = 1;

X1A_EtOH_struc = 1/3; X1A_EtOH = 0.333; X1B_EtOH = 0.333;
X5_EtOH = 0.333;

X1A_ActA_struc = 1/2; X1A_ActA = 0.5; X20_ActA = 0.5;

X1A_Hdec_struc = 1/3; X1A_Hdec = 0.333; X1B_Hdec = 2.0;
X20_Hdec = 0.333;

Theta56_CO2 = (Q_56 * X56_CO2)/(Q_56 * X56_CO2);
```

```
Theta7_H2O = (Q_7 * X7_H2O)/(Q_7 * X7_H2O);

Theta1A_EtOH = (Q_1A * X1A_EtOH)/((Q_1A * X1A_EtOH)+(Q_1B
* X1B_EtOH)+(Q_5 * X5_EtOH));
Theta1B_EtOH = (Q_1B * X1B_EtOH)/((Q_1A * X1A_EtOH)+(Q_1B
* X1B_EtOH)+(Q_5 * X5_EtOH));
Theta5_EtOH = (Q_5 * X5_EtOH)/((Q_1A * X1A_EtOH)+(Q_1B *
X1B_EtOH)+(Q_5 * X5_EtOH));

Theta1A_ActA = (Q_1A * X1A_ActA)/((Q_1A * X1A_ActA)+(Q_20
* X20_ActA));
Theta20_ActA = (Q_20 * X20_ActA)/((Q_1A * X1A_ActA)+(Q_20
* X20_ActA));

Theta1A_Hdec = (Q_1A * X1A_Hdec)/((Q_1A * X1A_Hdec)+(Q_1B
* X1B_Hdec)+(Q_20 * X20_Hdec));
Theta1B_Hdec = (Q_1B * X1B_Hdec)/((Q_1A * X1A_Hdec)+(Q_1B
* X1B_Hdec)+(Q_20 * X20_Hdec));
Theta20_Hdec = (Q_20 * X20_Hdec)/((Q_1A * X1A_Hdec)+(Q_1B
* X1B_Hdec)+(Q_20 * X20_Hdec));


ln_TA56_CO2 = Q_56*(1-log(Theta56_CO2)-
(Theta56_CO2/Theta56_CO2));

ln_TA7_H2O = Q_7*(1-log(Theta7_H2O)-
(Theta7_H2O/Theta7_H2O));

ln_TA1A_EtOH = Q_1A*(1-log(Theta1A_EtOH + (Theta5_EtOH *
psi5_1))-(Theta1A_EtOH/...
    (Theta1A_EtOH + (Theta5_EtOH * psi5_1)) + (Theta5_EtOH
* psi1_5)/((Theta1A_EtOH * psi1_5) + Theta5_EtOH)));
ln_TA1B_EtOH = Q_1B*(1-log(Theta1B_EtOH + (Theta5_EtOH *
psi5_1))-(Theta1B_EtOH/...
    (Theta1B_EtOH + (Theta5_EtOH * psi5_1)) + (Theta5_EtOH
* psi1_5)/((Theta1B_EtOH * psi1_5) + Theta5_EtOH)));
ln_TA5_EtOH = Q_5*(1-log((Theta1A_EtOH * psi1_5)+
(Theta1B_EtOH * psi1_5) + Theta5_EtOH)-...
    ((Theta1A_EtOH * psi5_1) + (Theta1B_EtOH *
psi5_1)/(Theta1A_EtOH + (Theta5_EtOH * psi5_1)) +...
    (Theta1B_EtOH + (Theta5_EtOH * psi5_1)) +
(Theta5_EtOH)/((Theta1A_EtOH * psi1_5) + (Theta1B_EtOH *
psi1_5)...
    + Theta5_EtOH)));
```

```
ln_TA1A_ActA = Q_1A*(1-log(Theta1A_ActA + (Theta20_ActA *
psi20_1))-(Theta1A_ActA/(Theta1A_ActA +...
    (Theta20_ActA * psi20_1)) + (Theta20_ActA *
psi1_20)/((Theta1A_ActA * psi1_20) + Theta20_ActA)));
ln_TA20_ActA = Q_20*(1-log((Theta1A_ActA * psi1_20) +
Theta20_ActA )-((Theta1A_ActA * psi20_1)/...
    (Theta1A_ActA + (Theta20_ActA * psi20_1)) +
(Theta20_ActA)/((Theta1A_ActA * psi1_20) +
Theta20_ActA)));

ln_TA1A_Hdec = Q_1A*(1-log(Theta1A_Hdec + (Theta20_Hdec *
psi20_1))-(Theta1A_Hdec/...
    (Theta1A_Hdec + (Theta20_Hdec * psi20_1)) +
(Theta20_Hdec * psi1_20)/((Theta1A_Hdec * psi1_20) +
Theta20_Hdec)));
ln_TA1B_Hdec = Q_1B*(1-log(Theta1B_Hdec + (Theta20_Hdec *
psi20_1))-(Theta1B_Hdec/...
    (Theta1B_Hdec + (Theta20_Hdec * psi20_1)) +
(Theta20_Hdec * psi1_20)/((Theta1B_Hdec * psi1_20) +
Theta20_Hdec)));
ln_TA20_Hdec = Q_20*(1-log((Theta1A_Hdec * psi1_20)+
(Theta1B_Hdec * psi1_20) + Theta20_Hdec)-...
    ((Theta1A_Hdec * psi20_1) + (Theta1B_Hdec *
psi20_1)/(Theta1A_Hdec + (Theta20_Hdec * psi20_1)) +...
    (Theta1B_Hdec + (Theta20_Hdec * psi20_1)) +
(Theta20_Hdec)/((Theta1A_Hdec * psi1_20) +...
    (Theta1B_Hdec * psi1_20) + Theta20_Hdec)));

%%%%%%%%%%%%%%% Group Residual Activity
%%%%%%%%%%%%%%%%%%%%%%%%%%%%%%%%%%%%%%%%%%%%%%%%%%%

v_i = [1 1 3 2 8]; % Number of Structural Groups
% Types of Structural Groups
v_56 = 1;  v_7 = 1; v_1A = 1; v_1B = 6; v_5 = 1; v_20 = 1;

denominator_X_V = sum(y.*v_i);

X_56V = v_56 * 0.06 / denominator_X_V;

X_7V = v_7 * 0.9556 / denominator_X_V;

X_1AV = (v_1A * 0.00044)+(v_1A * 0.00033)+(v_1A * 0.01125)
/ denominator_X_V;

X_1BV = (v_1A * 0.00044)+(v_1B * 0.01125) /
denominator_X_V;
```

```
X_5V = v_5 * 0.00044 / denominator_X_V;

X_20V = (v_20 * 0.00033)+(v_20 * 0.01125) /
denominator_X_V;

Q_XV = (Q_56 * X_56V)+(Q_7 * X_7V)+(Q_1A * X_1AV)+(Q_1B *
X_1BV)+(Q_5 * X_5V)+(Q_20 * X_20V);

Theta_56V = (Q_56 * X_56V)/Q_XV;

Theta_7V = (Q_7 * X_7V)/Q_XV;

Theta_1AV = (Q_1A * X_1AV)/Q_XV;

Theta_1BV = (Q_1B * X_1BV)/Q_XV;

Theta_5V = (Q_5 * X_5V)/Q_XV;

Theta_20V = (Q_20 * X_20V)/Q_XV;


ln_TA56V = Q_56*(1-
log(Theta_56V+(Theta_7V*psi7_56)+(Theta_1AV*psi1_56)+(Thet
a_1BV*psi1_56)+(Theta_5V*psi5_56)...
    +(Theta_20V*psi20_56))-
((Theta_56V/(Theta_56V+(Theta_7V*psi7_56)+(Theta_1AV*psi1_
56)+(Theta_1BV*psi1_56)+...

(Theta_5V*psi5_56)+(Theta_20V*psi20_56)))+((Theta_7V*psi56
_7)+(Theta_1AV*psi56_1)+(Theta_1BV*psi56_1)+...
    (Theta_5V*psi56_5)+(Theta_20V*psi56_20)/((Theta_56V *
psi56_7) + Theta_7V)+((Theta_56V * psi56_1) +
Theta_1AV)...
    +((Theta_56V * psi56_1) + Theta_1BV)+((Theta_56V *
psi56_5) + Theta_5V)+((Theta_56V * psi56_20) +
Theta_20V))));

ln_TA7V = Q_7*(1-
log(Theta_7V+(Theta_56V*psi56_7)+(Theta_1AV*psi1_7)+(Theta
_1BV*psi1_7)+(Theta_5V*psi5_7)...
    +(Theta_20V*psi20_7))-
((Theta_7V/(Theta_7V+(Theta_56V*psi56_7)+(Theta_1AV*psi1_7
)+(Theta_1BV*psi1_7)+...

(Theta_5V*psi5_7)+(Theta_20V*psi20_7)))+((Theta_56V*psi7_5
6)+(Theta_1AV*psi7_1)+(Theta_1BV*psi7_1)+...
```

```
    (Theta_5V*psi7_5)+(Theta_20V*psi7_20)/((Theta_7V *
psi7_56) + Theta_56V)+((Theta_7V * psi7_1) + Theta_1AV)...
    +((Theta_7V * psi7_1) + Theta_1BV)+((Theta_7V *
psi7_5) + Theta_5V)+((Theta_7V * psi7_20) + Theta_20V))));

ln_TA1AEtV = Q_1A*(1-
log(Theta_1AV+(Theta_56V*psi56_1)+(Theta_7V*psi7_1)+(Theta
_5V*psi5_1)+...
    (Theta_20V*psi20_1))-
((Theta_1AV/(Theta_1AV+(Theta_56V*psi56_1)+(Theta_7V*psi7_
1)+(Theta_5V*psi5_1)...

+(Theta_20V*psi20_1)))+((Theta_56V*psi1_56)+(Theta_7V*psi1
_7)+(Theta_5V*psi1_5)+(Theta_20V*psi1_20)/...
    ((Theta_1AV * psi1_56) + Theta_56V)+((Theta_1AV *
psi1_7) + Theta_7V)+((Theta_1AV * psi1_5) + Theta_5V)+...
    ((Theta_1AV * psi1_20) + Theta_20V))));
ln_TA1BEtV = Q_1B*(1-
log(Theta_1BV+(Theta_56V*psi56_1)+(Theta_7V*psi7_1)+(Theta
_5V*psi5_1)+...
    (Theta_20V*psi20_1))-
((Theta_1BV/(Theta_1BV+(Theta_56V*psi56_1)+(Theta_7V*psi7_
1)+(Theta_5V*psi5_1)...

+(Theta_20V*psi20_1)))+((Theta_56V*psi1_56)+(Theta_7V*psi1
_7)+(Theta_5V*psi1_5)+(Theta_20V*psi1_20)/...
    ((Theta_1BV * psi1_56) + Theta_56V)+((Theta_1BV *
psi1_7) + Theta_7V)+((Theta_1BV * psi1_5) + Theta_5V)...
    +((Theta_1BV * psi1_20) + Theta_20V))));
ln_TA5EtV = Q_5*(1-
log(Theta_5V+(Theta_56V*psi56_5)+(Theta_7V*psi7_5)+((Theta
_1AV+Theta_1BV)*psi1_5)+...
    (Theta_20V*psi20_5))-
(((Theta_56V*psi5_56)+(Theta_7V*psi5_7)+((Theta_1AV+Theta_
1BV)*psi5_1)+...

(Theta_20V*psi5_20)/(Theta_1AV+(Theta_56V*psi56_1)+(Theta_
7V*psi7_1)+(Theta_5V*psi5_1)+(Theta_20V*psi20_1)))...
    +((Theta_5V)/((Theta_1AV * psi1_56) +
Theta_56V)+((Theta_1AV * psi1_7) + Theta_7V)+((Theta_1AV *
psi1_5) ...
    + Theta_5V)+((Theta_1AV * psi1_20) + Theta_20V))));

ln_TA1AAcV = ln_TA1AEtV;
ln_TA20AcV = Q_20*(1-
log(Theta_20V+(Theta_56V*psi56_20)+(Theta_7V*psi7_20)+((Th
eta_1AV+Theta_1BV)*psi1_20)+...
```

```
    (Theta_5V*psi5_20))-
(((Theta_56V*psi20_56)+(Theta_7V*psi20_7)+((Theta_1AV+Thet
a_1BV)*psi20_1)+...

(Theta_5V*psi20_5)/(Theta_1AV+(Theta_56V*psi56_1)+(Theta_7
V*psi7_1)+(Theta_5V*psi5_1)+(Theta_20V*psi20_1)))...
    +((Theta_20V)/((Theta_1AV * psi1_56) +
Theta_56V)+((Theta_1AV * psi1_7) + Theta_7V)+((Theta_1AV *
psi1_5) ...
    + Theta_5V)+((Theta_1AV * psi1_20) + Theta_20V))));

ln_TA1AHdV = ln_TA1AEtV;
ln_TA1BHdV = ln_TA1BEtV;
ln_TA20HdV = ln_TA20AcV;

%%%%%%%%%%%%%%% Total Residual Activity
%%%%%%%%%%%%%%%%%%%%%%%%%%%%%%%%%%%%%%%%%%%%%%%%%%%%

ln_gammaR_CO2V = 1* (ln_TA56V - ln_TA56_CO2);
ln_gammaR_H2OV = 1* (ln_TA7V - ln_TA7_H2O);
ln_gammaR_EtOHV = 1* (ln_TA1AEtV - ln_TA1A_EtOH)+1*
(ln_TA1BEtV - ln_TA1B_EtOH)+1* (ln_TA5EtV - ln_TA5_EtOH);
ln_gammaR_ActAV = 1* (ln_TA1AAcV - ln_TA1A_ActA)+1*
(ln_TA20AcV - ln_TA20_ActA);
ln_gammaR_HdecV = 1* (ln_TA1AHdV - ln_TA1A_Hdec)+14*
(ln_TA1BHdV - ln_TA1B_Hdec)+1* (ln_TA20HdV -
ln_TA20_Hdec);

ln_gammaR_V =[ln_gammaR_CO2V ln_gammaR_H2OV
ln_gammaR_EtOHV ln_gammaR_ActAV ln_gammaR_HdecV];

%%%%%%%%%%%%%%% Final Activity
%%%%%%%%%%%%%%%%%%%%%%%%%%%%%%%%%%%%%%%%%%%%%%%%%%%%

Gamma_V=(ln_gemaCV+ln_gammaR_V);

%%%%%%%%%%%%%%% Excess Gibbs Free Energy
%%%%%%%%%%%%%%%%%%%%%%%%%%%%%%%

G_EV = R*T*(sum(y.*Gamma_V));

%%%%%%%%%%%%%% START OF FUGACITY F_V FOR VAPOR PHASE
THROUGH PSRK EoS %%%%%%%%%%%%%%%

part_3 = sum(y.*ai./bi);
part_4 = R*T*sum(y.*log(bmV./bi));
```

```
%%%%%%%%%%%%%%% FINDING MIXTURE CO-ENERGY PARAMETER am
%%%%%%%%%%%%%%%

am_equ_V = bmV*( part_3 + 1/q1*(G_EV + part_4));

%%%%%%%%%%%%%%%%%%%%%%%%%%%%%%%%%%%%%%%%%%%%%%%%%%%%

A = (P_Bub * am_equ_V) / (R^2 * T^2);
B = (P_Bub * bmV) / (R * T);
%Newt Rhaps method to get final Z
Zi = 1;
abs_tol=1e-8; %required tolerance for iteration loop to
find Z
Z(1)=Zi;
f_Z = (Z.^3) - (Z.^2) + Z*(A - B - (B.^2)) - (A*B);
f_der_Z = 3*Z.^2 - 2*Z + (A - B- B.^2);
Z(2)=Z(1)-f_Z/f_der_Z;
cur_err=abs(Z(2)-Z(1));
i=0;
while cur_err>abs_tol
    if i>=100
        disp('iteration limit reached without making
tolerance')
        disp(' ')
        disp('press <ctrl> c to quit, press enter to
continue (will use current value of Z)')
        pause
        cur_err
        cur_err=0;
    else
    Z(1)=Z(2);
    f_Z = (Z(1).^3) - (Z(1).^2) + Z(1)*(A - B - (B.^2)) -
(A*B);
    f_der_Z = 3*Z(1).^2 - 2*Z(1) + (A - B- B.^2);
    Z(2)=Z(1)-f_Z/f_der_Z;
    cur_err=abs(Z(2)-Z(1));
    i=i+1;
    end
end
Z=Z(2);

alpha_V = am_equ_V/((bmV)*R*T);
alpha = ai./(bi*R*T);

Part_V=(1/q1) *( (alpha*q1 + Gamma_V+ log(bmV./bi) +
(bi/bmV) -1 ));
```

```
%%%%%%%%%%%%%%%% Fugacity Coefficient for Vapor Phase
%%%%%%%%%%%%%%%%%%%%%%%%%%%%%%%%

t1=Z-B; t2=P_Bub/(R*T); t3=alpha_V*t2; t4=Z+B; t5=t4/Z;
Fc_V =  (1/t1).*(  exp( bi.*(  (t2/t1) - (t3/t4) )) )./
exp(Part_V.*log(t5));

%%%%%%%%%%%%%%%% Fugacity for Vapor Phase
%%%%%%%%%%%%%%%%%%%%%%%%%%%%%%%%%%%%%%%%%%%%%%%%%%%%%%%%
FV=y.*Fc_V*P_Bub;
```

REFERENCES

Aguado, R., Olazar, M., Jose, M.J.S., Aguirre, G., Bilbao, J., 2000. Pyrolysis of sawdust in a conical spouted bed reactor. Yields and product composition. Industrial and Engineering Chemistry Research 39 (6), 1925-1933.

Ahluwalia, K.S., 1996. United States Patent: 5, 571, 424.

Ahluwalia, K.S., 1997. United States Patent: 5, 670, 040.

Akiya, N., Savage, P., 2002. Roles of water for chemical reactions in high-temperature water. Chemical Reviews 102 (8), 2725-2750.

Antal Jr, M.J., Mok, W.S.L., 1990. Mechanism of formation of 5-(hydroxymethyl)-2-furaldehyde from D-fructose and sucrose. Carbohydrate Research 199, 91-109.

Asghari, F.S., Yoshida, H., 2006. Acid catalyzed production of 5-Hydroxymethyl Furfural from d-Fructose in subcritical water. Industrial & Engineering Chemistry Research 45 (7), 2163-2173.

Behrendt, F., Neubauer, Y., Oevermann, M., Wilmes, B., Zobel, N., 2008. Direct liquefaction of biomass-Review. Chem. Eng. Technology 31 (5), 667-677.

Beltrán, G.J., Servio, P., 2008. Equilibrium studies for the system Methane + Carbon Dioxide +Neohexane + Water. Journal of Chemical and Engineering Data 53, 1745-1749.

Bermejo, M.D., Cocero, M.J., 2006a. Supercritical water oxidation: A technical review. AIChE Journal 52 (11), 3933-3951.

Bermejo, M.D., Cocero, M.J., 2006b. Destruction of an industrial wastewater by supercritical water oxidation in a transpiring wall reactor. Journal of Hazardous Materials B137, 965-971.

Bobleter, O., 1994. Hydrothermal degradation of polymers derived from plants. Polymer Science 19, 797-841.

Bouvier, J.M., Gelus, M., Maugendre, S., 1988. Wood liquefaction-An overview, Applied Energy 30 (2), 85-98.

Bridgwater, A.V., 2001. Progress in thermochemical biomass conversion, Blackwell Science Ltd. London, Vol. 2, pp. 1312.

Bridgwater, A.V., Meier, D., Radlein, D., 1999. An overview of fast pyrolysis of biomass. Organic Chemistry 30, 1479-1493.

Bröll, D., Kaul, C., Krämer, A., Krammer, P., Richter, T., Jung, M., Vogel, H., Zehner, P., 1999. Chemistry in Supercritical Water. Angew. Chem. Int. Ed. 38, 2998±3014.

Brunner, G., 2009. Near critical and supercritical water. Part I. Hydrolytic and hydrothermal processes. Journal of Supercritical Fluids 47, 373-381.

Bruusgaard, H., Beltrán, G.J., Servio, P., 2008. Vapor-liquid water-hydrate equilibrium data for the system N_2 + CO_2 + H_2O. Journal of Chemical and Engineering Data 53, 2594-2597.

Changing World Technology, 2010. www.changingworldtech.com

Chisti, Y., 2007. Biodiesel from microalgae. Biotechnology Advances 25, 294-306.

Chornet, E., Overend, R.P., 1985. Biomass liquefaction: An overview, in fundamentals of thermochemical biomass conversion: Overend, R.P., Milne T.A., Mudge, L.K. (Eds.), Elsevier., London.

Chum, H.L., Overend, R.P., 2001. Biomass and renewable fuels. Fuel Processing Technology 71, 187-195.

Cocero, M.J., Alonso, E., Sanz, M.T., Fdz-Polanco, F., 2002. Supercritical water oxidation process under energetically self-sufficient operation. Journal of Supercritical Fluids 24, 37-46.

Constantinou, L., Gain, R., 1994. New group contribution method for estimating properties of pure compounds. AIChE J 40 (10), 1697-1710.

Constantinou, L., Gain, R., O'Connell, J.P., 1995. Estimation of the acentric factor and the liquid molar volume at 298 K using a new group contribution method. Fluid Phase Equilibria 103, 11-22.

Danish Energy Agency, 2010. http://www.ens.dk/en-US/supply/Renewable-energy/Bioenergy/Sider/Forside.aspx

Dell'Orco, P.C., Li, L., Gloyna, E.F., 1993. The separation of particles from supercritical water oxidation processes. Separation Science and Technology 28, 624-642.

Demirbaş, A., 2005. Thermochemical conversion of biomass to liquid products in the aqueous medium. Energy Source 27, 1235-1243.

Demirbas, A., 2000. Mechanisms of liquefaction and pyrolysis reaction of biomass. Energy Convers. Manage. 41, 633-46.

Demirbas, A., 2008. Biodiesel-A realistic fuel alternative for diesel engines. Springer, ISBN: 978-1-84628-994-1.

DIAS Report, 2003. Plant production no.86.

Domínguez, A., Menéndez, J.A., Inguanzo, M., Bernad, P.L., Pis, J.J., 2003. Gas chromatographic- mass spectrometric study of the oil fractions produced by microwave-assisted pyrolysis of different sewage sludges, Journal of Chromatography A 1012, 193-206.

Ebrahim, M., Kawari, Al., 2000. Pinch technology: an efficient tool for chemical-plant energy and capital-cost saving. Applied Energy 65, 45-49.

Elliott, D.C., Beckman, D., Bridgwater, A.V., Diebold, J.P., Gevert, S.B., Solantausta, Y., 1991. Developments in direct thermochemical liquefaction of biomass: 1983-1990. Energy and Fuels 5, 399-410.

Elliot, D.C., Sealock Jr, L.J., Baker, E. G., 1993. Chemical processing in high-pressure aqueous environments. 2. Development of catalysts for

gasification. Industrial & Engineering Chemistry Research 32, 1542-1548.

Elliot, D.C., Phelps, M.R., Sealock Jr, L.J., Baker, E.G., 1994a. Chemical processing in high-pressure aqueous environments. 3. Continuous-flow reactor process development experiments for organics destruction. Industrial & Engineering Chemistry Research 33, 566-574.

Elliot, D.C., Sealock Jr, L.J., Baker, E.G., 1994b. Chemical processing in high-pressure aqueous environments. 3. Batch reactor process development experiments for organics destruction. Industrial & Engineering Chemistry Research 33, 558-565.

Energy, 2009. Annual report on Danish energy research programmes.

EREC, 2006. Renewable energy scenario to 2040.
Faaij, A.P.C., 2006. Bio-energy in Europe: changing technology choices. Energy Policy 34, 322-342.

Feng, w., van der Kooi, H.J., de Swaan Arons, J., 2004. Phase equilibria for biomass conversion processes in subcritical and supercritical water. Chem. Eng. Journal 98, 105-113.

Franck, E.U., 1968. Supercritical water. Endeavour 27, 55-59.

Franck, E.U., 1983. Thermochemical properties of supercritical fluids with special consideration of aqueous Systems. Fluid Phase Equilibr.10, 211-222.

Franck, E.U., Weingärtner, H., 1999. Chemical Thermodynamics. A Chemistry for the 21 st Century Monograph 105-119.

Fredenslund, A., Jones, R.L., Prausnitz, J.M., 1975. Group-contribution estimation of activity coefficients in nonideal liquid mixtures. AIChE J 21 (6), 1086-1099.

Global Renewable Fuels Alliance, 2010. http://www.globalrfa.org/

He, B.J., Zhang, Y., Funk, T.L., Riskowski, G.L., Yin, Y., 2000. Thermochemical conversion of swine manure: An alternative process for

waste treatment and renewable energy production. American Society of Agricultural Engineers 43(6), 1827-1833.

Heger, K., Uematsu, M., Franck, E.U., 1980. The static dielectric constant of water at high pressures and temperatures to 500 MPa and 550 ^{0}C. Ber. Bunsen-Gas. Phys. Chem. 84, 758-762.

Hodes, M., Marrone, P.A., Hong, G.T., Smith, K.A., Tester, J.W., 2004. Salt precipitation and scale control in supercritical water oxidation-Part A: fundamentals and research. Journal of Supercritical Fluids 29, 265-288.

Holderbaum, T., Gmehling, J., 1991. PSRK: A group contribution equation of state based on UNIFAC. Fluid Phase Equilibria 70, 251-265.

Holliday, R.L., King, J.W., List, G.R., 1997. Hydrolysis of vegetable oils in sub- and supercritical water. Industrial & Engineering Chemistry Research 36, 932-935.

Horstmann, S., Jabloniec, A., Krafczyk, J., Fischer, K., Gmehling, J., 2005. PSRK group contribution equation of state: comprehensive revision and extension IV, including critical constants and α-function parameters for 1000 components. Fluid Phase Equilibria 227, 157-164.

Hunter, S.E., Savage, P.E., 2004. Recent advances in acid-and base-catalyzed organic synthesis in high-temperature liquid water. Chemical Engineering Science 59, 4903-4909.

IEA, 2009. Key world energy statistics 2009.

IEA, 2007. Renewables in global energy supply- An IEA factsheet 2007.

IEO, 2009. World marketed energy consumption and CO_2 emissions.

Kabyemela, B.M., Adschiri, T., Malaluan, R.M., Arai, K., 1997a. Degradation kinetics of dihydroxyacetone and glyceraldehyde in subcritical and supercritical water. Industrial & Engineering Chemistry Research 36 (6), 2025-2030.

Kabyemela, B.M., Adschiri, T., Malaluan, R.M., Arai, K., 1997b. Kinetics of Glucose Epimerization and Decomposition in Subcritical and Supercritical Water. Industrial & Engineering Chemistry Research 36 (5), 1552-1558.

Kabyemela, B.M., Adschiri, T., Malaluan, R.M., Arai, K., 1999. Glucose and Fructose Decomposition in Subcritical and Supercritical Water: Detailed Reaction Pathway, Mechanisms, and Kinetics. Industrial & Engineering Chemistry Research 38 (8), 2888-2895.

Karagöz, S., Bhaskar, T., Muto, A., Sakata, Y., Oshiki, T., Kishimoto, T., 2005a. Low-temperature catalytic hydrothermal treatment of wood biomass: analysis of liquid products. Chemical Engineering Journal 108, 127–137.

Karagöz, S., Bhaskar, T., Muto, A., Sakata, Y., 2005b. Comparative studies of oil compositions produced from sawdust, rice husk, lignin and cellulose by hydrothermal treatment. Fuel 84, 875-884.

Karagöz, S., Bhaskar, T., Muto, A., Sakata, Y., 2006. Hydrothermal upgrading of biomass: Effect of K_2CO_3 concentration and biomass/water ratio on products distribution. Bioresource Technology 97, 90–98.

Kevin, B., 2001. The SlurryCarb^{TM} Process: Turning Municipal Wastewater solids into a Profitable Renewable Fuel. Proceedings of the Water Environment Federation 15, 1456-1470.

Khuwijitjaru, P., Adachi, S., Matsuno, R., 2002. Solubility of saturated fatty acids in water at elevated temperatures. Biosci. Biotechnol. Biochem. 66 (8), 1723-1726.

Kikic, I., Alessp, P., Rasmussen, P., Fredenslund, A., 1980. On the combinatorial part of the UNIFAC and UNIQUAC models. The Canadian Journal of Chemical Engineering 58, 253-258.

Kim, Y., Mosier, N.S., Hendrickson, R., Ezeji, T., Blaschek, H., Dien, B., Cotta, M., Dale, B., Ladisch, M.R., 2008. Composition of corn dry-grinde ethanol by-products: DDGS, wet cake, and thin stillage. Bioresource Technology 99, 5165-5176.

King, J.W., Holliday, R.L., List, G.R., 1999. Hydrolysis of soybean oil in a subcritical water flow reactor. Green Chemistry 1 (6), 261–264.

Klingler, D., Berg, J., Vogel, H., 2007. Hydrothermal reactions of alanine and glycine in sub- and supercritical water. Journal of Supercritical Fluids 43, 112–119.

Krammer, P., Vogel, H., 2000. Hydrolysis of esters in subcritical and supercritical water. J. Supercrit. Fluids 16, 189-206.

Kritzer, P., 2004. Corrosion in high-temperature and supercritical water and aqueous solutions: a review. Journal of Supercritical Fluids 29, 1-29.

Kritzer, P., Dinjus, E., 2001. An assessment of supercritical water oxidation (SCWO) Existing problems, possible solutions and new reactor concepts. Chemical Engineering Journal 83, 207-214.

Kruse, A., Dinjus, E., 2007a. Hot compressed water as reaction medium and reactant properties and synthesis reactions. J. Supercrit. Fluids 39, 362-380.

Kruse, A., Dinjus, E., 2007b. Hot compressed water as reaction medium and reactant 2. Degradation reactions. Journal of Supercritical Fluids 41, 361-379.

Kruse, A., Gawlik, A., 2003. Biomass conversion in water at 330-410 ^{0}C and 30-50 MPa. Identification of key compounds for indicating different chemical reaction pathways. Industrial & Engineering Chemistry Research 42, 267-279.

Kruse, A., Maniam, P., Spieler, F., 2007c. Influence of proteins on the hydrothermal gasification and liquefaction of biomass. 2. Model compounds. Industrial & Engineering Chemistry Research 46 (1), 87-96.

Lee, S., Speight, J.M., Loyalka, S.K., 2007. Handbook of alternative fuel technologies. CRC Press, ISBN: 978-0-8247-4069-6.

Lien, Y.C., Nawar, W.W., 1974. Thermal decomposition of some amino acids Valine, Leucine and Isoleucine. Journal of Food Science 39, 911-913.

Liu, A., Park, Y.K., Huang, Z., Wang, B., Ankumah, R.O., Biswas, P.K., 2006. Product identification and distribution from hydrothermal conversion of walnut shells. Energy and Fuel 20, 446-454.

Luijkx, G.C.A., Rantwijk, F.V., Bekkum, H.V., 1993. Hydrothermal formation of 1,2,4-benzenetriol from 5 hydroxymethyl-2-furaldehyde and D-fructose. Carbohydrate Research 242, 131-139.

Marrone, P.A., Hodes, M., Smith, K.A., Tester, J.W., 2004. Salt precipitation and scale control in supercritical water oxidation-Part B: commercial/full-scale applications. Journal of Supercritical Fluids 29, 289-312.

Marshall, W.L., Franck, E.U., 1981. Ion product of water substance, 0-1000 ^{0}C, 1-10,000 bar new international formulation and its background. J. Phys. Chem. Ref. Data 10, 295-304.

Mathias, P.M., Copeman, T.W., 1983. Extension of the Peng-Robinson equation of state to complex mixtures: Evaluation of the various forms of the local composition concept. Fluid Phase Equilibria 13, 91-108.

Matsumura, Y., Minowa, T., Potic, B., Kersten, S.R.A., Prins, W., van Swaaij, W.P.M., van de Beld, B., Elliott, D.C., Neuenschwander, G.G., Kruse, A., Antal Jr, M.J., 2005. Biomass gasification in near- and super-critical water: Status and prospects. Biomass and Bioenergy 29, 268-292.

McKendry, P., 2002. Energy production from biomass (part 2): conversion technologies. Bioresource Technology 83, 47-54.

Michelsen, M.L., 1990. A modified Huron-Vidal mixing rule for cubic equations of state. Fluid Phase Equilibria 60, 213-219.

Minowa, T., Inoue, S., 1999. Hydrogen production from biomass by catalytic gasification in hot compressed water. Renewable Energy 16, 1114-1117.

Minowa, T., Kondo, T., Sudirjo, s., 1998a. Thermochemical liquefaction of Indonesian biomass residues. Biomass Bioenergy 14, 517-24.

Minowa, T., Murakami, M., Dote, Y., Ogi, T., Yokoyama, S., 1995. Oil production from garbage by thermochemical liquefaction. Biomass and Bioenergy 8 (2), 117-120.

Minowa, T., Ogi, T., 1998b. Hydrogen production from cellulose using a reduced nickel catalyst. Catalysis Today 45, 411-416.

Minowa, T., Zhen, F., Ogi, T., 1998c. Cellulose decomposition in hot-compressed water with alkali or nickel catalyst. Journal of Supercritical Fluids 13, 253-259.

Mok, W.S.L., Antal Jr, M.J., Varhegyi, G., 1992. Productive and parasitic pathways in dilute acid-catalyzed hydrolysis of cellulose. Industrial & Engineering Chemistry Research 31 (1), 94-100.

Molton, P.M., Fassbender, A.G., Brown, M.D., 1986. STORS: The sludge-to-oil reactor system. U.S. Environmental Protection Agency EPA/600/S2-86/034.

Moreau, C., Durand, R., Roux, A., Tichit, D., 2000. Isomerization of glucose into fructose in the presence of cation-exchanged zeolites and hydrotalcites. Applied catalysis A 193, 257-264.

Naber, J.E., Goudriaan, F., 2005. HTU®-Diesel from biomass. ACS Division of FuelChemistry.http://membership.acs.org/P/PETR/2005-Biorefineries/Presentation-08.ppt.

Osada, M., Sato, T., Watanabe, M., Shirai, M., Arai, K., 2006. Catalytic gasification of wood biomass in subcritical and supercritical water. Combustion Science and Technology 178, 537-552.

Peterson, A.A., Vogel, F., Lachance, R.P., Fröling, M., Antal, M.J., Tester, J.W., 2008. Thermochemical biofuel production in hydrothermal media: A review of sub- and supercritical water technologies. Energy and Environmental Science 1, 32-65.

Qian, Y., Zuo, C., Tan, J., He, J., 2007. Structural analysis of bio-oils from sub-and supercritical water liquefaction of woody biomass. Energy 32, 196-202.

Qu, Y., Wei, X., Zhong, C., 2003. Experimental study on the direct liquefaction of *Cunninghamia lanceolata* in water. Energy 28, 597-606.
Renewables, 2007. Global status report-REN 21.

Reid, R.C., Prausnitz, J.M., Poling, B.E., 1987. The Properties of Gases and Liquids. 4th Edition, McGraw-Hill, Singapore.

Rogalinski, T., Herrmann, S., Brunner, G., 2005. Production of amino acids from bovine serum albumin by continuous sub-critical water hydrolysis. Journal of Supercritical Fluids 36, 49-58.

Rogalinski, T., Liu, K., Albrecht, T., Brunner, G., 2008. Hydrolysis kinetics of biopolymers in subcritical water. Journal of Supercritical Fluids 46, 335–341.

Russell, J.A., Miller, R.K., Motton, P.M., 1983. Formation of aromatic compounds from condensation reactions of cellulose degradation products. Biomass 3, 43-57.

Sandler, S. I., Orbey, H., 1998. Modeling Vapor-Liquid Equilibria-Cubic Equations of State and Their Mixing rules. Cambridge University Press ISBN: 0-521-62027-9 (hb).

Sasaki, M., Fang, Z., Fukushima, Y., Adschiri, T., Arai, K., 2000. Dissolution and Hydrolysis of Cellulose in Subcritical and Supercritical Water. Industrial & Engineering Chemistry Research 39 (8), 2883-2890.

Sasaki, M., Goto, K., Tajima, K., Adschiri, T., Arai, K., 2002. Rapid and selective retro-aldol condensation of glucose to glycoaldehyde in supercritical water. Green Chemistry 4, 285-287.

Sato, N., Quitain, A.T., Kang, K., Daimon, H., Fujie, K., 2004. Reaction kinetics of amino acid decomposition in high-temperature and high-pressure water. Industrial & Engineering Chemistry Research 43, 3217-3222.

Schubert, M., Regler, J.W., Vogel, F., 2010. Continuous salt precipitation and separation from supercritical water. Part 1: Type 1 salts. Journal of Supercritical Fluids 52, 99-112.

Sealock, L.J., Elliott, D.C., Baker, E.G., Butner, R.S., 1993. Chemical processing in high-pressure aqueous environments. 1. Historical perspective and continuing developments. Industrial and engineering Chemistry Research 32, 1535-1541.

Soave, G., 1972. Equilibrium constants from a modified Redlich-Kwong equation of state. Chemical Engineering Science 27, 1197-1203.

Song, C., Hu, H., Zhu, S., Wang, G., Chen, G., 2004. Nonisothermal catalytic liquefaction of corn stalk in subcritical and supercritical water. Energy & Fuels 18, 90-96.

Speck Jr, J.C., 1953. The Lobry de Bruyn-Alberda van Ekenstein Transformation, Advance Carbohydrate Chemistry 13, 63.

Srokol, Z., Bouche, A.G., Estrik, A.V., Strik, RC.J., Maschmeyer, T., Peters, J.A., 2004. Hydrothermal upgrading of biomass to biofuel; studies on some monosaccharide model compounds. Carbohydrate Research 339, 1717–1726.

Stevens, D.J., 1994. Review and analysis of the 1980–1989 biomass thermochemical conversion program. U.S. Department of Energy NREL/TP-421-7501.

Uematsu, M., Franck, E.U., 1980. Static dielectric constant of water and steam. J. Phys. Chem. Ref. Data. 9 (4), 1291-1306

Watanabe, M., Aizawa, Y., Iida, T., Aida, T.M., Levy, C., Sue, K., Inomata, H., 2005a. Glucose reactions with acid and base catalysts in hot compressed water at 473 K. Carbohydrate Research 340, 1925–1930.

Watanabe, M., Aizawa, Y., Iida, T., Nishimura, R., Inomata, H., 2005b. Catalytic glucose and fructose conversions with TiO2 and ZrO2 in water at 473K: Relationship between reactivity and acid-base property determined by TPD measurement. Applied Catalysis A 295, 150–156.

Watanabe, M., Iida, T., Aizawa, Y., Ura, H., Inomata, H., Arai, K., 2003. Conversions of some small organic compounds with metal oxides in supercritical water at 673 K. Green Chemistry 5, 539–544.

Watanabe, M., Iida, T., Inomata, H., 2006. Decomposition of a long chain saturated fatty acid with some additives in hot compressed water. Energy Conversion and Management 47, 3344–3350.

Watanabe, M., Inomata, H., Arai, K., 2002. Catalytic hydrogen generation from biomass (glucose and cellulose) with ZrO_2 in supercritical water. Biomass and Bioenergy 22, 405 – 410.

Xian, Z., Chao, Z., Liang, Z., Hongbin, C., 2008. Amino acid production from fish proteins hydrolysis in subcritical Water. Chinese Journal of Chemical Engineering 16 (3), 456-460.

Yang, B.Y., Montgomery, R., 1996. Alkaline degradation of glucose: effect of initial concentration of reactants. Carbohydrate Research 280, 27-45.

Yoshida, H., Terashima, M., Takahashi, Y., 1999. Production of organic acids and amino acids from fish meat by sub-critical water hydrolysis. Biotechnology Progress 15, 1090-1094.

Yu, Y., Lou, X., Wu, H., 2008. Some recent advances in hydrolysis of biomass in hot-compressed water and its comparisons with other hydrolysis methods. Energy & Fuels 22, 46-60.

Zhang, B., Huang, H.J., Ramaswamy, S., 2008. Reaction kinetics of the hydrothermal treatment of lignin. Appl Biochem Biotechnol 147, 119-131.

Zhang, B., Keitz, M.v., Valentas, K., 2008. Thermal effects on hydrothermal biomass liquefaction. Applied Biochemistry and Biotechnology 147, 143-150.

Zhong, C., Peters, C.J., Swaan Arons, J.de., 2002. Thermodynamic modeling of biomass conversion processes. Fluid Phase Equilibria 194-197, 805-815.

Zhong, C., Sato, Y., Masuoka, H., Chen, X., 1996. Improvement of predictive accuracy of the UNIFAC model for vapor-liquid equilibria of polymer solutions. Fluid Phase Equilibria 123, 97-106.

Zhong, C., Wei, X., 2004. A comparative experimental study on the liquefaction of wood. Energy 29, 1731-1741.

PUBLICATIONS

POSTER-1

Structural analysis of CatLiq® bio-oil produced by catalytic liquid conversion of biomass *(Presented)*

4th International conference on renewable resources and biorefineries, Rotterdam, Holland, 1-4 June 2008.

POSTER-2

Thermodynamic modelling of CatLiq® biomass conversion process *(Presented)*

6th International conference on renewable resources and biorefineries, Dusseldorf, Germany, 7-9 June 2010.

PAPER-1

Hydrothermal Liquefaction of biomass: A review of sub-critical water technologies *(Submitted)*

Bioresource Technology.

PAPER-2

Production and evaluation of CatLiq® bio-oil from catalytic liquid conversion of DDGS *(Submitted)*

Chemical Engineering Science.

PAPER-3

Bubble point pressures of the selected model system for CatLiq® bio-oil process *(Accepted)*

Bioten Conference, 21-23 September 2010. Birmingham, United Kingdom.

Hydrothermal Liquefaction of biomass: A review of sub-critical water technologies

TOOR, S. S., ROSENDAHL, L. and RUDOLF, A.
Institute of Energy Technology
Aalborg University
Pontoppidanstraede 101, DK-9220 Aalborg
DENMARK
sst@iet.aau.dk http://www.iet.aau.dk

Abstract: - This article reviews the hydrothermal liquefaction of biomass with the aim of describing the current status of the technology. Hydrothermal liquefaction is a medium-temperature, high pressure thermochemical process, which produces a liquid product, often called bio-oil or bi-crude. During the hydrothermal liquefaction process, the macromolecules of the biomass are first hydrolyzed and/or degraded into smaller molecules. Many of the produced molecules are unstable and reactive and can recombine into larger molecules. During the process a substantial part of the oxygen in the biomass is removed by dehydration or decarboxylation. The reaction patterns are highly dependant of the biomass composition since, the reaction patterns of biomass components such as protein; carbohydrates, lignin and fat, are very different. In spite of the potential for hydrothermal production of renewable fuel, only a few techniques have so-far gone beyond lab or bench-scale.

Key-Words: - hydrothermal liquefaction; biomass conversion; bio-oil

1 INTRODUCTION

Biomass is one of the most abundant sources of renewable energy and will be an important part of a more sustainable future energy system. Apart from direct combustion there is also growing attention in converting the biomass into liquid energy carriers (IEO, 2009). Biomass energy conversion methods are divided into biochemical/biotechnical methods (Hahn-Hägerdal et al., 2006; Lin and Tanaka, 2006; Wheals et al., 1999; Mata-Alvarez et al., 2000) and the thermochemical methods; such as direct combustion, pyrolysis, gasification, liquefaction etc. (Elliott et al., 1991; Matsumura et al., 2005; Peterson et al., 2008). In this article, however, the focus is on conversion of wet biomass through what is often referred to as hydrothermal liquefaction. Hydrothermal liquefaction is generally carried out at 280 to 370 ^{o}C and between 10 and 25 MPa. At these conditions water is in a liquid state. The phase diagram of water can be seen in (Fig. 1.1). In hydrothermal liquefaction, water is an important

reactant and catalyst, and thus the biomass can be directly converted without an energy consuming drying step, such as in the case of flash pyrolysis (Bridgwater et al., 1999). The process chemistry of hydrothermal liquefaction is complicated and highly substrate dependant and it will be addressed in the following section. The main products are bio-crude with a relatively high heating value, char, water-soluble substances and gas. Addition of various alkaline catalysts can suppress the char formation and thus improve the oil yield and quality. As the temperature is increased above the critical limit, gasification becomes the dominating process.

Due to the severe process conditions, industrial application of these processes suffers from various challenges. Corrosion requires the use of expensive alloys and the high operation pressures put tough requirements on process components such as feed pumps. Most work on hydrothermal liquefaction has so far been carried out in lab- or bench-scale, especially high investment costs is a considerable hurdle for commercialization. Nevertheless, a few pilot/demonstration processes do exist such as; HTU® (hydrothermal upgrading), LBL (Lawrence Berkeley Laboratory), CatLiq® (Catalytic Liquefaction) and the TDP process (Thermal Depolymerization) (Bridgwater, 2001; Bouvier et al., 1988; Changing World Technologies, Inc.). The SlurrCarb™ process is a similar technique; however, the main product is a solid carbonaceous fuel (Kevin, 2001). Other liquefaction processes, such as the PERC-process have utilized organic solvents instead of water (Bouvier et al., 1988).

In addition to hydrothermal liquefaction, a range of other hydrothermal conversion processes exist, however they usually are carried out at higher pressures and temperatures. Supercritical water oxidation (SCWO) utilizes temperatures above the critical temperature of water (374 ^{o}C) and oxidative conditions to produce thermal energy and a CO_2 rich gas phase (Cocero et al., 2002). The SCWO process has mainly been applied on industrial waste water and sludges. The major disadvantages with the SCWO process are salt precipitation, which occurs extensively at such high temperatures and corrosion due to high temperatures and oxidative conditions (Kritzer and Dinjus, 2001). The SCWO process was extensively reviewed by (Bermejo and Cocero, 2006a). Another hydrothermal process is SCWG (supercritical water gasification). Here the biomass is gasified to mainly CO_2, H_2, and CH_4 under supercritical but not oxidative conditions. Gasification of biomass in the presence of water has been extensively reviewed by (Matsumura et al., 2005). In temperatures up to 500 ^{o}C, effective reforming and gasification generally requires heterogeneous catalytic enhancement to achieve reasonable rates and selectivity (Peterson et al., 2008). At temperatures above 500 ^{o}C, homogeneous gasification is possible.

The scope of the paper is hydrothermal liquefaction with the aim of producing liquid fuels. In the next chapters, the reactions patterns for various biomasses

and biomass components are investigated and various pilot and commercial scale hydrothermal techniques are discussed.

2 Properties of Water

In hydrothermal liquefaction water is an active component as solvent, reactant and catalyst, and this make the process significantly different from pyrolysis.

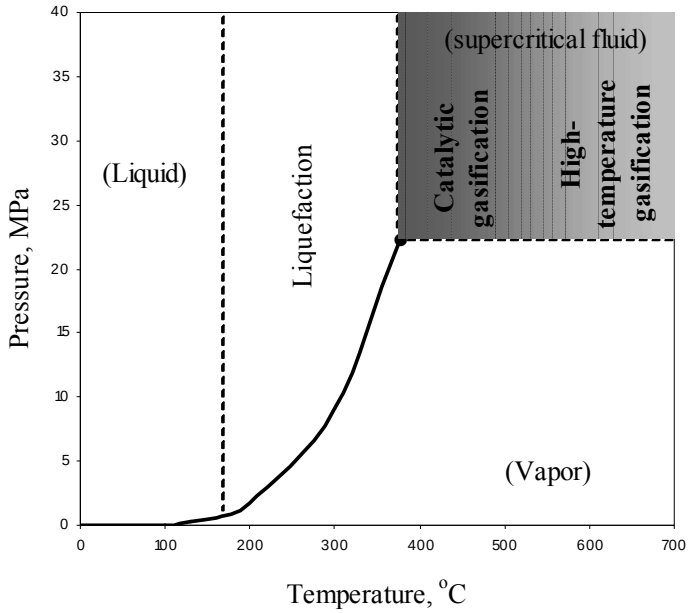

Fig. 1.1. The phase diagram of water, adapted from (Peterson et al., 2008).

At conditions close to the critical point, water has several very interesting properties. Among them are low viscosity and high solubility of organic substances, which make sub and supercritical water an excellent medium for fast, homogeneous and efficient reactions. (Franck, 1968; Heger et al., 1980; Marshall and Franck, 1981; Franck, 1983; Franck and Weingärtner, 1999; Kruse and Dinjus, 2007a). Therefore, during the last decades, there have been strong research interests in using sub and super-critical water as a solvent and reaction medium for biomass conversion. (Table 1.1) lists some properties of sub- and supercritical water (Bröll et al., 1999; Krammer and Vogel, 2000; Kruse and Dinjus, 2007a).

Table 1.1 Properties of water under various conditions.

	Ordinary Water T<150 ^{0}C P<0.4 MPa	**Subcritical water 150 ^{o}C < T <350 ^{o}C 0.4< P <20 MPa**		**Supercritical water T>370 ^{0}C**	
		5 MPa	**25 MPa**	**25 MPa**	**50 MPa**
Temp. (^{o}C)	25	250	350	400	400
Pressure, (MPa)	0.1	5	25	25	50
Density, ρ (g cm^{-3})	1	0.80	0.6	0.17	0.58
Dielectric constant, ϵ (Fm^{-1})	78.5	27.1	14.07	5.9	10.5
Ionic product, IP (K_w)	14.0	11.2	12	19.4	11.9
Heat capacity Cp (kJ kg^{-1} K^{-1})	4.22	4.86	10.1	13.0	6.8
Dynamic viscosity η (mPas)	0.89	0.11	0.064	0.03	0.07

Subcritical water has several properties that differ from those of water at room temperature as shown in (Table 1.1). The dielectric constant decreases from 78 Fm^{-1}at 25 ^{o}C to 14.07 Fm^{-1}at 350 ^{o}C (Uematsu and Franck, 1980). This decrease in dielectric constant gives rise to increase solubility otherwise hydrophobic organic compounds, for example free fatty acids are insoluble in water (Holliday et al., 1997; King et al., 1999). On the other hand the solubility of salts decreases. At supercritical conditions salts are almost insoluble, at subcritical conditions the solubility of most salts are much lower than at room temperature, however there are some important variations between different salts. So-called Type 1 salts such as NaCl still exhibit high solubility at subcritical conditions, whereas so-called Type 2 salts such as Na_2SO_4 have low solubility at these conditions (Hodes et al., 2004).

The low solubility might cause the formation of fine-crystalline, slimy "shock precipitate". The precipitating salts easily attaches to the walls of process components such as heat exchangers and reactor and thereby causes fouling or even blockage. (Kritzer and Dinjus, 2001; Marrone et al., 2004).

The ionic product of water (K_W) is relatively high in the subcritical range (10^{-12} compared to 10^{-14} at ambient conditions). The high levels of H^+ and OH^- at subcritical conditions means that many acid- or base catalyzed reactions, such as biomass hydrolysis, are accelerated. (Akiya and Savage, 2002; Hunter et al., 2004).

The density of subcritical water is significantly lower than at ambient conditions but at the same time higher than at supercritical conditions. The compressibility is also lower than at supercritical conditions. The relatively high density combined with the high dissociation constant of subcritical water, favors ionic reactions, whereas at supercritical conditions with low densities radical reaction dominates. At subcritical conditions hot compressed water

supports water eliminations from carbohydrates and alcohols and other reactions such as aldol splitting is enhanced by the special properties of subcritical water. Radical reactions at supercritical conditions first of all results in gas formation. (Kruse and Dinjus, 2007b; Osada et al., 2006).

Although the properties of sub/super critical water in many aspects are favorable, this also causes problems and limitations. Corrosion in the sub/super critical water environment is a critical issue. In particular acid and oxidizing conditions can cause rapid corrosion. The corrosion can even be more severe at subcritical conditions than supercritical conditions due to the relatively dense and polar character of supercritical water. Main forms of corrosion are pitting corrosion, general corrosion, intercrystalline corrosion and stress corrosion cracking (Kritzer, 2004). Pitting corrosion is a localized form of corrosion occurring in the passive state of the metal. High temperatures weaken the protective oxide film, and thus, pitting occurs much easier at high temperatures. In contrast to pitting corrosion, general corrosion attacks the entire surface of the metal. During the intercrystalline corrosion, either the grain boundaries or neighboring grain areas might be attacked. Stress cracking corrosion is an extremely dangerous form of corrosion and is observed along the grain boundaries or through the grains (Kritzer, 2004). Several materials have been tested at these conditions, however only a few do have sufficient corrosion resistance. The most widely used in sub and supcritical applications are Ni alloys such as Inconel 625 and Hasteloy C-276. Furthermore, titanium alloys also have good resistance; however their mechanical strength is limited (Table 1.2). (Bermejo and Cocero, 2006b; Kritzer and Dinjus, 2001; Bröll et al, 1999).

As mentioned salt precipitation due to the unpolar properties of the water solvent poses a problem at conditions close to or above the critical point of water. Several approaches have been evaluated to alleviate the problem, among them on-line salt separation through specially designed separators and reactors (Schubert et al., 2010; Kritzer and Dinjus, 2001; Marrone et al., 2004). One example is the transpiring wall reactor a modified reactor concept e.g. transpiring with an inner porous pipe, which is rinsed with water to prevent salt deposits at the wall (Bermejo and Cocero, 2006b; Ahluwalia, 1996, 1997). Dell'Orco et al (Dell'Orco et al., 1993) studied the used of hydrocyclons to eliminate particles with a known size distribution, under sub- and supercritical conditions. These devices proved to be effective in the elimination of particles of microscopic size and their efficiency is increased with temperature.

Another solution to avoid salt precipitation inside the reactor is to reduce the quantity of salt present in the feed. This can be achieved using solid-fluid separation methods. However, if the inorganic matter is bound the biomass matrix this cannot be easily carried out (Kritzer and Dinjus, 2001).

Table 1.2 Corrosion resistance of nickel-based alloys and titanium against different media.

	$T<T_c$; high density		**$T>T_c$; low density**	
	Good resistance resistance	**Poor**	**Good resistance**	**Poor resistance**
Nickel-based alloys	H_3PO_4, HF	HCl, HBr	All acids	$[H_3PO_4]>0.1$mol/kg
	Alkaline solutions	H_2SO_4, HNO_3	-	NaOH
Titanium	All acids	F^{-1}	HCl	H_2SO_4, H_3PO_4

3 Reaction Pathways for Liquefaction

Biomass is a broad definition and includes a wide range of materials with varying compositions. The main biomass components are: carbohydrates, lignin, protein and lipids (Table 2) (Sun and Cheng, 2002; Bobleter, 1994; Kim et al., 2008; Heddle, 1979). The degradation pattern of these components in sub and supercritical water differs; however, the basic mechanisms can be described as (Demirbas, 2000; Chornet and Overend, 1985; Peterson et al, 2008):

a. Hydrolysis of the biomass
b. Depolymerization of the main components
c. Chemical and thermal defragmentation, dehydration, decarboxylisation and deammination.
d. Recombination of reactive fragments.

The degradation pattern for the different biomass components differs widely and so does the product. There is also most likely a synergy between the different biomass components.
In the following sections the reactions patterns of the various biomass components will be reviewed.

Table 2 Typical Lignocellulosic Biomass Compositions (% Dry Basis)

Lignocellulosic materials	Cellulose	Hemicelluloses	lignin	Crude-Protein	Crude-Fat
	Hard Woods				
White poplar	49.0	25.6	23.1	-	-
European birch	48.5	25.1	19.4	-	-
White willow	49.6	26.7	22.7	-	-
	Soft Woods				
White spruce	44.8	30.9	27.1	-	-
Monterey pine	41.7	20.5	25.9	-	-
Douglas fir	42.0	23.5	27.8	-	-
	Agricultural Residues				
Corn stover	37.1	24.2	18.2	-	-
Sugarcane bagasse	39.0	24.9	23.1	-	-
Wheat straw	44.5	24.3	21.3	-	-
	Other Wastes				
Newspaper	40-55	25-40	18-30	-	-
Swine waste	6.0	28	-	-	-
Switch grass	45	31.4	12.0	-	-
Dried Distillers Grains with Solubles (DDGS)	-	-	-	30.2	10.9
Slaughter house waste	-	-	-	45-60	15-25

4 Conversions of Carbohydrates

The most abundant carbohydrates in biomass are the polysaccharides cellulose, hemicelluloses and starch. Under hydrothermal conditions carbohydrates undergo hydrolysis to form glucose and other monosaccharides.

The hydrolysis is acid-catalyzed and the rate of hydrolysis varies between different carbohydrates. Hemicelluloses and starch are hydrolyzed much faster than cellulose, which to a large extent has a crystalline structure. The degradation of carbohydrates in sub and supercritical water has been

thoroughly reviewed by several authors (Yu et al., 2008; Behrendt et al., 2008; Bobleter, 1994).

4.1 Cellulose hydrolysis

Cellulose consists of glucose units, linked by β-(1→ 4) - glycosidic bonds, which allows formation of strong intra-and inter-molecule hydrogen bonds. Thus cellulose has a high degree of crystallinity, which makes it insoluble in water and resistant to attack by enzymes. However at subcritical conditions cellulose is rapidly solubilized and hydrolyzed to its constituents (Delmer and Amor, 1995; Bobleter, 1994).

Rogalinski *et al* (Rogalinski et al., 2008) found that the cellulose hydrolysis rate in water at 25 MPa increased tenfold between 240-310 ^{o}C, and that cellulose hydrolysis is considerably slower starch hydrolysis. At 280 ^{o}C 100% cellulose conversion was achieved within 2 min. The glucose decomposition rate increased rapidly with temperature and became higher than the glucose release rate already between 250 and 270 ^{o}C. It was observed that the addition of carbon dioxide yielded a significant rate enhancement of cellulose liquefaction; this effect however, CO_2 was believed to promote the acid catalyzed hydrolysis due to the formation of carbonic acid. However, the effect got less pronounced above 260°C. The relationship between cellulose hydrolysis rate and glucose decomposition rate was also seen by conducting decomposition experiments of microcrystalline cellulose in subcritical and supercritical water (320-400 ^{o}C, 25MPa, and 0.05-10.0s). At 400 ^{o}C hydrolysis products (cellohexaose, cellopentaose, cellotetraose, cellotrioase, cellobiose, glucose and fructose) were mainly obtained, whereas in 320-350 ^{o}C water, aqueous decomposition products (1, 6-anhydroglucose, erythrose, glycolaldehyde, glyceraldehyde, dihydroxyacetone, pyruvaldehyde, furfural and 5-HMF) of glucose and fructose were the main products. These results were explained by kinetic studies which, showed that below 350 ^{o}C the cellulose hydrolysis rate was slower than the glucose decomposition rates, whereas above 350 ^{o}C, the cellulose hydrolysis rate drastically increased and became higher than the glucose decomposition rate (Sasaki et al., 2000). The estimated reaction mechanism for the conversion of microcrystalline cellulose in subcritical and supercritical water at 25 MPa can be seen in (Fig. 1.2). Once the cellulose is depolymerized the monosaccharides are susceptible to further degradation.

Kamio *et al* (Kamio et al., 2008) reported that cellulose hydrolysis drastically increased above 240 ^{o}C and that the hydrolysis proceeded by initial formation of oligosaccharides and trisaccharides, which are subsequently converted into glucose and pyrolysis products.

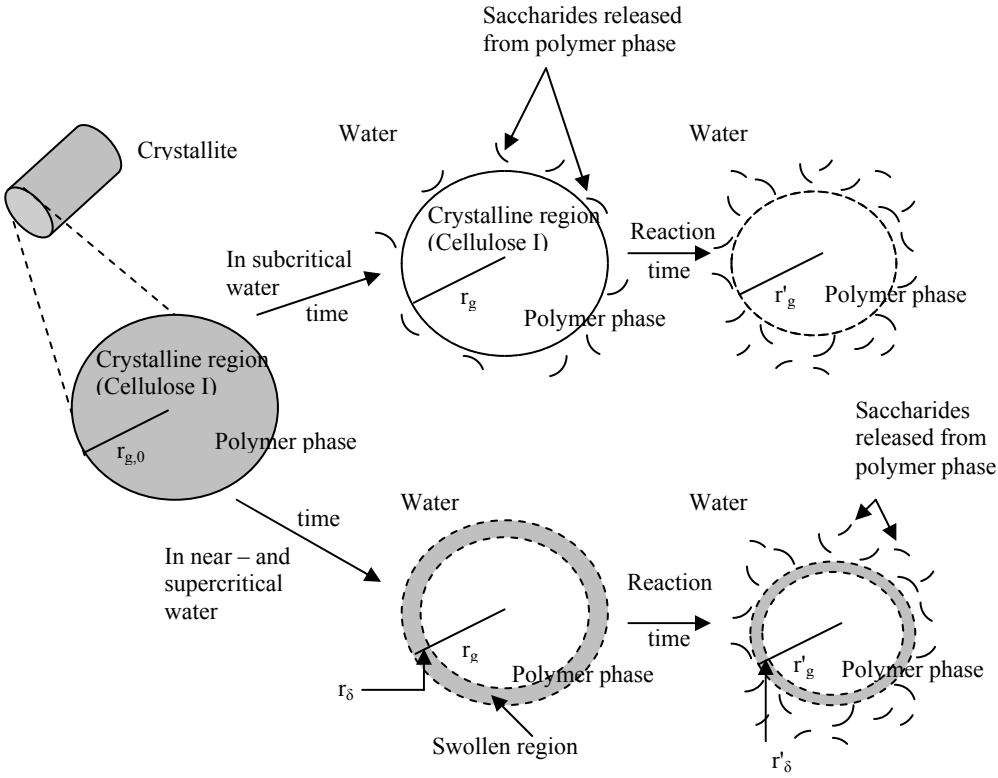

Fig. 1.2. Estimated reaction mechanism for the conversion of microcrystalline cellulose in subcritical and supercritical water at 25 MPa, adapted from (Sasaki et al., 2004).

4.2 Hemicelluloses hydrolysis

Hemicelluloses make up 20-40% of plant biomass. It is a heteropolymer composed of various monosaccharides, including xylose, mannose, glucose and galactose (Bobleter, 1994). The composition varies significantly between plant types, grass hemicellulose is mainly composed of xylane, whereas wood hemicelluloses are rich in mannan, glucan and galactan. Due to the abundance of side-groups and the less uniform structure of the hemicelluloses polymer, it does not form as crystalline and resistant of a structure as cellulose does (Peterson et al., 2008). Hemicelluloses are easily dissolved in water at temperatures above about 180 ^{o}C and the hydrolysis is both acid and base-catalyzed (Bobleter, 1994). Mok *et al* (Mok and Antal, 1992a) found they could extract an average of 95% monomeric of sugars at 34.5 MPa and 200 to 230 ^{o}C from uncatalyzed hydrolysis of hemicelluloses over a span of just a few

minutes. Pessoa *et al* (Pessoa et al., 1997) obtained a maximum xylose yield of 83.3% at 140 ^{o}C, 20 min, and addition of 100 mg of sulphuric acid per gram of dry matter in a semi-pilot reactor during acid hydrolysis of hemicelulosic fraction of sugarcane bagasse.
Sasaki *et al* (Sasaki et al., 2003) conducted decomposition experiments of D-xylose in subcritical and supercritical water at temperatures 360-420 ^{o}C, pressure 25-40 MPa and residence time of 0.02-1 seconds. They proposed two reactions on the primary decomposition of D-xylose, namely retro-aldol condensation and dehydration. Retro-aldol condensation results in the formation of glycolaldehyde and glyceraldehyde. Glyceraldehyde can be converted to dihydroxyacetone via keto-enol tautomerism or to pyruvaldehyde via dehydration. In addition, D-xylose can also convert to 2-furaldehyde via dehydration. The analysis showed that retro-aldol condensation of D-xylose was dominant and the contribution of dehydration was negligible small in near- and supercritical water.

4.3 Starch hydrolysis

Starch is a polysaccharide consisting of glucose monomers bound with β-(1→ 4) and α-(1→ 6) bonds (Peterson et al., 2008). There are two different forms of starch, amylose with a linear structure, and amylopectin with a more branched structure. Compared to cellulose, starch is relatively readily hydrolyzed.
Starch (from sweet potato) was decomposed using water under hydrothermal conditions in the absence of any additives and quantified the yields of glucose, fructose, maltose, and 5-hydromethylfurfural (5-HMF) versus time at 180- 240 ^{o}C in a batch reactor at unspecified pressures. The starch was completely solubilized already after 10 min in 180 ^{o}C, however glucose yields were negligible. The maximum glucose yield was about 60% and was obtained both at 200 ^{o}C and a residence time of 30 min and at 220 ^{o}C and 10 min. At 240 ^{o}C and a 10 min, the yield was considerably lower due to glucose degradation. The main degradation product was 5-hydroxymethylfurfural (Nagamori and Funazukuri, 2004). In a similar study on hydrolysis of sweet potato, Miyazawa *et al* (Miyazawa and Funazukuri, 2005) reported a glucose yield of just 4% after 15 min. at 200 ^{o}C and unspecified pressures. It was observed that the hydrolysis rate increased drastically if the medium was acidified with CO_2. The amount of glucose released increased approximately linearly with increasing CO_2 concentration, in the range of 0 to 0.1 g CO_2 per g H_2O. Addition of 0.32g of carbon dioxide resulted in a glucose yield of 53.0 % at 200 ^{o}C after 15 min. In a similar study on hydrolysis of starch from sweet potato, a maximum glucose yield of 43.8 % was attained (from sweet potato) at 240 ^{o}C in 3.64 min without any additives. (Miyazawa et al., 2006)

4.4 Hydrothermal conversion of carbohydrates

The carbohydrates in biomass are as mentioned above rapidly hydrolyzed to monosaccharides at subcritical conditions. One of the main hydrolysis products is glucose. The glucose itself reacts by isomerization, dehydration and fragmentation and at sub and super critical conditions, producing a wide range of products. The fragments from the degradation may recombine to form lager molecules such as phenols.

Several attempts to describe a general degradation mechanism have been made. The models vary in detail however the over-all pattern is similar (Fig. 2) (Kruse et al., 2007c). At supercritical conditions, the main products are gaseous ones, which are formed via defragmentation segments. At subcritical conditions the degradation of glucose proceeds via both isomerization to fructose, dehydration and defragmentation. Furans, defragmentation products and phenols are major products; however the distribution is dependent on pH and temperature. Glucose reversibly isomerizes into fructose via the LBAE (Lobry de Bruyn, Alberda van Ekenstein) transformation (Peterson et al., 2008; Antal and Mok, 1990). The LBAE transformation has been well-studied and proof of its occurrence is supported well by deuterium exchange reactions of glucose (Speck, 1953). Antal *et al* (Antal and Mok, 1990) saw that, when starting with glucose, the amount of fructose formed was quite small compared to the amounts of other degradation products. Kabyemela et al (Kabyemela et al., 1997b) observed that the rate of glucose isomerization to fructose was important in hydrothermal media, whereas the reverse reaction was rather insignificant. His observations are based on experiment in which glucose or fructose were the starting material at temperatures of 300 to 400 ^{o}C and pressures of 25 to 40 MPa. Glucose decomposition products were fructose, saccharinic acids, erythrose, glyceraldehyde, 1, 6-anhydroglucose, dihydroxyacetone, pyruvaldehyde, and small amounts of 5-HMF.

In general glucose and fructose have different reaction patterns at subcritical conditions and fructose is in general more reactive than glucose. Glucose degrades mostly to fragmentation products (glycolaldehyde, pyruvaldehyde, glyceraldehyde, etc.) through retro-aldol condensation reaction (Srokol et al., 2004; Bonn and Bobleter, 1983), whereas fructose to a higher extent forms dehydration products such as 5-hydroxymethylfurfural (5-HMF) (Antal and Mok, 1990; Srokol et al., 2004; Bonn and Bobleter, 1983; Boon et al., 1994).

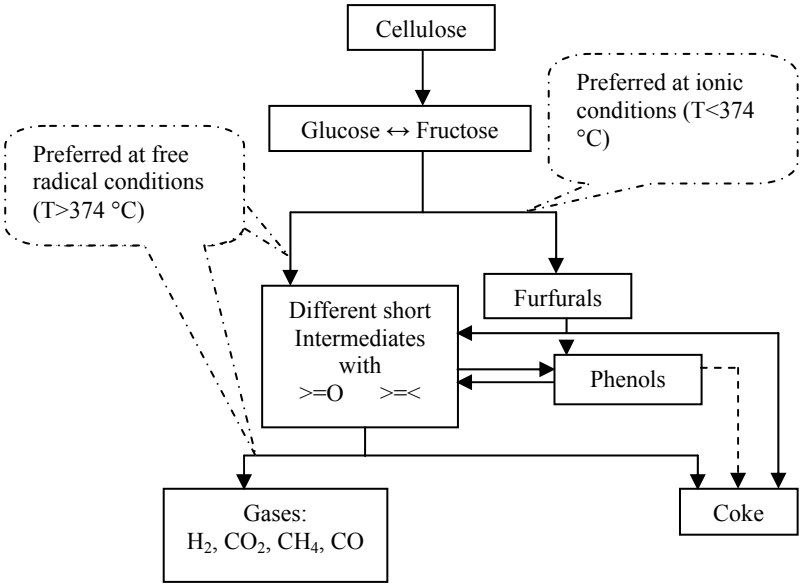

Fig. 2. A simplified reaction mechanism for biomass degradation at supercritical conditions, adapted from (Kruse et al., 2007c; Kruse and Gawlik, 2003)

Watanabe *et al* (Watanabe et al., 2005b) studied the effect of reaction conditions and additives on glucose and fructose reactions with 5 min. residence time (Fig. 3). The primary reactions of glucose were found to be as follows: (1) glucose isomerization into fructose via keto-enol tautomerization, (2) glucose dehydration into 1, 6-anhydroglucose, and (3) glucose decomposition into aldehyde and ketone via retro-aldol condensation. Further, (4) dehydration of tautomerization intermediate and fructose produce 5-HMF.
It has been shown that the contribution of retro-aldol condensation is predominant at higher temperatures (400-500 ^{o}C), whereas that of the dehydration reaction is significant at lower temperatures (250-350 ^{o}C) (Yang and Montgomery, 1996; Kabyemela et al., 1997b; Moreau et al., 2000; Sasaki et al., 2002; Watanabe et al., 2005b).
Srokol *et al* (Srokol et al., 2004) studied hydrothermal treatment (340 ^{o}C, 27.5 MPa, 25-204 s) of dilute (50mM) solutions of D-glucose and some other monosaccharides (D-fructose, D-mannose, D-galactose). It was found that dehydrations, producing 5-hydroxymethylfurfural were favored under acidic conditions, whereas basic conditions resulted in fragmentation products such as glycolaldehyde and glyceraldehyde. Further fragmentations and dehydrations lead to the formation of a variety of low molecular weight compounds such as formic acid, acetic acid, lactic acid, acrylic acid, 2-furaldehyde and 1, 2, 4-benzenetriol.

In another study, the decomposition of D-fructose to 5-HMF was studied over a temperature range of 200-320 ^{o}C and pH 1.5-5 (Asghari and Yoshida, 2006). It was found that phosphoric acid showed good catalytic ability on the dehydration of fructose in sub-critical water. That is, ~ 65% absolute yield of HMF was obtained in 120s at 240 ^{o}C which was only 23% in uncatalyzed reactions. It was concluded that not only the pH, but also the nature of the acids, had great influence on the decomposition pathway. At lower pH, a rehydration of HMF to leyulinic and formic acids occurred, whereas at higher pH, polymerization reactions occurred.

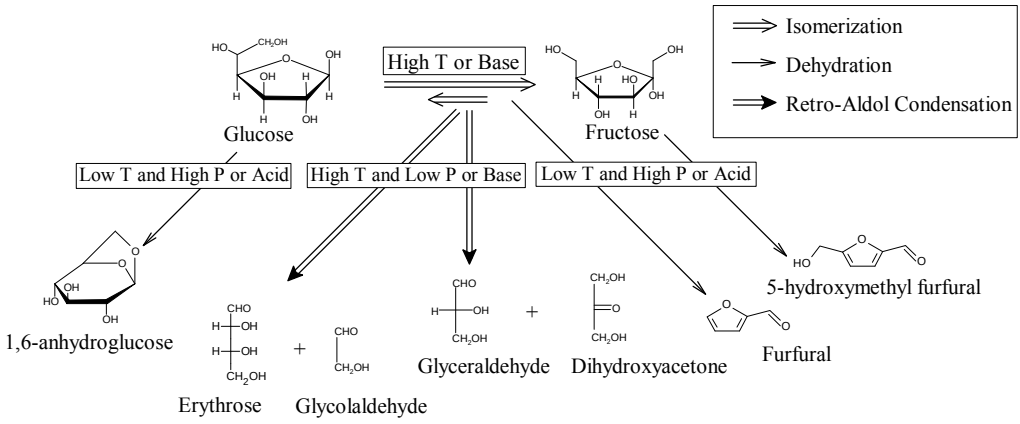

Fig. 3. Effect of reaction conditions and additives on glucose and fructose reactions, adapted from (Watanabe et al., 2005b)

The formation of aromatic compounds during hydrothermal treatment of glucose has been reported.

Luijkx *et al* (Luijkx et al., 1993) reported that the aromatic compound 1, 2, 4-benzenetriol could be formed in significant yields from the glucose degradation product, 5-HMF at 27.5 MPa and 290-400 ^{o}C. At neutral conditions, a yield of 46% was attained. The addition of HCl (0.01M) also resulted in complete HMF conversion at 330 ^{o}C with residence time ranging from 1-5 min. Under these conditions, the normal product of HMF degradation was 4-oxopentanoic acid but formation of 1, 2, 4-benzenetriol was still substantial.

(Table 3) summarizes research performed with biomass and model compounds.

Table 3 Summary of conversion of biomass and model compound

Substrate	Conditions	Compounds	Reference
Glucose	300-400 ^{o}C 25-40 Mpa 0.02-2s (neutral pH)	Fructose Dihydroxyacetone Glyceraldehyde Erythrose Glycolaldehyde Pyruvaldehyde 1,6 anhydroglucose Acetic, formic acid 5-HMF	(Kabyemela *et al.* 1997a; Kabyemela *et al.* 1997b) Kabyemela *et al.* 1999;
D-glucose and other monosaccharides	340 ^{o}C 27.5 Mpa 25-204s (acid and base catalyzed)	5-HMF Glycolaldehyde Glyceraldehyde formic acid, acetic acid, lactic acid, acrylic acid, 2-furaldehyde 1, 2, 4-benzenetriol	(Srokol *et al.* 2004)
D-fructose	200-320 ^{o}C 120s pH range (1.5-5)	5-HMF Formic acid Levulinic acid	(Asghari and Yoshida 2006)
Microcrystalline cellulose	320-400 ^{o}C 25MPa 0.05-10.0s (neutral pH)	1, 6-anhydroglucose Erythrose Glycolaldehyde Glyceraldehyde Pyruvaldehyde Dihydroxyacetone Furfural 5-HMF	(Sasaki *et al.* 2000)
5-HMF	290-400 ^{o}C 27.5 MPa 0.107-0.308min^{-1}	1,2,4-benzenetriol 4-oxopentanoic acid (330 ^{o}C, 1-5 min., acidic media)	(Luijkx *et al.* 1993)
Cellulose	250-407 ^{o}C Alkaline environment	o-,m-or p-Xylene Ethylbenzene n-Propylbenzene 1 -Methyl-2-ethylbenzene 1 -Methyl-3-ethylbenzene Phenol o-, m-,p-Cresol 2-Phenoxyethanol	(Russell *et al.* 1983)

Russell *et al* (Russell et al., 1983) detected many aromatic compounds from the oily product obtained after liquefaction of cellulose with aqueous Na_2CO_3 at 250-470 ^oC. The most abundant were substituted benzenes, phenols and cresols. They proposed that, under liquefaction conditions, the cellulose degrades to low molecular weight aldehydes and ketones, as been previously mentioned for glucose. These aldehydes and ketones may then form aromatic compounds by condensation and dehydration.

5 Conversions of Lignin

Lignin is together with cellulose and hemicellulose major part of plant materials. It is an aromatic heteropolymer consisting of p-hydroxyphenylpropanoid units held together by C-C or C-O-C bonds. The three basic building blocks are trans-p-coumaryl alcohol, coniferyl alcohol and sinapyl alcohol (Fig. 4). Lignin is relatively resistant to chemical or enzymatic degradation (Bobleter, 1994). During hydrothermal degradation various phenol derivates are formed by hydrolysis of ether-bonds. The lignin hydrolysis is catalyzed by alkaline pH.

Hydrothermal treatment process of Kraft pine and organosolv lignin was conducted at 374 ^oC and 22MPa for 10 min. The liquid yields were between 57.8 and 79.1 % and the solid residue yields were between 12.1 and 37.6%. The product profile differed between the two substrates, but in general the major lignin hydrolysis products were: guaiacol, 4-ethylguaiacol, 4-ethyl phenol and 2-Methoxy-4-propy-phenol (Zhang et al., 2008). Liu *et al* (Liu et al., 2006) studied hydrothermal processing of walnut shell by both acid- (HCl) and base-catalyzed (KOH, Na_2CO_3) at reaction temperature of (200-300 ^oC), corresponding to a pressure range of (1.5-8.6 MPa) for 1h. Several phenol derivates such as 2-methoxy phenol, 3, 4-dimethoxy phenol and 1, 2-benzenediol most likely were produced by base-catalyzed lignin hydrolysis followed by hydrolysis of methoxy groups.

Karagöz *et al* (Karagöz et al., 2005b) also obtained phenolic compounds (2-methoxy phenol, 1, 2-benzenediol, 4-methyl-1,2-benzenediol, 3-methyl-1,2-benzenediol and phenol) from hydrothermal treatment (280 ^oC for 15 min.) of lignin.

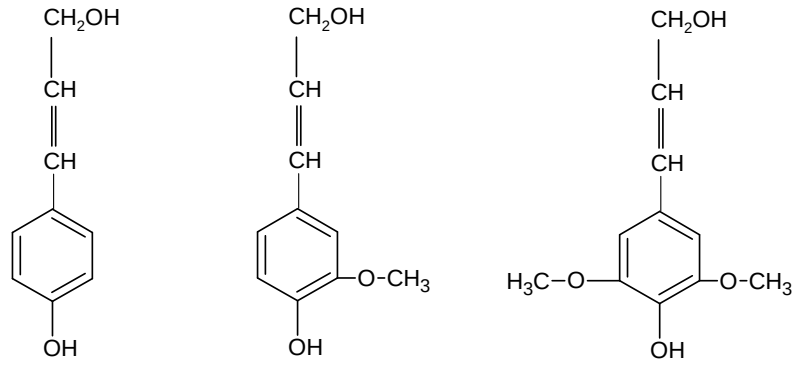

Fig. 4. Monomeric lignin building units: Cou= p-coumaryl alcohol, Con= coniferyl alcohol and Sin= sinapyl alcohol (Bobleter, 1994)

6 Conversions of Lipids

Fats and oils are non-polar compounds with mainly aliphatic character, which are insoluble in water at normal conditions. As shown in Table. 1, the dielectric constant of water decreases drastically under subcritical and supercritical conditions, allowing greater miscibility. (Peterson et al., 2008; Khuwijitjaru et al., 2002).

Fats and oils in biological systems are typically in the form of triacylglycerides (TAGs), which consist of three fatty acids bound to a glycerol backbone. Hot compressed water is one of the candidates for treating the fats/oils to produce long chain hydrocarbons because of its capability to hydrolyze TAGs into free fatty acid and glycerol without catalyst. On the other hand, free fatty acids are relatively stable in subcritical water (Holliday et al., 1997; King et al., 1999). At higher rapid hydrolysis of soybean oil was achieved in liquid water, at temperatures of 330 to 340 ^{o}C, P = 13.1 MPa, and water-to-oil ratios of 2.5 to 5.0 : 1, giving 90 to 100% yields of free fatty acids in 10 to 15 minutes. Using an optically accessible reactor, the phase behavior was found to be extremely important. King *et al* noted that the reaction quickly went to completion when the mixture became a single phase at 339 ^{o}C.

Glycerol

Glycerin ($C_3H_8O_3$) is one of the products of triglyceride hydrolysis and therefore a major coproduct in bio-diesel production. It can be used to synthesize specialty chemicals but is also considered as an important source for producing energy or fuel. Glycerol is not converted to an oily phase during

hydrothermal liquefaction but rather to water-soluble compounds. Lehr *et al* (Lehar et al., 2007) found that glycerol is converted into acrolein in subcritical water (360 ^{o}C, 34 MPa, 0-180 s) with catalytic amounts of $ZnSO_4$. Glycerol was decomposed in near critical and supercritical water in plug-flow reactor at 349-475 ^{o}C, 25-45 MPa and reaction times from 32-165s at different initial concentrations. Conversion between 0.4 and 31% was observed. The main products of glycerol degradation were methanol, acetaldehyde, propionaldehyde, acrolein, allyl alcohol, ethanol, formaldehyde, carbon monoxide, carbon dioxide and hydrogen (Bühler et al., 2002).

6.1 Fatty acids

Fatty acids can be degraded in hydrothermal systems to produce long-chained hydrocarbons. The reaction is however slow at subcritical conditions. Stearic acid ($C_{17}H_{35}COOH$) was decomposed at temperature of 400 ^{o}C and pressure of 25 MPa in a batch reactor at a fixed density of 0.17 gcm^{-3} for 30 min. At uncatalyzed conditions the alkane yield was only a few percent. However, addition of KOH accelerated the decomposition and a yield of 32% was achieved. At alkaline conditions, the major decomposition mechanism was decarboxylization of the fatty acid producing the corresponding alkane. The reaction in a hydrothermal system was compared to pyrolysis of water-free stearic acid. Degradation tests were also carried out at water-free conditions and this revealed that supercritical water stabilized the fatty acid and suppressed the degradation (Watanabe et al., 2006).

7 Conversions of Proteins

Proteins are a major biomass component in particular in animal, plant and microbial biomass. Proteins are made up from one or several peptide-chains. The smallest buildings-blocks are the amino acids. The structural bond that links amino acids together into protein is the peptide bond, which is an amide bond between carboxyl and amine groups of the amino acids. Hydrolysis rates of various biopolymers, strongly depend on the type of bond. Peptide bonds in the proteins are much more stable than the glycosidic bonds in cellulose and starch, and only slow hydrolysis occurs below 230 ^{o}C (Brunner, 2009; Rogalinski et al., 2008). In addition, yields of amino acids are generally significantly lower than by conventional acid hydrolysis since the degradation rate of amino acids at hydrothermal conditions is much higher than for example glucose (Peterson et al., 2008).

Some researchers have reported ways to enhance hydrolysis yields. Rogalinski *et al* (Rogalinski et al., 2008) reported that the yield of amino acids quadrupled with the addition of CO_2 due to acceleration of acid hydrolyzed catalysis steps: at 250 ^{o}C, 25MPa and 300 s residence time total amino acid yield increased

from 3.7 to 15 wt%. It was also observed that the catalytic influence of carbon dioxide decreases with increasing temperature. Xian *et al* (Xian et al., 2008) investigated the hydrolysis and reaction kinetics for amino acids production from fish proteins in subcritical water reactor without catalyst at 180-320 ^{o}C, 5-26 MPa and residence time from 5-60 min. It was found that the hydrolysis rate increased five-fold between 220 and 260 ^{o}C. Another phenomenon described was that the stability of the various amino acids differed markedly and that both process temperature as well as process gas had an influence. Rogalinski *et al* (Rogalinski et al., 2005) observed production of amino acids from bovine serum albumin (BSA) by continuous sub-critical water hydrolysis. The highest amino acid yield in sub-critical water was obtained at 290 ^{o}C and 65s. For a residence time of 30s the optimum temperature was found to be 310 ^{o}C and yield was 32 mg/g BSA.

7.1 Amino acids

The monomeric components of proteins are amino acids. All 21 different amino acids contain an amine group, a carboxylic acid group and a side chain. The side chains vary significantly between different amino acids, there hydrophilic, hydrophobic, aromatic, charged ones etc. Due to the differences in the chemical structure the individual amino acids have somewhat different degradation patterns. However, all amino acids have the same peptide backbone, and undergo similar decarboxylation and deamination reactions resulting mainly in hydrocarbons, amines, aldehydes and acids (Peterson et al., 2008).

Lien *et al* (Lien and Nawar, 1974) investigated the thermal decomposition of valine, leucine and isoleucine at 220 ^{o}C to 270 ^{o}C under non-oxidative conditions. They detected NH_3, CO_2 and CO in all of the three amino acids, whereas the remaining compounds consisted of hydrocarbons (propane, butane, isobutane and isopentane), ketones, aldehydes, primary amines, imines and secondary amines. They concluded that decarboxylation and deamination are responsible for the production of olefins and that the corresponding paraffins result upon reaction with hydrogen.

Klinger *et al* (Klinger et al., 2007) recently studied glycine and alanine, two of the simplest amino acids. Similarly, they found that the primary mechanisms of degradation of these amino acids to be decarboxylation and deamination (Fig. 5). About 50% of their starting material was degraded in 5-15 s in 350 ^{o}C water at 34 MPa. Klinger found no effect of pressure on the decomposition rate between 24 and 34 MPa at 300- 350 ^{o}C. Major compounds were acetaldehyde, acetaldehyde-hydrate, diketopiperazine, ethylamine, methylamine, formaldehydes, lactic acid and propionic acid.

In another study the decomposition behavior of alanine and its derivatives (leucine, phenylalanine, serine, and aspartic acid) was analyzed in the

temperature range of 200-340 ^{o}C and pressure of 20 MPa. The general reaction network of amino acids under hydrothermal conditions proceeded via two main paths: deamination to produce ammonia and organic acids, and decarboxylation to produce carbonic acid and amines. It was found that alanine decomposed at 300 ^{o}C and 20 MPa to produce ammonia, carbonic acid, lactic acid, and pyruvic acid. Traces of acrylic acid, acetic acid, propionic acid, and formic acid were also detected (Sato et al., 2004).

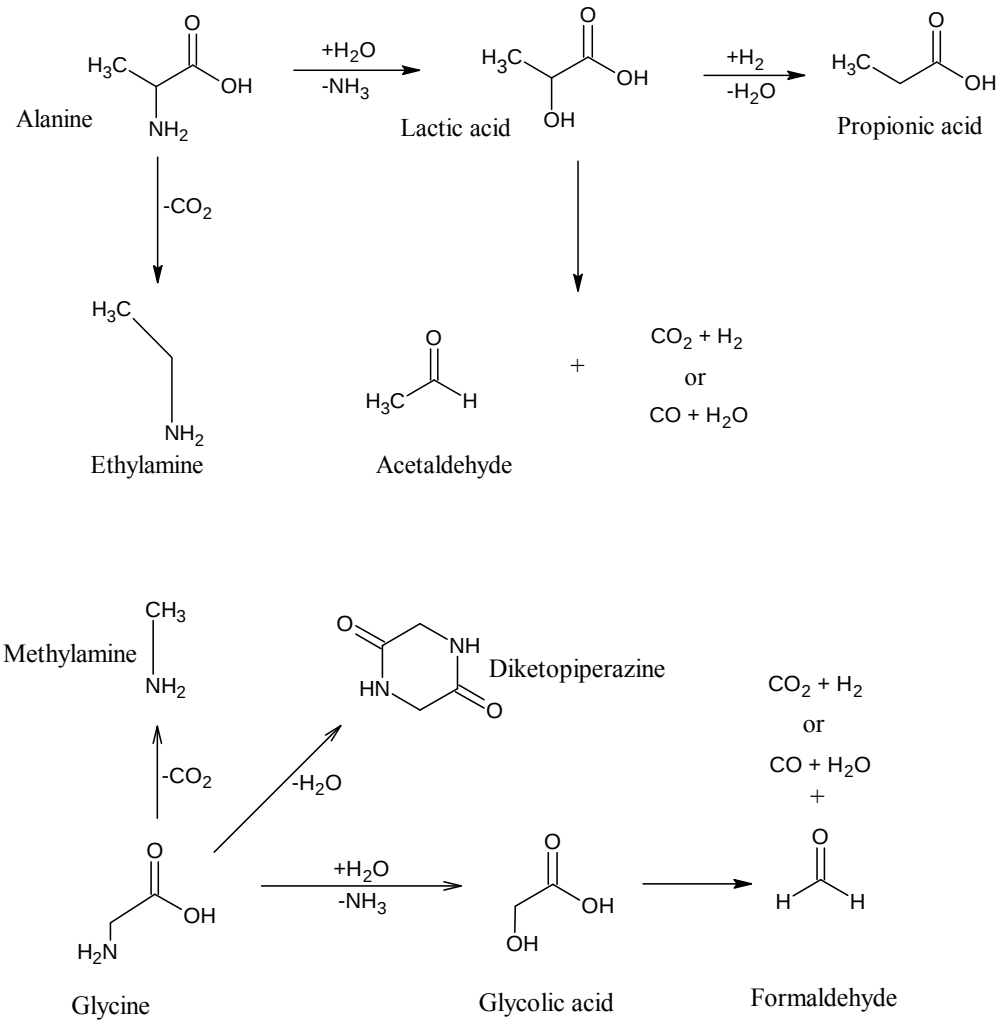

Fig. 5. Reaction network of hydrothermal alanine and glycine decomposition, adapted from (Klinger et al., 2007)

Rogalinski *et al* (Rogalinski et al., 2005) observed production and decomposition of amino acids from bovine serum albumin (BSA) by continuous sub-critical water hydrolysis at 25 MPa, 250-330 ^{o}C and 4-180 sec. The highest total amino acid yields were achieved at 270 ^{o}C and 90 sec. During hydrolysis, in particular, considerable quantities of glycine and alanine was produced, whereas other amino acids like Aspargine was unstable and considerable yields was only seen at a temperature at mild conditions, 250 ^{o}C and a 30 sec. At harsh conditions, 330 ^{o}C and 90 sec there was almost complete degradation of all amino acids.

Besides different gaseous compounds (e.g. CO_2, CO, H_2, and CH_4), in particular low alkanes and alkenes, alcohols (up to C_5), amides, aldehydes, and carboxylic acids were produced.

A summary of the studies on hydrothermal degradation of amino acids is shown in (Table 4).

Table 4 Summary of conversion of amino acids

Substrate	Conditions	Compounds	Reference
Valine, Leucine and Isoleucine	at 220 ^{0}C and above under non-oxidative conditions	NH_3, CO_2 and CO propane, butane, isobutane,isopentane, 3-methyl-1-butene, 2-methyl-1-butene, Propene, butane, isobutylene Acetone, Iso-butylamine	(Lien *et al.* 1974)
glycine and alanine	350 ^{0}C 34 MPa 5-15s	acetaldehyde, acetaldehyde-hydrate diketopiperazine, ethylamine, methylamine, formaldehydes, lactic acid, Propionic acid.	(Klinger *et al.* 2007)
alanine	300 ^{0}C 20 MPa	NH_3, carbonic acid, lactic acid, pyruvic acid, acrylic acid, acetic acid, propionic acid, formic acid	(Sato *et al.* 2004)
bovine serum albumin (BSA)	310 ^{o}C 25 MPa 30s	CO_2, CO, H_2, and CH_4 acetic acid, propanoic acid, n-butyric acid, iso-butyric acid, Iso-valeric acid	(Rogalinski *et al.* 2005)

During hydrolysis of biomass both amino acids and sugars are formed and these can react via the so-called Maillard reaction (Fig. 6). These types of reactions lead to the formation of nitrogen containing cyclic organic compounds, which are more or less strong free radical scavengers and inhibit free radical chain reactions that are highly relevant for gas formation (Kruse et al., 2007c).

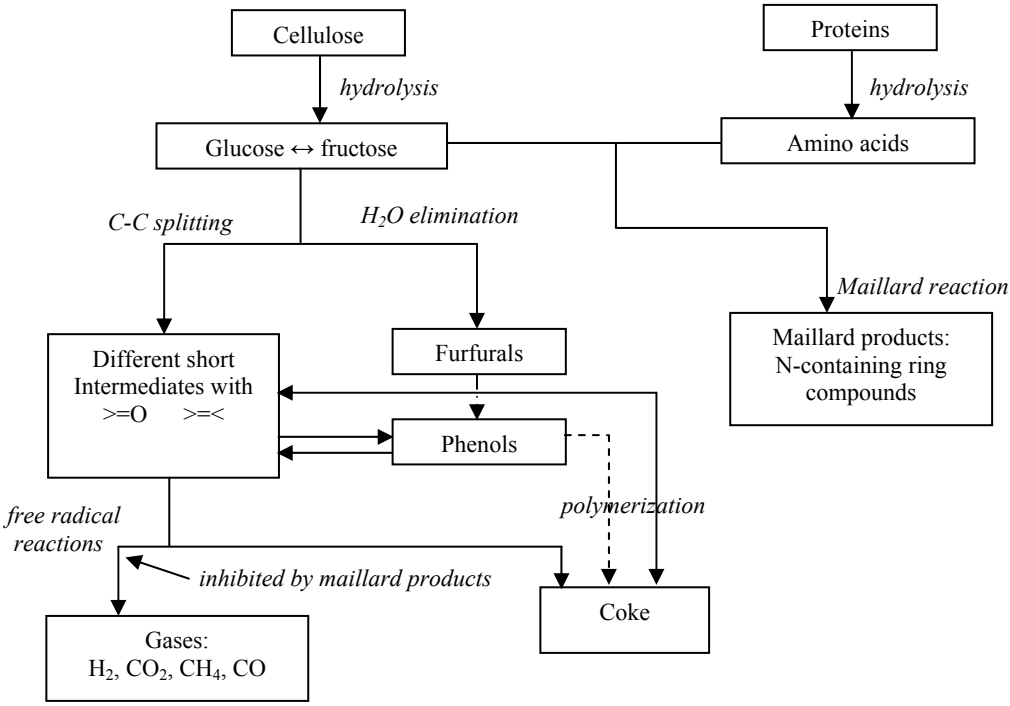

Fig. 6. Reaction pathways of hydrothermal biomass degradation in the presence of proteins, adapted from (Kruse et al., 2007c)

8 Effects of Catalysts

Catalysts are important in hydrothermal liquefaction processes and are used for improving gasification efficiency, suppress tar and char formation etc. Homogeneous catalysts in form of alkali salts have been frequently used, whereas heterogeneous catalysts such as various form for Ni-catalysts has been less frequently utilized in hydrothermal liquefaction. On the other hand, heterogeneous catalysts are widely used in low-temperature water gasification of biomass.

8.1 Homogeneous catalysts

It is well-known that the addition of alkali salts has a positive influence on hydrothermal processes. It improves gasification, accelerates the water-gas shift, suppresses tar and char formation and increases liquid yields.

It was reported that the addition of alkali promoted the yield of fructose and inhibited the yield of anhydrous glucose (AHG) by isomerization reaction of glucose, whereas the addition of acid promoted the dehydration reaction of glucose by providing anhydrous glucose and hydroxymethyl furfural (HMF) (Watanabe et al., 2005a; Yang and Montgomery, 1996; Mok et al., 1992b; Watanabe et al., 2003).

Song *et al* (Song et al., 2004) investigated the effect of Na_2CO_3 on the liquefaction of corn stalk and concluded that the catalyst has a positive effect on the liquefaction process and can increase the yield of liquid products, as well as increase the quality of the liquid product. With a catalyst, more bio-oil and less gas could be obtained than without using a catalyst. The catalyst mainly improved the yield of bio-oil, from 33.4% without a catalyst, increasing to 47.2% with 1.0 wt% of Na_2CO_3.

Alkali also favors the so-called water gas shift and thus favours H_2 and CO_2 formation at the expense of CO. The mechanism proceeds via formation of a formate salt (Sinag et al., 2003; Sinag et al., 2004) and is more thoroughly described below.

A formate salt ($HCOO^-K^+$) is formed by adding alkaline salts. The formation of the formate salt in the presence of K_2CO_3 can be shown by the reactions given below.

$$K_2CO_3 + H_2O \rightarrow KHCO_3 + KOH \quad (1)$$

$$KOH + CO \rightarrow HCOOK \quad (2)$$

Hydrogen is obtained when formate reacts with water.

$$HCOOK + H_2O \rightarrow KHCO_3 + H_2 \quad (3)$$

In the next step, CO_2 is produced by the reaction of $KHCO_3$.

$$2KHCO_3 \rightarrow H_2O + K_2CO_3 + CO_2 \quad (4)$$

$$H_2O + CO \leftrightarrow HCOOH \leftrightarrow H_2 + CO_2 \quad (5)$$

Karagöze *et al* (Karagöze et al., 2006; Karagöze et al., 2005a) performed catalytic hydrothermal treatment of wood biomass at 280 ^oC for 15 min. in the presence of K_2CO_3 with different concentration. They found that the concentrations of base solutions have an important effect on the degradation of wood biomass in terms of both oil yield and conversion. Their study showed that the use of alkali catalyst during the hydrothermal treatment of biomass

inhibits the char formation, and subsequent increase in oil yields. They concluded that the concentration of base solutions has an important effect on the inhibition of char (solid residue) formation. Decreasing the concentration of base solutions decreased the water-soluble hydrocarbons (WSH). They concluded that alkaline salts are more effective than the hydroxides and ranked the order of catalysts activity as follows: K_2CO_3 > KOH > Na_2CO_3 > NaOH. This may come from one possible reason, which is alkaline salts react with water and form their bases and bicarbonates and act as secondary catalyst.
Minowa *et al* (Minowa et al., 1998) tested the catalytic action of Na_2CO_3 during hydrothermal conversion of cellulose. Above 300°C the catalyst decreased secondary tar formation from the oil product and catalyzed the gasification of the aqueous organics.
Watanabe *et al* (Watanabe et al., 2006) enhanced the conversion of C_{17}-acid (fatty acid) decomposition from 2% to 32 % with the addition of KOH catalyst by promoting the decarboxylation of C_{17}-acid.

8.2 Heterogeneous catalysts

Heterogeneous catalysts have so far mostly been used in gasification processes, where they are reported to have a significant positive effect on low-temperature processes. In hydrothermal liquefaction, where the main purpose is to produce liquid products, though, the number of studies is limited. Watanabe and co-workers (Watanabe et al., 2002) studied the influence of heterogeneous acid and base additives, such as metal oxides, on the glucose reactions. They found that the addition of ZrO_2 also promotes isomerization of glucose and fructose, and thus, ZrO_2 can be considered to be a base catalyst for glucose.
Gasification of cellulose was conducted over nickel, palladium, and platinum catalysts with a batch-type reactor at reaction conditions 350 ^oC, 25 MPa, and 10 to 180 min reaction time. It was reported that methane and carbon dioxide were mainly produced over supported nickel catalysts, whereas hydrogen and carbon dioxide were obtained over supported palladium and platinum catalysts (Minowa and Ogi, 1998b; Minowa et al., 1998c; Minowa and Inoue, 1999).
Elliott *et al* (Elliott et al., 1993, 1994a, 1994b) examined the activities of supported ruthenium and nickel catalysts for the gasification with a bench-scale flow type reactor at 350 ^0C and 21 MPa. Various wastewaters such as manure grain and brewer's spent grain were completely gasified to methane and carbon dioxide. They also reported that ruthenium was more stable catalyst than nickel at these conditions.
Watanabe *et al* (Watanabe et al., 2006) studied effect of metal oxide (ZrO_2) on stearic acid ($C_{17}H_{35}COOH$) decomposition at 400 ^oC and 25 MPa for 30 min. They observed metal oxide (ZrO_2) enhanced the decarboxylation of C_{17}-acid and the main products were CO_2 and C_{16} alkene.
Various other heterogeneous catalysts have been tested in hydrothermal conversion processes; however the main focus has been to improve

gasification, not the liquid yields. Examples of these catalysts are Ni/Al_2O_3, Ru/TiO_2 and ZrO_2. Catalysis of gasification at conditions below 400 ^oC was extensively reviewed by (Peterson et al., 2008).

9 Studies on hydrothermal liquefaction of various biomasses

A large amount of studies on hydrothermal liquefaction on various biomasses have been carried out. In general an oily phase, aqueous organics and a CO_2 rich gas phase are formed. However, the yields, oil characteristics and char formation varies widely between different biomasses. In general the energy density in these oils is 30-37 MJ/kg i.e. almost 50% higher than in the biomass itself (Peterson et al., 2008).

Waste materials from the fishing industry and slaughter houses are rich in protein and triglycerides can be converted into water-insoluble bio-oils. Yoshida *et al* (Yoshida et al., 1999) liquefied raw fish meat under subcritical conditions. Aqueous phase and solids were formed as the reaction products at 200 ^oC (1.52 MPa) in 5 min. Amino acids such as cystine, alanine, glycine, and leucine were produced at the optimum conditions of 270 ^oC (5.51 MPa). At 300 ^oC (8.40 MPa), the amount of solids decreased, and water-insoluble phase was formed above the aqueous phase. This water-insoluble phase contains oil and fat-like solids, and the oil with 0.922 g/cm^3 density could be extracted with hexane. When the temperature was further increased to 350 ^oC (16.1 MPa), the solids disappeared, and the amount of water-insoluble phase decreased. This behavior can be explained as follows; the solids formed at low temperature were unconverted substrate and the water-insoluble phase was produced from a part of the solids as the reaction temperature increased. At higher temperature, the water-insoluble phase was increasingly degraded to other organic compounds. Their preliminary analysis with GC/MS showed that the oil extracted with hexane contains useful fatty acids such as arachidonic acid, eicosapentanoic acid (EPA), and docosahexianoic acid (DHA). The total organic carbon (TOC) of the aqueous phase increased from 0.2 at 200 ^oC and reached 0.58 above 300 ^oC, indicating that about 60% of the organic carbon in the raw fish meat was recovered in the aqueous phase. Organic acids produced in the aqueous phase were lactic acid, pyroglutamic acid, phosphoric acid, and acetic acid. Formation of gaseous products such as CO_2 and NH_3 was not significant under the employed reaction conditions.

Cellulose and lignin rich materials represent a large pool of abundant and cheap raw materials. These include not only wood products but also household and agricultural wastes. At the University of Illinois, He and co-workers (He et al., 2000) have worked to convert swine manure into oil via conversion at temperatures of 275-350 ^oC and pressures of 5.5-18 MPa. Carbon monoxide was used as a reducing agent. The process was carried out on a bench scale thermochemical conversion (TCC) reactor operated in a batch mode. Retention time varied from 5 to 180 min. for different operating conditions. The produced

oil was found to have heating values of approximately 35 MJ/kg and to be made up of 71% carbon, 14.2% oxygen, 8.9% hydrogen, 4.1% nitrogen, and 0.21 ppm of sulfur. CO_2 was the sole detected gaseous by-product. In another study the liquefaction of garbage was studied (Minowa et al., 1995), generally at conditions of 340 ^oC, 18 MPa with Na_2CO_3 catalyst and 0.5h residence time. The oil was obtained in the highest yield of 27.6% with heating value of 36 MJ/kg.

In another study on liquefaction of Indonesian biomass residue, heavy oil was produced in the presence of Na_2CO_3 as the catalyst at 300 ^oC and around 10MPa in 30 min. The oil yield was between 21-36 wt%, the calorific value around 30MJ/kg and the viscosity>10^5 mPa.s (Minowa et al., 1998a).

Karagöz *et al* (Karagöz et al., 2005b) conducted hydrothermal liquefaction of wood (saw dust) and non-wood biomass (rice husk), and major biomass components (lignin and cellulose) at 280 ^oC for 15 min. Total oil yield was 3.9% from lignin and highest solid residue of 60%. The major hydrocarbons from hydrothermal liquefaction of lignin were 2-methoxy-phenol and 1, 2-benzenediol derivatives. They concluded decomposition of lignin in water (280 ^oC, 15 min.) was comparatively less than other samples.

Demirbaş (Demirbaş et al., 2005) obtained the highest heavy oil yield of 28% from beech wood at liquefaction temperature around 376 ^oC in 25 min. The oil was found to have heating values of approximately 34.9 MJ/kg.

Table 5 Summary of conversion of various biomasses

Substrate	Conditions	Compounds	Reference
Raw fish meat	350 °C 16.1 MPa 5 min. Without oxidants	NH_3, CO_2 lactic acid, pyroglutamic acid phosphoric acid, acetic acid citric acid, malic acid sussinic acid, formic acid Arachidonic acid Eicosapentanoic acid (EPA) Docosahexianoic acid (DHA)	(Yoshida *et al.* 1999)
Swine manure	275-350 °C 5.5-18 MPa 5 to 180 min.	Raw oil Average yield = 53.8% heating value = 35MJ/kg	(He *et al.* 2000)
Garbage	340 °C , 18 MPa, 0.5 h Na_2CO_3 as catalyst	Oil Highest yield = 27.6% calorific value = 36 MJ/kg	(Minowa et al., 1995)
Indonesian biomass residues	300 °C 10MPa, 30min. Na_2CO_3 as catalyst	Heavy oil yields between 21-36% calorific value = 30MJ/kg	(Minowa *et al.* 1998a)
Saw dust, rice husk lignin and cellulose	280 °C 15 min.	2-methoxy-phenol 4-methyl phenol Hexadecanoic acid Octadecanoic acid 1, 2-benzenediol derivatives	(Karagöz *et al.* 2005b)
Beech wood	376 °C 25 min.	Heavy oil yields =28% heating value = 34.9MJ/kg	(Demirbas *et al.* 2005)
Phytomass	330-410 °C 30-50 MPa 15 min.	CO_2, H_2, CH_4 Ethane, ethane, propane, propene, isobutene,methylpropene, cis/trans-butene, Phenol, o-cresol, m- and p-cresol, Methylfurfural Leyulinic acid, acetic acid, formic acid	(Kruse and Gawlik, 2003)

(Kruse and Gawlik, 2003) studied reaction of wet biomass (phytomass) at 330, 370, and 410 °C and at 30, 40, and 50 MPa in 15 min. reaction time. In gas-phase they obtained CO_2 as a major product but above the critical temperature

they found the increase in the yields of H_2 and CH_4 and a decrease of CO. Ethane, ethane, propane, propene, isobutene, methylpropene, and cis/trans-butene were identified as minor hydrocarbon products. In liquid-phase they mainly focused on phenols and furfurals. Phenol, o-cresol, and the sum of m- and p-cresol were determined. Only very small amount of methylfurfural could be detected. The aqueous liquid phase possessed leyulinic acid, acetic acid, formic acid and some acetic and formic aldehydes.

10 Review of different Processes

This section contains a brief detail of historic and ongoing approaches to the liquefaction process. (Table 6) shows an overview of direct liquefaction processes of different biomass materials.

Pioneering liquefaction work was done by Appell and coworkers at the Pittsburgh Energy Research Center in the 1970s, which was later demonstrated at a pilot plant in Albany, Oregon. This process differed from most modern processes in that the high-pressure reaction took place in an oil-rich phase (anthracene oil), rather than a water-rich phase. In their continuous process wood flour was heated to about 330 to 370 ^{o}C and a pressure of 20 MPa in the presence of ~5 % Na_2CO_3 catalyst and water at a ratio of about 2.8 kg water per kg wood for residence time of 10 to 30 min. They obtained heavy oil with heating value of 34.52 MJ/kg on dry basis. Later on, researchers at Lawrence Berkeley Laboratory pointed out that the high-pressure liquefaction could take place in a water-rich phase, rather than an oil-rich phase, which eliminated the need for recycle but employed subsequent alkaline and acid treatments (Bouvier et al., 1988; Stevens, 1994). Both processes were demonstrated at the Albany, Oregon facility starting from the late 1970s, but research was halted by the US Department of Energy in the early 1980s as the price of petroleum began to drop and national interests shifted to fuel additives, such as ethanol.

The HTU® process has been investigated in 1981-1988 at Shell Laboratory in Amsterdam, as a reaction to the two oil crisis of 1973 and 1980. Due to the commercial circumstances in the late eighties, the research on the promising HTU® technology was discontinued after only a few hundred hours of continuous bench scale operation. On November 1st, 1997, with support from the Dutch Government, a consortium with Shell Netherlands and Stork Engineers & Contractors as the main partners started a R&D program that ran till the end of 2000.

Table 6 Overview of direct liquefaction processes

Process Name	Developer/Supplier of the Process	Raw Material	Temperature, ^{0}C	Pressure, MPa
PERC-Process	Pittsburg Energy Research Center (USA)	Wood Chips	330-370	20
LBL-Process	Lawrence Berkeley Laboratory (USA)	Wood Chips	330-360	10-24
HTU-Process	Shell Research Institute (NL)	All types of biomass, domestic, agricultural, and industrial residues, wood	300-350	12-18
DoS-Process	HAW (GER)	Lignocellulosic biomass (e.g. wood, straw)	350-500	8.0
CatLiq-Process	SCF Technologies A/S (DK)	DDGS	280-350	22.5-25

Its purpose was a validated process on pilot plant scale for the generation of data for the reliable design of the first commercial applications. Based on the results of R&D project, including the process design studies, a technical and economic feasibility study was carried out for a first commercial demonstration plant at a scale of 25000 tons biomass (dry basis)/year for the conversion of the wet organic fraction of domestic waste. This feasibility study intends to establish the potential for a first commercial demonstration of the HTU® process.

In the Hydrothermal Upgrading process a number of different biomass (also with high moisture content) can be liquefied under high pressure (Naber and Goudriaan, 2005; Feng et al., 2004). The biomass is suspended and pumped into the reactor using a high pressure pump. At temperatures of 300 to 350 ^{o}C, pressure between 12 and 18 MPa and a residence time of 5 to 20 min. a bio-crude is produced. The oxygen in the biomass is removed by water and CO_2. The product consists of 45 % bio-crude (wt% of input material, dry and without ash), 25% gas (>90% CO_2), 20% H_2O and 10% dissolved organic materials (e.g. acetic acid, ethanol). Bio-crude is a heavy organic fluid that becomes solid at 80 ^{o}C. The heating value is 30-35 MJ/kg, the H/C ratio is 1:1

and the oxygen content is between 10 to 18%. The thermal efficiency for one variant of this process amounts to 74.9% (theoretically a maximum of 78.6% could be reached) (Behrendt et al., 2008).
HAW (Hochschule für Angewandte Wissenschaften Hamburg, Germany) developed the DoS process which is a direct one-step liquefaction process for lignocellulosic biomass (e.g. wood, straw). It works under a pressure of about 8.0 MPa and at temperatures between 350 and 500 ^{o}C. The conversion of hackled and dried biomass is carried out in a bottom phase reactor under high-pressure using hydrogen to produce oil, water, coal and gas. The thermal efficiency of the whole system is around 70% (Behrendt et al., 2008).
The Danish company SCF Technologies has developed the CatLiq technology and operates a 20 L/h capacity pilot plant in Copenhagen, Denmark. In the CatLiq® process the organic fraction of DDGS (Dried Distillers Grains with Solubles), is converted to oil in the presence of a homogeneous (K_2CO_3) and a heterogeneous (Zirconia) catalyst, at subcritical conditions (280-350 ^{o}C and 22.5-25 MPa). The full product consists of a top-phase of bio-oil, a gas-phase mainly consisting of CO_2, a water phase with soluble organic compounds (e.g. ethanol, acetic acid.) and a bottom-phase mainly consisting of inorganic salts.
The CatLiq® process has been demonstrated to be an effective technology for catalytic liquid conversion of DDGS, giving a high yield of bio-crude oil. Even though the oil is not directly suitable as transportation fuel it may well be used for direct green electricity production, as input for refineries or as marine diesel. The CatLiq® technique offers an alternative use of WDGS and thus flexibility in terms of product spectrum. In addition a CatLiq process based on WDGS process with optimized energy integration will consume less energy than a drying process for DDGS production, since the CatLiq process is carried out in the liquid state.
EPA's Water Engineering Research Laboratory, Cincinnati, OH developed a prototype sludge-to-oil reactor system (STORS) capable of processing undigested municipal sewage sludge with 20% solids at a rate of 30L/hr. Approximately 73% of the energy content of the feedstock was recovered as combustible products (oil and char), suitable for use as a boiler fuel. The oil product had a heating value of 80 to 90% that of diesel fuel. Sludge liquefaction occurred rapidly above 265 ^{o}C. The feedstock conversion was completely achieved at 300 ^{o}C with nominal 1.5h residence time (Molton et al., 1986).

Conclusion

Thermochemical conversion can be subdivided into gasification, pyrolysis, and direct liquefaction. Direct liquefaction is attractive from the view point of energy consumption and it's a promising method for the biomass conversion. The carbonaceous materials are converted to liquefied products through a complex sequence of changes in physical structure and chemical bonds.

Liquefaction process may become an important technology for converting wet biomass or organic waste into bio-oil or other types of fuels. Technical hurdles are not yet solved completely but significant progress has been made through experimentation.
Catalyst has a positive effect on the liquefaction process and can increase the yield of liquid product, as well as improve the quality of liquid product. With a catalyst, more bio-oil and less gas can be obtained than that without using a catalyst.
Among the available solutions, biomass liquefaction has been regarded as a long-term option and so might appear now as unimportant. Nonetheless, its potential does really exist, particularly for producing specific fuels. Research and development have to progress in order to solve the associated technological problems and integrate the product into existing markets.

References

Ahluwalia, K.S., 1996. United States Patent: 5, 571, 424.

Ahluwalia, K.S., 1997. United States Patent: 5, 670, 040.

Akiya, N., Savage, P., 2002. Roles of water for chemical reactions in high-temperature water. Chemical Reviews 102 (8), 2725-2750.

Antal Jr, M.J., Mok, W.S.L., 1990. Mechanism of formation of 5-(hydroxymethyl)-2-furaldehyde from D-fructose and sucrose. Carbohydrate Research 199, 91-109.

Asghari, F.S., Yoshida, H., 2006. Acid catalyzed production of 5-Hydroxymethyl Furfural from d-Fructose in subcritical water. Industrial & Engineering Chemistry Research 45 (7), 2163-2173.

Behrendt, F., Neubauer, Y., Oevermann, M., Wilmes, B., Zobel, N., 2008. Direct liquefaction of biomass-Review. Chem. Eng. Technology 31 (5), 667-677.

Bermejo, M.D., Cocero, M.J., 2006a. Supercritical water oxidation: A technical review. AIChE Journal 52 (11), 3933-3951.

Bermejo, M.D., Cocero, M.J., 2006b. Destruction of an industrial wastewater by supercritical water oxidation in a transpiring wall reactor. Journal of Hazardous Materials B137, 965-971.

Bobleter, O., 1994. Hydrothermal degradation of polymers derived from plants. Polymer Science 19, 797-841.

Bonn, G., Bobleter, O., 1983. Determination of the hydrothermal degradation products of D- (U-^{14}C) glucose and D- (U-^{14}C) fructose by TLC. Journal of Radioanalytical Chemistry 79 (2), 171-177.

Boon, J.J., Pastorova, I., Botto, R.E., Arisz, P.W., 1994. Structural studies on cellulose pyrolysis and cellulose char by PYMS, PYGCMS, FTIR, NMR and by wet chemical techniques. Biomass and Bioenergy 7 (1-6), 25-32.

Bouvier, J.M., Gelus, M., Maugendre, S., 1988. Wood liquefaction-An overview, Applied Energy 30 (2), 85-98.

Bridgwater, A.V., 2001. Progress in thermochemical biomass conversion, Blackwell Science Ltd. London, Vol. 2, pp. 1312.

Bridgwater, A.V., Meier, D., Radlein, D., 1999. An overview of fast pyrolysis of biomass. Organic Geochemistry 30, 1479-1493.

Bröll, D., Kaul, C., Krämer, A., Krammer, P., Richter, T., Jung, M., Vogel, H., Zehner, P., 1999. Chemistry in Supercritical Water. Angew. Chem. Int. Ed. 38, 2998±3014.

Brunner, G., 2009. Near critical and supercritical water. Part I. Hydrolytic and hydrothermal processes. Journal of Supercritical Fluids 47, 373-381.

Bühler, W., Dinjus, E., Ederer, H.J., Kruse, A., Mas, C., 2002. Ionic reactions and pyrolysis of glycerol as competing reaction pathways in near- and supercritical Catalytic dehydration of biomass-derived polyols in sub- and supercritical water. Journal of Supercritical Fluids 22, 37-53.

Changing World Technologies. Thermal Depolymerization Process. http://www.changingworldtech.com/who/index.asp (accessed 01-07-10).

Chornet, E., Overend, R.P., 1985. Biomass liquefaction: An overview, in fundamentals of thermochemical biomass conversion: Overend , R.P., Milne T.A., Mudge, L.K. (Eds.), Elsevier., London.

Cocero, M.J., Alonso, E., Sanz, M.T., Fdz-Polanco, F., 2002. Supercritical water oxidation process under energetically self-sufficient operation. Journal of Supercritical Fluids 24, 37-46.

Dell'Orco, P.C., Li, L., Gloyna, E.F., 1993. The separation of particles from supercritical water oxidation processes. Separation Science and Technology 28, 624-642.

Delmer, D.P., Amor, Y., 1995. Cellulose Biosynthesis. The Plant Cell 7, 987-1000.

Demirbaş, A., 2000. Mechanisms of liquefaction and pyrolysis reactions of biomass. Energy Convers. Manage. 41, 633-46.

Demirbaş, A., 2005. Thermochemical conversion of biomass to liquid products in the aqueous medium. Energy Source 27, 1235-1243.

Elliott, D.C., Beckman, D., Bridgwater, A.V., Diebold, J.P., Gevert, S.B., Solantausta, Y., 1991. Developments in direct thermochemical liquefaction of biomass: 1983-1990. Energy and Fuels 5, 399-410.

Elliot, D.C., Sealock Jr, L.J., Baker, E. G., 1993. Chemical processing in high-pressure aqueous environments. 2. Development of catalysts for gasification. Industrial & Engineering Chemistry Research 32, 1542-1548.

Elliot, D.C., Phelps, M.R., Sealock Jr, L.J., Baker, E.G., 1994a. Chemical processing in high-pressure aqueous environments. 3. Continuous-flow reactor process development experiments for organics destruction. Industrial & Engineering Chemistry Research 33, 566-574.

Elliot, D.C., Sealock Jr, L.J., Baker, E.G., 1994b. Chemical processing in high-pressure aqueous environments. 3. Batch reactor process development experiments for organics destruction. Industrial & Engineering Chemistry Research 33, 558-565.

Feng, w., van der Kooi, H.J., de Swaan Arons, J., 2004. Phase equilibria for biomass conversion processes in subcritical and supercritical water. Chem. Eng. Journal 98, 105-113.

Franck, E.U., 1968. Supercritical water. Endeavour 27, 55-59.

Franck, E.U., 1983. Thermochemical properties of supercritical fluids with special consideration of aqueous Systems. Fluid Phase Equilibr.10, 211-222.

Franck, E.U., Weingärtner, H., 1999. Chemical Thermodynamics. A Chemistry for the 21 st Century Monograph 105-119.

Hahn-Hägerdal, B., Galbe, M., Gorwa-Grauslund, M.F., Lidén, G., Zacchi, G., 2006. Bio-ethanol-the fuel of tomorrow from the residues of today. Trends in Biotechnology 24, 549-556.

He, B.J., Zhang, Y., Funk, T.L., Riskowski, G.L., Yin, Y., 2000. Thermochemical conversion of swine manure: An alternative process for waste treatment and renewable energy production. American Society of Agricultural Engineers 43(6), 1827-1833.

Heddle, J.F., 1979. Activated sludge treatment of slaughter house wastes with protein recovery. Water Research 13, 581-584.

Heger, K., Uematsu, M., Franck, E.U., 1980. The static dielectric constant of water at high pressures and temperatures to 500 MPa and 550 ^{0}C. Ber. Bunsen-Gas. Phys. Chem. 84, 758-762.

Hodes, M., Marrone, P.A., Hong, G.T., Smith, K.A., Tester, J.W., 2004. Salt precipitation and scale control in supercritical water oxidation-Part A: fundamentals and research. Journal of Supercritical Fluids 29, 265-288.

Holliday, R.L., King, J.W., List, G.R., 1997. Hydrolysis of vegetable oils in sub- and supercritical water. Industrial & Engineering Chemistry Research 36, 932-935.

Hunter, S.E., Savage, P.E., 2004. Recent advances in acid-and base-catalyzed organic synthesis in high-temperature liquid water. Chemical Engineering Science 59, 4903-4909.

IEO, 2009. International Energy Outlook 2009. Liquid fuels.

Kabyemela, B.M., Adschiri, T., Malaluan, R.M., Arai, K., 1997a. Degradation kinetics of dihydroxyacetone and glyceraldehyde in subcritical and supercritical water. Industrial & Engineering Chemistry Research 36 (6), 2025-2030.

Kabyemela, B.M., Adschiri, T., Malaluan, R.M., Arai, K., 1997b. Kinetics of Glucose Epimerization and Decomposition in Subcritical and Supercritical Water. Industrial & Engineering Chemistry Research 36 (5), 1552-1558.

Kabyemela, B.M., Adschiri, T., Malaluan, R.M., Arai, K., 1999. Glucose and Fructose Decomposition in Subcritical and Supercritical Water: Detailed Reaction Pathway, Mechanisms, and Kinetics. Industrial & Engineering Chemistry Research 38 (8), 2888-2895.

Kamio, E., Sato, H., Takahashi, S., Noda, H., Fukuhara, C., Okamura, T., 2008. Liquefaction kinetics of cellulose treated by hot compressed water under variable temperature conditions. Journal of Materials Science 43, 2179-2188.

Karagöz, S., Bhaskar, T., Muto, A., Sakata, Y., Oshiki, T., Kishimoto, T., 2005a. Low-temperature catalytic hydrothermal treatment of wood biomass: analysis of liquid products. Chemical Engineering Journal 108, 127–137.

Karagöz, S., Bhaskar, T., Muto, A., Sakata, Y., 2005b. Comparative studies of oil compositions produced from sawdust, rice husk, lignin and cellulose by hydrothermal treatment. Fuel 84, 875-884.

Karagöz, S., Bhaskar, T., Muto, A., Sakata, Y., 2006. Hydrothermal upgrading of biomass: Effect of K_2CO_3 concentration and biomass/water ratio on products distribution. Bioresource Technology 97, 90–98.

Kevin, B., 2001. The SlurryCarb^{TM} Process: Turning Municipal Wastewater solids into a Profitable Renewable Fuel. Proceedings of the Water Environment Federation 15, 1456-1470

Khuwijitjaru, P., Adachi, S., Matsuno, R., 2002. Solubility of saturated fatty acids in water at elevated temperatures. Biosci. Biotechnol. Biochem. 66 (8), 1723-1726.

Kim, Y., Mosier, N.S., Hendrickson, R., Ezeji, T., Blaschek, H., Dien, B., Cotta, M., Dale, B., Ladisch, M.R., 2008. Composition of corn dry-grind ethanol by-products: DDGS, wet cake, and thin stillage. Bioresource Technology 99, 5165–5176.

King, J.W., Holliday, R.L., List, G.R., 1999. Hydrolysis of soybean oil in a subcritical water flow reactor. Green Chemistry 1 (6), 261–264.

Klingler, D., Berg, J., Vogel, H., 2007. Hydrothermal reactions of alanine and glycine in sub- and supercritical water. Journal of Supercritical Fluids 43, 112–119.

Krammer, P., Vogel, H., 2000. Hydrolysis of esters in subcritical and supercritical water. J. Supercrit. Fluids 16, 189-206.

Kritzer, P., 2004. Corrosion in high-temperature and supercritical water and aqueous solutions: a review. Journal of Supercritical Fluids 29, 1-29.

Kritzer, P., Dinjus, E., 2001. An assessment of supercritical water oxidation (SCWO) Existing problems, possible solutions and new reactor concepts. Chemical Engineering Journal 83, 207-214.

Kruse, A., Dinjus, E., 2007a. Hot compressed water as reaction medium and reactant properties and synthesis reactions. J. Supercrit. Fluids 39, 362-380.

Kruse, A., Dinjus, E., 2007b. Hot compressed water as reaction medium and reactant 2. Degradation reactions. Journal of Supercritical Fluids 41, 361-379.

Kruse, A., Gawlik, A., 2003. Biomass conversion in water at 330-410 ^{0}C and 30-50 MPa. Identification of key compounds for indicating different chemical reaction pathways. Industrial & Engineering Chemistry Research 42, 267-279.

Kruse, A., Maniam, P., Spieler, F., 2007c. Influence of proteins on the hydrothermal gasification and liquefaction of biomass. 2. Model compounds. Industrial & Engineering Chemistry Research 46 (1), 87-96.

Lehr, V., Sarlea, M., Ott, L., Vogel, H., 2007. Catalytic dehydration of biomass-derived polyols in sub- and supercritical water. Catalysis Today 121, 121-129.

Lien, Y.C., Nawar, W.W., 1974. Thermal decomposition of some amino acids Valine, Leucine and Isoleucine. Journal of Food Science 39, 911-913.

Lin, Y., Tanaka, S., 2006. Ethanol fermentation from biomass resources: current state and prospects. Applied Microbiology and Biotechnology 69, 627-642.

Liu, A., Park, Y.K., Huang, Z., Wang, B., Ankumah, R.O., Biswas, P.K., 2006. Product identification and distribution from hydrothermal conversion of walnut shells. Energy and Fuel 20, 446-454.

Luijkx, G.C.A., Rantwijk, F.V., Bekkum, H.V., 1993. Hydrothermal formation of 1,2,4-benzenetriol from 5 hydroxymethyl-2-furaldehyde and D-fructose. Carbohydrate Research 242, 131-139.

Marrone, P.A., Hodes, M., Smith, K.A., Tester, J.W., 2004. Salt precipitation and scale control in supercritical water oxidation-Part B: commercial/full-scale applications. Journal of Supercritical Fluids 29, 289-312

Marshall, W.L., Franck, E.U., 1981. Ion product of water substance, 0-1000 ^{0}C, 1-10,000 bar new international formulation and its background. J. Phys. Chem. Ref. Data 10, 295-304.

Mata-Alvarez, J., Macé, S., Llabrés, P., 2000. Anaerobic digestion of organic solid wastes: An overview of research achievements and prospectives. Bioresource Technology, 74, 3-16.

Matsumura, Y., Minowa, T., Potic, B., Kersten, S.R.A., Prins, W., van Swaaij, W.P.M., van de Beld, B., Elliott, D.C., Neuenschwander, G.G., Kruse, A., Antal Jr, M.J., 2005. Biomass gasification in near- and super-critical water: Status and prospects. Biomass and Bioenergy 29, 268-292.

Minowa, T., Inoue, S., 1999. Hydrogen production from biomass by catalytic gasification in hot compressed water. Renewable Energy 16, 1114-1117.

Minowa, T., Kondo, T., Sudirjo, s., 1998a. Thermochemical liquefaction of Indonesian biomass residues. Biomass Bioenergy 14, 517-24.

Minowa, T., Murakami, M., Dote, Y., Ogi, T., Yokoyama, S., 1995. Oil production from garbage by thermochemical liquefaction. Biomass and Bioenergy 8 (2), 117-120.

Minowa, T., Ogi, T., 1998b. Hydrogen production from cellulose using a reduced nickel catalyst. Catalysis Today 45, 411-416.

Minowa, T., Zhen, F., Ogi, T., 1998c. Cellulose decomposition in hot-compressed water with alkali or nickel catalyst. Journal of Supercritical Fluids 13, 253-259.

Miyazawa, T., Ohtsu, S., Nakagawa, Y., Funazukuri, T., 2006. Solvothermal treatment of starch for the production of glucose and maltooligosaccharides. Journal of Materials Science 41, 1489-1494.

Mok, W.S.L., Antal Jr., M.J., 1992a. Uncatalyzed solvolysis of whole biomass hemicellulose by hot compressed liquid water. Industrial & Engineering Chemistry Research 31 (4), 1157-1161.

Mok, W.S.L., Antal Jr, M.J., Varhegyi, G., 1992b. Productive and parasitic pathways in dilute acid-catalyzed hydrolysis of cellulose. Industrial & Engineering Chemistry Research 31 (1), 94-100.

Molton, P.M., Fassbender, A.G., Brown, M.D., 1986. STORS: The sludge-to-oil reactor system. U.S. Environmental Protection Agency EPA/600/S2-86/034

Moreau, C., Durand, R., Roux, A., Tichit, D., 2000. Isomerization of glucose into fructose in the presence of cation-exchanged zeolites and hydrotalcites. Applied catalysis A 193, 257-264.

Naber, J.E., Goudriaan, F., 2005. HTU®-Diesel from biomass. ACS Division of Fuel Chemistry. http://membership.acs.org/P/PETR/2005-Biorefineries/Presentation-08.ppt.

Nagamori, M., Funazukuri, T., 2004. Glucose production by hydrolysis of starch under hydrothermal conditions. Journal of Chemical Technology & Biotechnology 79 (3), 229-233.

Osada, M., Sato, T., Watanabe, M., Shirai, M., Arai, K., 2006. Catalytic gasification of wood biomass in subcritical and supercritical water. Combustion Science and Technology 178, 537-552.

Pessoa JR, A., Mancilha, I.M., Sato, S., 1997. Acid hydrolysis of hemicellulose from sugarcane bagasse. Brazilian Journal of Chemical Engineering 14 (3).

Peterson, A.A., Vogel, F., Lachance, R.P., Fröling, M., Antal, M.J., Tester, J.W., 2008. Thermochemical biofuel production in hydrothermal media: A review of sub- and supercritical water technologies. Energy and Environmental Science 1, 32-65.

Rogalinski, T., Herrmann, S., Brunner, G., 2005. Production of amino acids from bovine serum albumin by continuous sub-critical water hydrolysis. Journal of Supercritical Fluids 36, 49-58.

Rogalinski, T., Liu, K., Albrecht, T., Brunner, G., 2008. Hydrolysis kinetics of biopolymers in subcritical water. Journal of Supercritical Fluids 46, 335–341.

Russell, J.A., Miller, R.K., Motton, P.M., 1983. Formation of aromatic compounds from condensation reactions of cellulose degradation products. Biomass 3, 43-57.

Sasaki, M. Adschiri, T., Arai, K., 2004. Kinetics of cellulose conversion at 25 MPa in sub- and supercritical water. AIChE Journal 50 (1), 192-202.

Sasaki, M., Fang, Z., Fukushima, Y., Adschiri, T., Arai, K., 2000. Dissolution and Hydrolysis of Cellulose in Subcritical and Supercritical Water. Industrial & Engineering Chemistry Research 39 (8), 2883-2890.

Sasaki, M., Goto, K., Tajima, K., Adschiri, T., Arai, K., 2002. Rapid and selective retro-aldol condensation of glucose to glycoaldehyde in supercritical water. Green Chemistry 4, 285-287.

Sasaki, M., Hayakawa, T., Arai, K., Adichiri, T., 2003. Measurement of the rate of retro-aldol condensation of D- xylose in subcritical and supercritical water. Presented at the Proceeding of the 7th International Symposium on Hydrothermal Reactions. 169-176.

Sato, N., Quitain, A.T., Kang, K., Daimon, H., Fujie, K., 2004. Reaction kinetics of amino acid decomposition in high-temperature and high-pressure water. Industrial & Engineering Chemistry Research 43, 3217-3222.

Schubert, M., Regler, J.W., Vogel, F., 2010. Continuous salt precipitation and separation from supercritical water. Part 1: Type 1 salts. Journal of Supercritical Fluids 52, 99-112.

Sinag, A., Kruse, A., Rathert, J., 2004. Influence of the heating rate and the type of catalyst on the formation of key intermediates and on the generation of gases during hydropyrolysis of glucose in supercritical water in a batch reactor. Industrial & Engineering Chemistry Research 43, 502-508.

Sinag, A., Kruse, A., Schwarzkopf, V., 2003. Key compounds of the hydropyrolysis of glucose in supercritical water in the presence of K2CO3. Industrial & Engineering Chemistry Research 42, 3516-3521.

Song, C., Hu, H., Zhu, S., Wang, G., Chen, G., 2004. Nonisothermal catalytic liquefaction of corn stalk in subcritical and supercritical water. Energy & Fuels 18, 90-96.

Speck Jr, J.C., 1953. The Lobry de Bruyn-Alberda van Ekenstein Transformation, Advance Carbohydrate Chemistry 13, 63.

Srokol, Z., Bouche, A.G., Estrik, A.V., Strik, RC.J., Maschmeyer, T., Peters, J.A., 2004. Hydrothermal upgrading of biomass to biofuel; studies on some monosaccharide model compounds. Carbohydrate Research 339, 1717–1726.

Stevens, D.J., 1994. Review and analysis of the 1980–1989 biomass thermochemical conversion program. U.S. Department of Energy NREL/TP-421-7501.

Sun, Y., Cheng, J., 2002. Hydrolysis of lignocellulosic materials for ethanol production: a review. Bioresource Technology 83, 1-11.

Uematsu, M., Franck, E.U., 1980. Static dielectric constant of water and steam. J. Phys. Chem. Ref. Data. 9 (4), 1291-1306.

Watanabe, M., Aizawa, Y., Iida, T., Aida, T.M., Levy, C., Sue, K., Inomata, H., 2005a. Glucose reactions with acid and base catalysts in hot compressed water at 473 K. Carbohydrate Research 340, 1925–1930.

Watanabe, M., Aizawa, Y., Iida, T., Nishimura, R., Inomata, H., 2005b. Catalytic glucose and fructose conversions with TiO2 and ZrO2 in water at 473K: Relationship between reactivity and acid-base property determined by TPD measurement. Applied Catalysis A 295, 150–156.

Watanabe, M., Iida, T., Aizawa, Y., Ura, H., Inomata, H., Arai, K., 2003. Conversions of some small organic compounds with metal oxides in supercritical water at 673 K. Green Chemistry 5, 539–544.

Watanabe, M., Iida, T., Inomata, H., 2006. Decomposition of a long chain saturated fatty acid with some additives in hot compressed water. Energy Conversion and Management 47, 3344–3350.

Watanabe, M., Inomata, H., Arai, K., 2002. Catalytic hydrogen generation from biomass (glucose and cellulose) with ZrO_2 in supercritical water. Biomass and Bioenergy 22, 405 – 410.

Wheals, A.E., Basso, L.C., Alves, D.M.G., Amorim, H.V., 1999. Fuel ethanol after 25 years. TIBTECH 17, 482 – 487.

Xian, Z., Chao, Z., Liang, Z., Hongbin, C., 2008. Amino acid production from fish proteins hydrolysis in subcritical Water. Chinese Journal of Chemical Engineering 16 (3), 456-460.

Yang, B.Y., Montgomery, R., 1996. Alkaline degradation of glucose: effect of initial concentration of reactants. Carbohydrate Research 280, 27-45.

Yoshida, H., Terashima, M., Takahashi, Y., 1999. Production of organic acids and amino acids from fish meat by sub-critical water hydrolysis. Biotechnology Progress 15, 1090-1094.

Yu, Y., Lou, X., Wu, H., 2008. Some recent advances in hydrolysis of biomass in hot-compressed water and its comparisons with other hydrolysis methods. Energy & Fuels 22, 46-60.

Zhang, B., Huang, H.J., Ramaswamy, S., 2008. Reaction kinetics of the hydrothermal treatment of lignin. Appl Biochem Biotechnol 147, 119-131.

Production and evaluation of CatLiq® bio-oil from catalytic liquid conversion of DDGS

TOOR, S. S.[1], ROSENDAHL, L.[1], NIELSEN, M.P.[1], OLOFSSON, G[2]. and RUDOLF, A[2].

[1]Institute of Energy Technology
Aalborg University
Pontoppidanstraede 101, DK-9220 Aalborg
sst@iet.aau.dk, http://www.iet.aau.dk
[2]SCF Technologies A/S
Smedeholm 13B
DK-2730 Herlev
anr@scf-technologies.com

Abstract: - The CatLiq® process is a second generation process for the production of bio-oil from various aqueous biomass-based waste products. The process is carried out at subcritical conditions (280-350 ^{o}C and 225-250 bar) in the presence of a homogeneous alkaline and a heterogeneous Zirconia catalyst. The raw material used in this study was DDGS (Dried Distillers Grains with Solubles), a byproduct in first generation ethanol production, available in large quantities. In the current work, catalytic conversion of DDGS was performed in a continuous pilot plant with a capacity of 10-20 L/h of wet biomass. In the process, DDGS was converted to bio-oil, combustible gases and water-soluble organic compounds. The oil obtained was characterized using several analysis methods, among them element analysis and GC-MS and these studies on the bio-oil showed that the oil obtained from DDGS has good fuel properties and potentially can be used for combustion or being further processed.

Key-Words: hydrothermal liquefaction, sub-critical, renewable fuel, bio-oil, DDGS, pilot-plant

2 INTRODUCTION

The rapid increase in global energy demand makes the search for new energy sources a major concern, and as a consequence, there is a big interest in the production and use of renewable energy.

Biomass in various forms is a huge source of renewable energy, and utilization of biomass, in contrast to utilization of fossil resources such as oil and gas, does not cause a net increase in atmospheric CO_2. The increasing level of CO_2 in the atmosphere is by most scholars considered to cause global warming (Mann et al., 1998; Karl and Trenberth, 2003; Börjesson and Gustavsson, 1996; Joos et al., 1999). There is globally a large and increasing demand for liquid fuels produced from biomass, not only for environmental reasons, but also for pure economical ones due to increasing oil prices

(International Energy Outlook, 2008). First generation ethanol production is the largest process for liquid biofuel production today. In 2007, global production of bioethanol reached 13.1 billion gallons, an increase of 9% compared with 2005 (Renewable Fuel Association, 2009). The largest producers are the US and Brazil. The main co-product in the process is DDGS (Dried Distillers Grains with soluble). In a typical first generation ethanol process, the amounts of DDGS produced almost equals the amount of ethanol produced. The residuals from the fermentation step are called WDGS (wet distiller's grain with solubles) and contain about 30% of water. The WDGS is further dewatered and dried to DDGS.

DDGS and WDGS are today mainly used as cattle feed (Pedersen et al., 2002). However, instead the WDGS could be used directly to produce a liquid fuel in a thermal liquefaction process, such as the CatLiq® process. This would offer a more flexible process, which allows for adjustment of the product profile depending of the price of DDGS and crude oil.

Several other processes for thermal transformation of biomass to liquids with fuel properties exists, however most of them are carried out on dry biomass such as pyrolysis. Pyrolysis is the process of thermochemical transformation of biomass under non-oxidative conditions (McKendry, 2002 a; Bridgewater et al., 1999b; Bridgewater, 1999a; McKendry, 2002 b; Yaman, 2004; Maschio et al., 1992). Typical pyrolysis conditions are 500-520 ^{o}C for most forms of woody biomass (Bridgewater et al., 1999b; Demirbas, 2007). Other thermal processes for liquid fuel production include Catalytic depolymerization (CDP) and biomass gasification combined with Fischer-Tropsch synthesis (BG-FT) (Laohalidanond et al., 2006).

Many of the above mentioned processes are not optimal for wet biomass. However, many biomass based materials, such as WDGS, contain a large fraction of water. To remove the water by evaporation consumes a considerable amount of energy. In hydrothermal liquefaction processes aqueous biomass is directly converted to oil, water soluble substances and gas at subcritical conditions (Srokol et al., 2004; Karagöz et al., 2006; Elliott et al., 1991; Sealock et al., 1993; He et al., 2000). Most of these processes such as Hydrothermal upgrading (HTU®) operates at pressures and temperatures in the range of 300-350 ^{o}C and 100-200 bar respectively, and alkaline catalysts such as NaOH, Na_2CO_3, KOH and K_2CO_3 are often added (Zhong et al., 2002; Feng et al., 2004; Karagöz et al., 2005). The CatLiq® process is similar to these processes, but the use of heterogeneous catalyst, as well as several process features, is unique. In particular, the heat-up of the feed to process temperature is carried out within seconds. This rapid heat-up is important to optimize oil yields and prevent tar and coke formation (Zhang et al., 2008).

The aim of the current work was to carry out an initial study of the conversion of DDGS to bio oil in the CatLiq pilot plant.

It was demonstrated that DDGS could be converted to bio oil with a heat value, comparable to that of gasoline. High oil yields and energy recovery was obtained.

2 Experimental

2.1 The CatLiq® process

The Danish company SCF Technologies has developed the CatLiq technology and operates a continuous 20 L/h capacity pilot plant in Copenhagen, Denmark. The study described in this paper was carried out in the pilot plant.

In the CatLiq® process the organic fraction of the feed stream is converted to oil in the presence of a homogeneous (K_2CO_3) and a heterogeneous (Zirconia) catalyst, at subcritical conditions (280-350^oC and 225-250 bar). The full product consists of a top-phase of bio-oil, a gas-phase mainly consisting of CO_2, a water phase with soluble organic compounds and a bottom-phase mainly consisting of inorganic salts.

The conditioned feed from the feed tanks is pumped through a high pressure feed pump. The feed is then preheated in the feed heater. The feed enters a recirculation loop, in which a recirculation pump ensures a high flow rate. This design ensures instantaneous heat up in the mixing point. The flow passes through a trim heater and a fixed-bed reactor filled with zirconia-catalyst. After the reactor a fraction of the product stream is withdrawn and passed through a cooler. After pressure reduction the oil is separated from the water by centrifugation or gravimetrical separation. A schematic flow sheet is shown in Fig. 1.

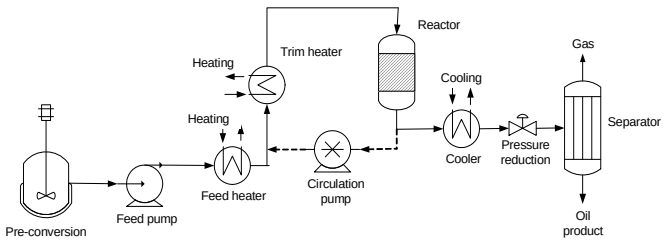

Fig. 1 Schematic of the CatLiq® process.

2.2 Feed Material

DDGS and WDGS are the major co-products of first generation ethanol production. The main components of DDGS are crude protein, crude fibe and crude fat (Kim et al., 2008). The content of the elements C, N and H were determined according to ASTM D 5291 and sulfur according to ASTM D 1552 (Table 1). The oxygen content was calculated from these results. The heating value of the DDGS was 18.8 MJ/kg and was determined according to ASTM D 240. Analysis of elementary composition and heat value was carried out at Karlshamns Kraft, Karlshamn, Sweden. The DDGS used in the current work comes from Agroetanol AB, Norrköping, Sweden. Due to storage reasons DDGS was used instead of WDGS. The DDGS was milled in a dry-mill to reduce particle size to 0.5 mm. Prior to the experiments milled DDGS was mixed with water to slurries with 25% dry matter.

Table 1
The composition of the DDGS used in the experiments

Elementary composition, daf *(wt %)	
C	45.50
H	7.0
N	8.10
S	0.79
O	38.7
Major components wt%	
Protein	35
Moisture	6.0
Fibers	47
Fat	5.5
Ash contents (db)	4.0
Starch	1.7

*daf, dry ash free; db, dry basis.

2.3 Experimental procedure

K_2CO_3 (homogeneous catalyst) corresponding to 2.5% of the slurry mass was added. The heterogeneous catalyst in the reactor was zirconia (ZrO_2). The catalytic conversion of DDGS was carried out at process temperature of 350°C and the feed rate was 11L/h. Each trial was run for 6 h and the process was considered to be in steady-state after 4 h. Each oil yield measurement was based on the oil production during 1 h at steady-state. The oil was separated from the water phase by a disc-stack centrifuge (Alfa-Laval, Sweden).

2.4 Oil properties

To evaluate the bio-oil quality, density, viscosity, heat value and elemental composition were determined. The heat value was determined according to ASTM D 240 and the elementary composition according to ASTM D 5291 and 1552. The oxygen content was calculated from these results. The Conradson

number, a measure of the oil stability, was measured according to ASTM D 189. The analyses mentioned above were carried out at Karlshamn Kraft, Karlshamn, Sweden. The water content was determined by Karl-Fischer titration performed with a TitraLab TIM 580 (Radiometer, France).

2.5 Composition analysis of oil, water and gas phase

Oil obtained from catalytic conversion of DDGS was analyzed by gas chromatograph equipped with a mass selective detector [GC-MS; Varian CP-3800; column, VF-5ms; (5% phenyl 95% dimethylpolysiloxane, 30m × 0.25mm × 0.25μm); temperature programmed: 75^{o}C (hold 2 min.) → 325^{o}C (20^{o}C/min, hold 15 min.). The compounds were identified by means of the NIST (National Institute of Standards and Technology) library of mass spectra.

The water phase was analyzed for short-chained alcohols and acids as well as acetone by GC (Varian 3800, column: fused silica, 25m × 0.32mm, temperature programmed: 50 ^{o}C hold 2 min. → 140 ^{o}C, 35 ^{o}C/min.). To detect other compounds such as amines and fatty acids, 24 mL of water-phase was acidified by addition of concentrated hydrochloric acid (2 mL). This made the water phase cloudy, indicating the presence of acidic organic compounds. The cloudy water phase was extracted using dichloromethane and the combined organic phases dried ($MgSO_4$) and evaporated *in vacuo* to give a colorless residue (240 mg, 1.0 wt%). The isolated residue was analyzed by GC-MS at the University of Copenhagen. The total organic content (TOC) in the water phase was measured by using a kit (LCK 387) and a spectrophotometrical analysis unit (DR 2800) from Hach & Lange, Germany.
The gas phase was sent for analysis at Statens Provningsanstalt, Borås, Sweden.

3 Results

The product from the process was a three-phase system of oil, water and salt. The oil was easily separated from water and salt by a disc-stack centrifuge.

3.1 The oil phase

The oil phase appeared as a black, viscous liquid, slightly lighter than water.

Table 2

Over-all results of the experiments, values are given with 95% confidence intervals

Oil yield on dry biomass (%)	33.9 ± 1.8
Energy recovery in oil (%)	73.2 ± 3.9
Carbon recovery from biomass to oil (%)	57.8 ± 2.8
Low heat value of oil* (MJ/kg)	35.8 ± 0.2
Elementary composition of oil (%)*	
C	78.3 ± 0.3
H	9.3 ± 0.1
O	5.1 ± 0.4
N	6.4± 0.4
S	0.4± 0.1

* corrected for the water content

Table 3

Properties of the bio-oil, representative sample

Viscosity at 40 ^{o}C, (cP)	499 ± 52
Viscosity at 60 ^{o}C, (cP)	116 ± 10
Viscosity at 80 ^{o}C, (cP)	39 ± 3
Water content in oil (%)	7.2 ± 0.9
Ash content in oil (%)*	0.6 ± 0.1
Conradson number	13± 1

* Water-free

The over-all results are given in table 2 and 3, expressed as average values with 95% confidence intervals. The values are based on five separate trials. The oil yield on dry matter in the feed was 34%. The oil contained more than 6 times less oxygen than the DDGS and thus the effective heat value was almost double, 35.8 MJ/kg. As much as 73.2% of the energy in the feed was recovered in the oil. The viscosity of the produced oil was high but decreased significantly with temperature and the rheological behavior was Newtonian. The oil contained some water that could be removed by a second centrifugation. The ash content in the oil was relatively low. The stability of the oil was checked by measuring the change in viscosity, elementary composition and heat value after extended storage at ambient conditions. After 4 months of storage at ambient conditions. In addition, there was no change in elementary composition and heat value after 8 months of storage.

GC-MS analysis of DDGS oil was performed and the identified compounds in the oil are presented in Table 4 and Fig. 2. The oil contained a large fraction of long chain aliphatic acids such as: tetradecanoic acid, hexadecanoic acid and octadecanoic acid.

In order to determine the distribution of compounds in the oil, a semi-quantitative study was made by means of the percentage of area of the chromatographic peaks. This type of qualitative analysis in which the concentrations of the components is related to the total area has also been used

by other researchers (Karagöz et al., 2005; Aguado et al., 2000; Domínguez et al., 2003). The deviation from 100% represents the area of unidentified compounds.

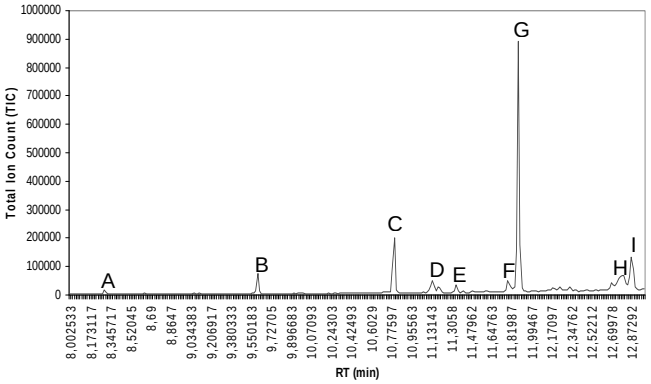

Fig. 2 GC-MS spectrum of bio-oil with peak identification. A=decanoic acid; B=dodecanoic acid; C=tetradecanoic acid; D=tridecanoic acid; E=n-pentadecanoic acid; F=palmitelaidic acid; G=hexadecanoic acid; H=11-cis-octadecenoic acid; I=octadecanoic acid.

Table 4
Identification of compounds in oil phase

RT(min)	Compound	Area (%)
8.299	Decanoic acid	0.571
9.616	Dodecanoic acid	3.039
10.809	Tetradecanoic acid	9.431
11.147	Tridecanoic acid	2.772
11.352	n-Pentadecanoic acid	1.216
11.790	Palmitelaidic acid	2.416
11.885	Hexadecanoic acid	37.376
12.793	11-cis-Octadecenoic acid	7.006
12.873	Octadecanoic acid	8.071
Σ Area		71.898

3.2 The water phase

The TOC (Total Organic Content) was 33.3 ± 0.8 g/L, corresponding to a carbon recovery to water-soluble compounds of 30%. A quantitative composition of the water is shown in Table 5. It can be seen that the content of short-chained alcohols and acids as well as acetone is 8% of the TOC content. The analysis of water-phase extract showed rather high levels of piperidone,

benzamine, cyclopentenone derivates and heptanoic acid, however only enough to account for about 10% of the TOC.

Table 5
The concentration of short-chained alcohols and acids in a water phase from one of the experiments

Compound	Quantity (mg/L)
Methanol	252
Ethanol	290
1-Propanol	40
Butanol	40
Acetone	110
Acetic acid	3320
Propionic acid	727
Butanic acid	305
Valeric acid	230
Isovaleric acid	241.23

3.3 The gas phase

The gas contained about 95% CO_2 and 1.6% H_2, small amounts of N_2, CO and CH_4 as well as traces of short-chain alkanes and alkenes. The product gas flow was about 350-410 L/h corresponding to a carbon recovery from biomass to gas of about 12%.

4 Discussion

Catalytic liquid conversion of DDGS was performed in a 20L/h continuous pilot-plant at subcritical conditions 350^{o}C and 250 bar in the presence of homogeneous K_2CO_3 and heterogeneous ZrO_2 catalysts. This represents the first study of hydrothermal conversion of DDGS.

The oil produced contained mainly long chain aliphatic acids and the oil yield on DDGS was 34% (w/w). More importantly, 73% of the energy in the DDGS was recovered in the oil. During the process more than 80% of the oxygen was removed. The oil had an effective heat value of 36 MJ/kg, not far from that of commercial diesel (42 MJ/kg, effective), and significantly higher than that of ethanol (28MJ/kg, effective).

There are only few similar techniques for utilization of wet materials that have reached further than bench-scale. The most important is the HTU® (Hydrothermal Upgrading) process, which has been evaluated in a 20 kg/h pilot plant. Even though the CatLiq and HTU process are based on the same principles there are basic differences; firstly, the use of heterogeneous catalysts in the CatLiq® and secondly that the design of the internal recirculation system differs (Goudriaan et al., 2000). The oil from the HTU-process in general has a low heating value (LHV) of 30-35 MJ/kg and an oxygen content of 12-21%. In

a specific case sugar beet pulp was converted and the lower heating value was 33.3 MJ/kg and the energy recovery 79%. In a different study made in a 1.8L stainless steel batch reactor swine manure was converted to oil with a heating value of 34.9 kJ/kg (He et al., 2000). It is obvious that the CatLiq process compares well to these results even though the raw materials were different. In addition the CatLiq oil from DDGS is stable during extended storage. Many pyrolysis oils and oils from similar processes often show poor stability (Bridgewater et al., 1999).

Only compounds corresponding to about 20% of the TOC could be identified with GC and GC-MS. The number of compounds was obviously large and thus not all compounds could be identified. In the GC-MS analysis of water extract, the detected compounds accounted only for 35% of the total area. It is over-all certain that the main components are short-chain alcohols and acids, amines and aliphatic acids and that the unidentified compounds are most likely derivates thereof. More careful analysis also including other analysis methods will be carried out.

The CatLiq® process has been demonstrated to be an effective technology for catalytic liquid conversion of DDGS, giving a high yield of bio-crude oil. Even though the oil due to the rather high viscosity, is not directly suitable as transportation fuel, it may well be used for direct green electricity production, as feed-stock for refineries or as marine diesel. The CatLiq technique offers an alternative use of WDGS and thus flexibility in terms of product spectrum.

Acknowledgement
We thank Erik G. Søgaard and Rudi P. Nielsen for their valuable discussions during this work at the CIChem research group, Aalborg University, Esbjerg.

References

Aguado, R., Olazar, M., Jose, M.J.S., Aguirre, G., Bilbao, J., 2000. Pyrolysis of sawdust in a conical spouted bed reactor. Yields and product composition. Industrial and Engineering Chemistry Research 39 (6), 1925-1933.

Börjesson, P., Gustavsson, L., 1996. Regional production and utilization of biomass in Sweden. Energy 21 (9), 747-764.

Bridgewater, A.V., 1999a. Principles and practice of biomass fast pyrolysis processes for liquids. Journal of Analytical and Applied Pyrolysis 51, 3-22.

Bridgewater, A.V., Meier, D., Radlein, D., 1999b. An overview of fast pyrolysis of biomass. Organic Geochemistry 30, 1479-1493.

Demirbas, A., 2007. The influence of temperature on the yields of compounds existing in bio-oils obtained from biomass samples via pyrolysis. Fuel Processing Technology 88, 591-597.

Domínguez, A., Menéndez, J.A., Inguanzo, M., Bernad, P.L., Pis, J.J., 2003. Gas chromatographic- mass spectrometric study of the oil fractions produced by microwave-assisted pyrolysis of different sewage sludges. Journal of Chromatography A 1012, 193-206.

Elliott, D.C., Beckman, D., Bridgwater, A.V., Diebold, J.P., Gevert, S.B., Solantausta, Y., 1991. Developments in direct thermochemical liquefaction of biomass: 1983-1990. Energy and Fuels 5, 399-410.

Feng, W., Van der Kooi, H.J., Swaan Arons, J.de., 2004. Biomass conversions in subcritical and supercritical water: driving force, phase equilibria and thermodynamic analysis. Chemical Engineering and Processing 43, 1459-1467.

Goudriaan, F., Van de Beld, B., Boerefijn, F.R., Bos, G.M., Naber, J.E., Van der Wal, S., Zeevalkink, J.A., 2000. Thermal efficiency of the HTU® process for biomass liquefaction. In: Conference on progress in thermochemical biomass conversion, Tyrol, Austria.

He, B.J., Zhang, Y., Funk, T.L., Riskowski, L., Yin, Y., 2000. Thermochemical conversion of swine manure: An alternative process for waste treatment and renewable energy production. American Society of Agricultural Engineers 43 (6), 1827-1833.

International Energy Outlook, 2008. World oil prices: Liquid fuels (http://www.eia.doe.gov/oiaf/ieo/)

Joos, F., Plattner, G.K., Stocker, T.F., Marchal, O., Schmittner, A., 1999. Global warming and marine carbon cycle feedbacks on future atmospheric CO_2. Science 284, 464-467.

Karagöz, S., Bhaskar, T., Muto, A., Sakata, Y., 2006. Hydrothermal upgrading of biomass: effect of K_2CO_3 concentration and biomass/water ratio on products distribution. Bioresource Technology 97, 90-98.

Karagöz, S., Bhaskar, T., Muto, A., Sakata, Y., Oshiki, T., Kishimoto, T., 2005. Low-temperature catalytic hydrothermal treatment of wood biomass: analysis of liquid products. Chemical Engineering Journal 108, 127-137.

Karl, T.R., Trenberth, K.E., 2003. Modern global climate change. Science 302, 1719-1723.

Kim, Y., Mosier, N.S., Hendrickson, R., Ezeji, T., Blaschek, H., Dien, B., Cotta, M., Dale, B., Ladisch, M.R., 2008. Composition of corn dry-grinde ethanol by-products: DDGS, wet cake, and thin stillage. Bioresource Technology 99, 5165-5176.

Laohalidanond, K., Heil, J., Writgen, C., 2006. The production of synthetic diesel from biomass. KMITL Science and Technology Journal 6 (1), 35-45.

Mann, M.E., Bradley, R.S., Hughes, M.K., 1998. Global-scale temperature patterns and climate forcing over the past six centuries. Nature 392, 779-787.

Maschio, G., Koufopanos, C., Lucchesi, A., 1992. Pyrolysis, a promising route for biomass utilization, Bioresource Technologies 42, 219-231.

McKendry, P., 2002 a. Energy production from biomass (part 1): overview of biomass, Bioresource Technologies 83, 37-46.

McKendry, P., 2002 b. Energy production from biomass (part 2): conversion technologies, Bioresource Technologies 83, 47-54.

Pedersen, C., Jonsson, H., Lindberg, J.E., Ross, S., 2002. Microbiological characterization of wet wheat distillers grain, with focus on isolation of lactobacilli with potential as probiotics. Applied and Environmental Microbiology 70 (3), 1522-1527.

Renewable Fuel Association, 2009. Ethanol production: Statistics (http://www.ethanolrfa.org/industry/statistics/)

Sealock, L.J., Elliott, D.C., Baker, E.G., Butner, R.S., 1993. Chemical processing in high-pressure aqueous environments. 1. Historical perspective and continuing developments. Industrial and engineering Chemistry Research 32, 1535-1541.

Srokol, Z., Bouche, A-G., Estrik, A.v., Strik, R.C.J., Maschmeyer, T., Peters, J.A., 2004. Hydrothermal upgrading of biomass to bio-fuel; studies on some monosaccharide model compounds. Carbohydrate Research 339, 1717-1726.

Yaman, S., 2004. Pyrolysis of biomass to produce fuels and chemical feedstocks. Energy Conversion and Management 45, 651-671.

Zhang, B., Keitz, M.v., Valentas, K., 2008. Thermal effects on hydrothermal biomass liquefaction. Applied Biochemistry and Biotechnology 147, 143-150.

Zhong, C., Peters, C.J., Swaan Arons, J.de., 2002. Thermodynamic modeling of biomass conversion processes. Fluid Phase Equilibria 194-197, 805-815.

BUBBLE POINT PRESSURES OF THE SELECTED MODEL SYSTEM FOR CATLIQ® BIO-OIL PROCESS

Toor, S.S[1]., Rosendahl, L[1]., Baig, M.N[2]., Robbins, P.T[2]., Santos, R.C.D[2]., Nøgaard, K.P[3]

[1]Department of Energy Technology, Aalborg University
Pontoppidanstraede 101, DK-9220 Aalborg
sst@iet.aau.dk, http://www.iet.aau.dk
[2]School of Chemical Engineering, University of Birmingham
Edgbaston B15 2TT, UK Birmingham
[3]SCF Technologies A/S, Smedeholm 13B, DK-2730 Herlev
kpn@scf-technologies.com

ABSTRACT: The CatLiq® process is a second generation catalytic liquefaction process for the production of bio-oil from WDGS (Wet Distillers Grains with Solubles) at subcritical conditions (280-350 °C and 225-250 bar) in the presence of a homogeneous alkaline and a heterogeneous Zirconia catalyst. In this work, the bubble point pressures of a selected model mixture (CO_2 + H_2O + Ethanol + Acetic acid + Octanoic acid) were measured to investigate the phase boundaries of the CatLiq® process. The bubble points were measured in the JEFRI-DBR high pressure PVT phase behavior system. The experimental results were presented for the temperatures between 40 °C and 75 °C. The results were correlated by the PSRK (Predictive Soave-Redlich-Kwong) model using Huron-Vidal first-order mixing rule of Michelsen coupled with the modified UNIFAC model. The average absolute deviation between the experimental and predicted data is 8.7% in the selected model mixture.

Introduction

Biomass is one of the most abundant sources of renewable energy and will be an important part of a more sustainable future energy system. Apart from direct combustion there is also growing attention in converting the biomass into liquid energy carriers. Biomass energy conversion methods [7,16,18,10,13,22] are divided into biochemical/biotechnical methods [14] and the thermochemical methods (such as direct combustion, pyrolysis, gasification, liquefaction etc.). In these methods, liquefaction is considered to be a promising method for converting biomass into higher value fuels. Hydrothermal liquefaction is generally carried out at 280 to 370 °C and between 100 and 250 bar. At these conditions water is in a liquid state. The main products are bio-crude with a relatively high heating value, char, water-soluble substances and gas. Addition of various alkaline catalysts can suppress the char formation and thus improve the oil yield and quality. As the temperature is increased above the critical limit of water, gasification becomes the dominating process. Due to the severe process conditions, industrial

application of these processes suffers from various challenges such as corrosion, which requires the use of special and expensive alloys in addition the high pressures put high requirements on other process components such as feed pumps. Most work on hydrothermal liquefaction has so far been carried out in lab or bench scale, especially high investment costs is a considerable hurdle for commercialization, however, a few pilot/demonstration processes do exist such as HTU® (hydrothermal upgrading), LBL (Lawrence Berkeley Laboratory), and CatLiq® (catalytic liquefaction) [2,3]. The purpose of the CatLiq® process is to convert WDGS (Wet Distillers Grains with Solubles), a byproduct in first generation ethanol production, available in large quantities into bio-oil, combustible gases and water-soluble organic compounds in the presence of a homogeneous (K_2CO_3) and a heterogeneous (Zirconia) catalyst, at subcritical conditions (280-350^oC and 225-250 bar). A schematic flow sheet of the CatLiq® process is shown in (Figure 1).

In the design and development of biomass conversion processes, the importance of accurate correlation and prediction of phase behavior should never be underestimated. In particular, accurate prediction depends on both a powerful model and high-quality experimental data. The full product of CatLiq® process consists of a top-phase of bio-oil, a gas-phase and a water phase with soluble organic compounds. The analysis of all these phases showed that the oil contained a large fraction of long chain aliphatic acids such as: tetradecanoic acid, hexadecanoic acid and octadecanoic acid, the gas consisting of 95 %CO_2 and some combustible gases. The water-phase contained short-chained alcohols and acids.

In this study, a mixture of a limited number of well-defined components resembling the products from the CatLiq® process was used instead of a real fraction. This method allows a thorough experimental investigation that can be used to verify the prediction and adjust the description by equations of state. Therefore bubble point pressures of a selected model mixture (CO_2 + H_2O + Ethanol + Acetic acid + Octanoic acid) were determined in the JEFRI-DBR high pressure PVT phase behavior system. The experimental results were presented for the temperatures (40 ^oC, 50 ^oC, 60 ^oC and 75 ^oC).

The results were correlated by the PSRK model proposed by Holderbaum and Gmehling [11], which is predictive Soave-Redlich-Kwong (SRK) equation of state (EOS) with the modified Huron-Vidal first-order (MHV1) mixing rule of Michelsen [17] coupled with the modified UNIFAC model.

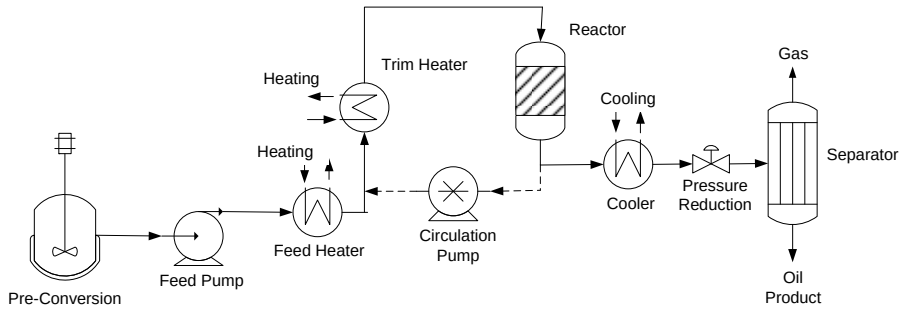

Figure 1. Schematic of the CatLiq® process.

Experimental

The experimental work was carried out in a high-pressure JEFRI-DBR phase behavior system. In this apparatus, pressures up to approximately 700 bar can be handled and the temperature can be range from 0 °C to 200 °C. An advantage of this apparatus is that the phase transitions can be observed visually. A schematic diagram of the system is shown in (Figure 2).

The heart of the system was a high-pressure PVT cell consisting of a glass cylinder, secured between two full-length sight glass windows, inside a stainless steel frame. This design allowed for unimpaired visibility of the entire contents of the cell. Pressure was regulated through an automated, high pressure, positive displacement pump. The hydraulic fluid inside the pump was connected to a floating isolation piston located inside the PVT cell. The piston isolated the hydraulic fluid from the process side of the PVT cell. Controlled displacement of the isolation piston allowed for volume changes in the process chamber, thus providing an effective way to control pressure. The PVT cell was mounted inside a temperature-controlled air bath by means of a bracket, attached to a horizontal shaft.

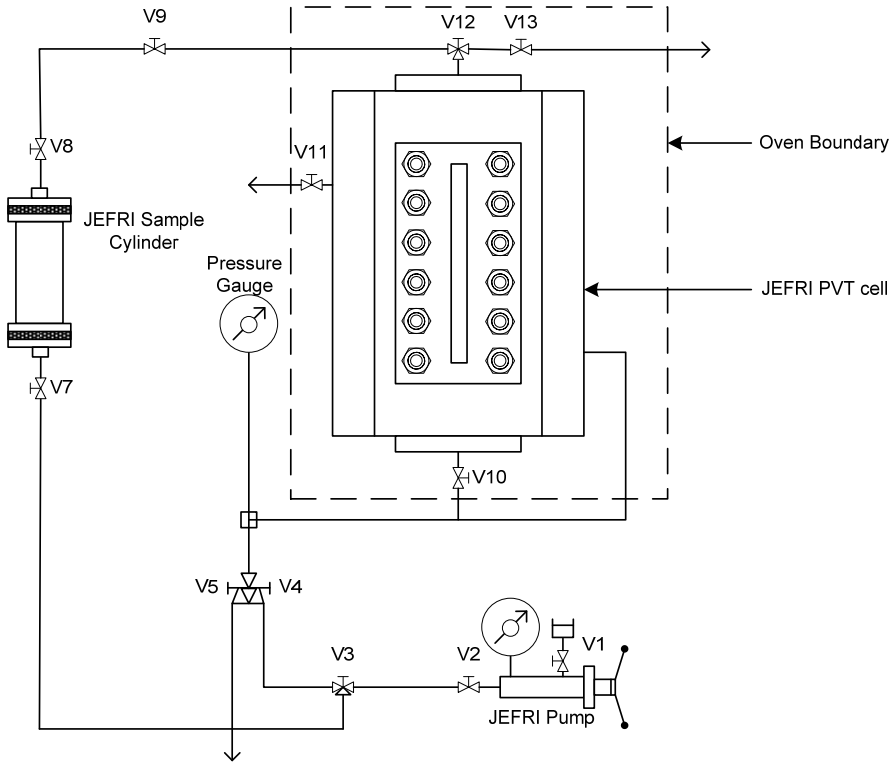

Figure 2. Schematic diagram of JEFRI-DBR PVT system.

The bubble point pressures were determined at different constant temperatures (40 ^{o}C, 50 ^{o}C, 60 ^{o}C, and 75 ^{o}C) by observing the appearance of gas bubble through the cell window as the pressurized liquid sample was decompressed. As soon as the bubble point pressure reached the overall compressibility of the system increased. Small changes in pressure resulted the large changes in the total fluid volume in the PVT cell. This was manifested graphically by the change of the slope when the sample pressure was plotted against the sample volume.

The applications of the JEFRI-DBR phase behavior system have also been described by Bruusgaard [4] and Beltrán [1].

Table 1. Suppliers and purities of the substances used in this work.

Substance	Supplier	Purity (mass %)
Carbon dioxide	Yara praxair	>99.95
Water	Sigma-Aldrich	>99
Ethanol	Sigma-Aldrich	>99
Acetic acid	Sigma-Aldrich	>99
Octanoic acid	Sigma-Aldrich	>99

Table 2. Approximate composition of the selected model mixture.

Component	(w/w %)
Carbon dioxide	7.0
Water	84.8
Ethanol	0.1
Acetic acid	0.1
Octanoic acid	8.0

Table 3. Pure component properties used in the mixing rule.

Substance	T_c (°C)	P_c(bar)	ω	c_1	c_2	c_3
Carbon dioxide	31.04[a]	73.8[a]	0.228[a]			
Water	374.15[a]	220.5[a]	0.344[a]	1.0783[b]	-0.5832[b]	0.5462[b]
Ethanol	243.01[a]	63.8[a]	0.637[a]	1.3327[b]	0.9695[b]	-3.1879[b]
Acetic acid	319.56[a]	57.86[a]	0.462[a]			
Octanoic acid	442.86[c]	27.35[c]	0.7653[c]			

a. [23].

b. [11].

c. Estimated by Aspen Plus software.

The pH of the mixture was adjusted to 8.0 with 5% NaOH solution.

Correlation

The equation of state The Soave-Redlich-Kwong (SRK) equation of state [11] is adopted in the PSRK model for phase equilibria calculations in this work:

$$P = \frac{RT}{v-b} - \frac{a}{v(v+b)} \tag{1}$$

The constants *a* and *b* can be obtained from the pure fluid critical properties using:

$$a = 0.42748 \frac{R^2 T_c^2}{P_c} f(T_i) \tag{2}$$

$$b = 0.08664 \frac{RT_c}{P_c} \tag{3}$$

Where T_c and P_c are the critical temperature and pressure, respectively. For large molecule (Octanoic acid) these properties were estimated by the group contribution method of Joback [19] and that of Constantinou and Gani [5].

$$f(T_i) = \left[1 + \left(0.48508 + 1.5517\omega - 0.15613\omega^2\right)\left(1 - T_r^{0.5}\right)\right]^2 \tag{4}$$

or

$$f(T_i) = \left[1 + c_1\left(1 - T_r^{0.5}\right) + c_2\left(1 - T_r^{0.5}\right)^2 + c_3\left(1 - T_r^{0.5}\right)^3\right]^2, T_r \langle 1 \tag{5}$$

$$f(T_i) = \left[1 + c_1\left(1 - T_r^{0.5}\right)\right]^2, T_r \rangle 1 \tag{6}$$

Eq. (4) is good enough for nonpolar substances (CO_2 and Octanoic acid) and the substance like acetic acid whose c_1, c_2, and c_3 cannot be obtained [21], however, for polar substances (H_2O and Ethanol) Eqs. (5) and (6) proposed by Mathias and Copeman [15] are much more accurate. Where T_r and ω are the reduced temperature and acentric factor, respectively. For large molecule (Octanoic acid) acentric factor was estimated with the Lee-Kesler method [19] and that of Constantinou and Gani [6].

The mixing rule The MHV1 mixing rule [17], a so-called EOS/G^E mixing rule, is used in the PSRK model:

$$\frac{a_m}{b_m} = \sum_i x_i \frac{a_i}{b_i} + 1/q_1 \left[G^E + RT \sum_i x_i \ln\left(b_m / b_i\right) \right] \tag{7}$$

$$b_m = \sum x_i b_i \tag{8}$$

Where a_m and b_m are the mixture co-energy and co-volume parameters, respectively and G^E is the molar excess Gibbs free energy, which can be calculated from a G^E model. The constant q_1 is set to be -0.64663 for the PSRK model.

The G^E model The system involved in the CatLiq® process is a highly asymmetric system. Therefore, modified UNIFAC model [24,12] is used, which reduces to the original UNIFAC model [9] for symmetric or slightly asymmetric systems.

$$\ln \gamma_i = \ln \gamma_i^C + \ln \gamma_i^R \tag{9}$$

Where the residual part $\ln \gamma_i^R$ is identical to the original UNIFAC model and combinatorial part $\ln \gamma_i^C$ is modified as follows:

$$\ln \gamma_i^C = \ln\left(\frac{\Phi'_i}{x_i}\right) + 1 - \left(\frac{\Phi'_i}{x_i}\right) - \left(\frac{z}{2}\right) q_i \left[\ln\left(\frac{\Phi_i}{\theta_i}\right) + 1 - \left(\frac{\Phi_i}{\theta_i}\right)\right] \tag{10}$$

With

$$\theta_i = \frac{x_i q_i}{\sum_j x_j q_j} \qquad \Phi_i = \frac{x_i r_i}{\sum_j x_j r_j} \tag{11}$$

and

$$\Phi'_i = \frac{x_i r'_i}{\sum_j x_j r'_j} \tag{12}$$

with

$r_i' = r_i$, for small molecules (13)

$r_i' = 0.6583\ r_i$, for large molecules (14)

Calculations were done using the pure component properties summarized in Table 3. The temperature-dependent UNIFAC group interaction parameters obtained by Holderbaum and Gmehling [11], and Fischer and Gmehling [8] are used, which allow the inclusion of gases in the calculation.

The proposed algorithm The general solution to vapor-liquid equilibria including high-pressure applications may be advantageously obtained using an equation of state by iteration methods. The proposed algorithm [20] for bubble pressure calculations is shown in (Figure 3). In this algorithm, y is iterated for convergence to a constant value $\sum y_i' = 1$ at a given *P*, which is iterated in the outer loop until the equilibrium conditions are satisfied.

Where the *K*-value is defined by:

$$K_i = \frac{\phi_i^L(T, P, x)}{\phi_i^V(T, P, y)} \tag{15}$$

$$y_i = K_i x_i \tag{16}$$

Here, *Øi* are fugacity coefficients of different phases, for the evaluation of which EOS are solved. Proper guess is very important in efficient computations. A good guess for the pressure may be obtained by the following equation.

$$P = \sum x_i P_i^{sat}(T) \tag{17}$$

A vapor composition is calculated by using guessed *K*-values obtained by:

$$K_i = \frac{P_i^{Sat}(T)}{P} \tag{18}$$

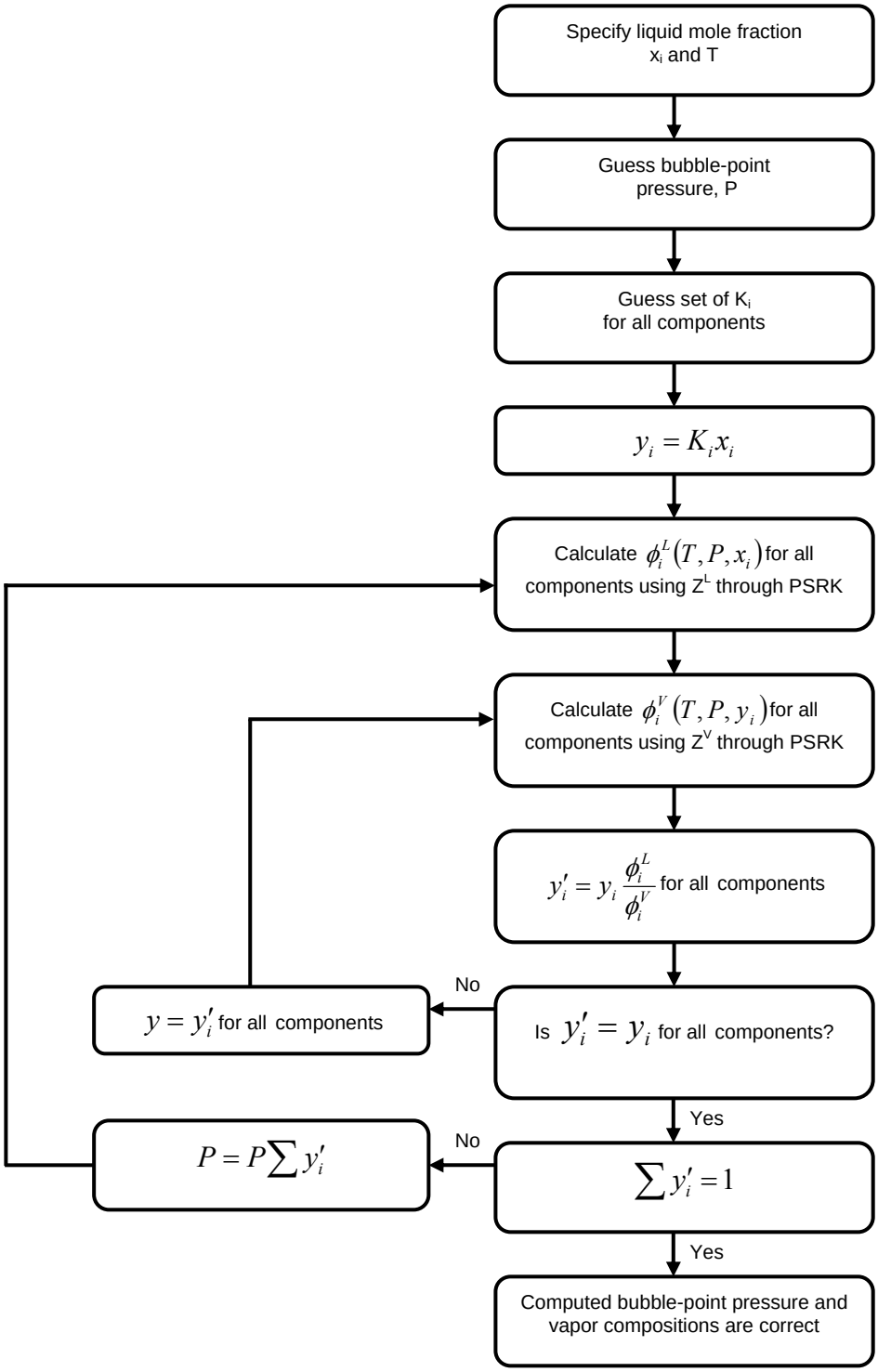

Figure 3. Flowchart for bubble P calculation.

Results and discussion

The experimental bubble point pressures for the selected model system (CO_2 + H_2O + Ethanol + Acetic acid + Octanoic acid) are given in (Table 4) and (Figure 4). The bubble point pressures, correlated by the PSRK model, are also shown in this table.

Table 4. Experimental ($P_{exp.}$) and PSRK-Estimated ($P_{calc.}$) Bubble point Pressures.

T/(°C)	$P_{exp.}$/(bar)	$P_{calc.}$/(bar)	Rel. Dev. (%)[d]
40	156.73	138.64	11.6123
50	190.88	169.43	11.3474
60	224.48	202.39	9.9786
75	258.97	254.35	1.9770
	AAD %[e]		8.728863

d. Relative Deviation (%) = $(P_{exp.} - P_{calc.})/ P_{exp.} \times 100$.

e. AAD % = $(\sum |\text{error \%}|)$ / number of data points.

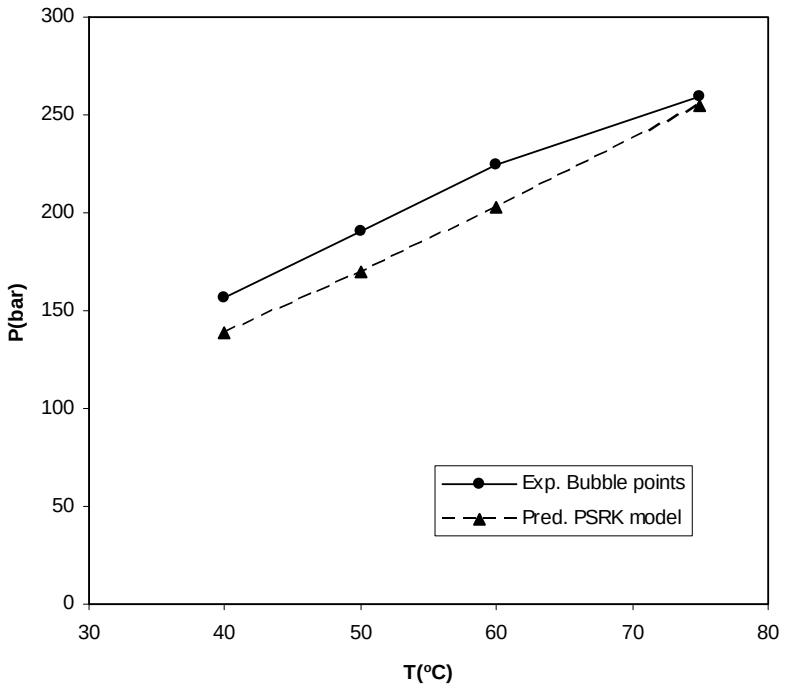

Figure 4. Measured and predicted phase boundaries for the selected model system.

For each measured point, the relative error between experimental and predictive values is given in the table and average absolute deviation of the system is determined. It can be seen that average absolute deviations (AAD %) are less than 10% or equal to 8.7%.
Comparison of the percentages of error and average absolute deviation between the experimental and predictive data shows that the capability of the PSRK model is reasonably good in predicting the phase behavior of such a model system for CatLiq® process. This modelling work is useful for the CatLiq® process design, development and optimization, which provides a general thermodynamic approach on how to model biomass conversion processes.

ACKNOWLEDGEMENTS

The authors would like to thank the SCF Technologies A/S for giving the opportunity to perform this research. Thanks are also due to Tor and Sivert for his help in the experimental work at the Department of Petroleum Engineering, Stavanger University, Norway.

REFERENCES

1. Beltrán G. J., Servio P. (2008) Equilibrium studies for the system Methane + Carbon Dioxide +Neohexane + Water. Journal of Chemical and Engineering Data, 53, 1745-1749.
2. Bouvier J. M., Gelus M., Maugendre S. (1988) Wood liquefaction-An overview. Applied Energy, 30 (2), 85-98.
3. Bridgwater A. V. (2001) Progress in thermochemical biomass conversion. Vol. 2, pp. 1312. Blackwell Science Ltd. London.
4. Bruusgaard H., Beltrán G. J., Servio P. (2008) Vapor-liquid water-hydrate equilibrium data for the system N_2 + CO_2 + H_2O. Journal of Chemical and Engineering Data, 53, 2594-2597.
5. Constantinou L., Gain, R. (1994) New group contribution method for estimating properties of pure compounds. AIChE Journal, 40 (10), 1697-1710.
6. Constantinou L., Gain R., O'Connell J. P. (1995) Estimation of the acentric factor and the liquid molar volume at 298 K using a new group contribution method. Fluid Phase Equilibria, 103, 11-22.
7. Elliott D. C., Beckman D., Bridgwater A. V., Diebold J. P., Gevert S. B., Solantausta Y. (1991) Developments in direct thermochemical liquefaction of biomass: 1983-1990. Energy and Fuels, 5, 399-410.
8. Fischer K., Gmehling J. (1996) Further development, status and results of the PSRK method for the prediction of vapor-liquid equilibria and gas solubilities. Fluid Phase Equilibria, 121, 185-206.

9. Fredenslund A., Jones R. L., Prausnitz J. M. (1975) Group-contribution estimation of activity coefficients in nonideal liquid mixtures. AIChE Journal, 21 (6), 1086-1099.
10. Hahn-Hägerdal B., Galbe M., Gorwa-Grauslund M. F., Lidén G., Zacchi G. (2006) Bio-ethanol-the fuel of tomorrow from the residues of today. Trends in Biotechnology, 24, 549-556.
11. Holderbaum T., Gmehling J. (1991) PSRK: A group contribution equation of state based on UNIFAC. Fluid Phase Equilibria, 70, 251-265.
12. Kikic I., Alessp P., Rasmussen P., Fredenslund A. (1980) On the combinatorial part of the UNIFAC and UNIQUAC models. The Canadian Journal of Chemical Engineering, 58, 253-258.
13. Lin Y., Tanaka S. (2006) Ethanol fermentation from biomass resources: current state and prospects. Applied Microbiology and Biotechnology, 69, 627-642.
14. Mata-Alvarez J., Macé S., Llabrés P. (2000) Anaerobic digestion of organic solid wastes: An overview of research achievements and prospectives. Bioresource Technology, 74, 3-16.
15. Mathias P. M., Copeman T. W. (1983) Extension of the Peng-Robinson equation of state to complex mixtures: Evaluation of the various forms of the local composition concept. Fluid Phase Equilibria, 13, 91-108.
16. Matsumura Y., Minowa T., Potic B., Kersten S. R .A., Prins W., van Swaaij W. P. M., van de Beld B., Elliott D. C., Neuenschwander G. G., Kruse A., Antal Jr M. J. (2005) Biomass gasification in near- and super-critical water: Status and prospects. Biomass and Bioenergy, 29, 268-292.
17. Michelsen M. L. (1990) A modified Huron-Vidal mixing rule for cubic equations of state. Fluid Phase Equilibria, 60, 213-219.
18. Peterson A. A., Vogel F., Lachance R. P., Fröling M., Antal M. J., Tester J. W. (2008) Thermochemical biofuel production in hydrothermal media: A review of sub- and supercritical water technologies. Energy and Environmental Science, 1, 32-65.
19. Reid R. C., Prausnitz J. M., Poling B. E. (1987) The Properties of Gases and Liquids. 4th edn. McGraw-Hill, Singapore.
20. Sandler S. I., Orbey H. (1998) Modeling Vapor-Liquid Equilibria- Cubic Equations of State and Their Mixing rules. pp. 110. Cambridge University Press, Cambridge.
21. Soave G. (1972) Equilibrium constants from a modified Redlich-Kwong equation of state. Chemical Engineering Science, 27, 1197-1203.
22. Wheals A. E., Basso L. C., Alves D. M. G., Amorim H. V. (1999) Fuel ethanol after 25 years. TIBTECH, 17, 482 – 487.
23. Yaws C. L. (2003) Yaws' Handbook of Thermodynamic and Physical Properties of Chemical Compounds. Knovel Publisher.
24. Zhong C., Sato Y., Masuoka H., Chen X. (1996) Improvement of predictive accuracy of the UNIFAC model for vapor-liquid equilibria of polymer solutions. Fluid Phase Equilibria, 123, 97-106.